Filamentous Co-Cultivation for the Conversion of Cellulose into Pigmented Antibiotics

Filamentöse Ko-Kultivierung für die Umwandlung von Zellulose in Pigmentierte Antibiotika

Von der Fakultät für Maschinenwesen der Rheinisch-Westfälischen Technischen Hochschule Aachen
zur Erlangung des akademischen Grades eines Doktors der Ingenieurwissenschaften
genehmigte Dissertation

vorgelegt von

Maurice Finger

Berichter/in: Universitätsprofessor Dr.-Ing. Dr. h. c. (Osaka) Jochen Büchs
Universitätsprofessorin Dr. rer. nat. Miriam Agler-Rosenbaum

Tag der mündlichen Prüfung: 11. Juli 2023

Danksagung

Die vorliegende Arbeit entstand während meiner Tätigkeit als wissenschaftlicher Mitarbeiter am Lehrstuhl für Bioverfahrenstechnik der RWTH Aachen. Die Arbeit wurde im Rahmen des Schwerpunktprograms SPP2170 „InterZell“ angefertigt, welches durch die DFG - Deutsche Forschungsgemeinschaft gefördert wurde.

Mein besonderer Dank gilt Prof. Dr.-Ing. Jochen Büchs für die Möglichkeit zur Promotion am Lehrstuhl für Bioverfahrenstechnik und die sehr gute Betreuung. Seine wissenschaftliche Neugier und die darauf bauenden Diskussionen haben meine Arbeit bereichert und zum Gelingen beigetragen. Weiterhin möchte ich mich bei Prof. Dr. rer. nat. Miriam Agler-Rosenbaum für die Übernahme des Koreferats und die produktive Zusammenarbeit im Forschungsprojekt bedanken. Vielmals danke ich auch Prof. Dr.-Ing. Thomas Bergs für die Übernahme des Prüfungsvorsitzes.

Kooperationen sind ein integraler Bestandteil wissenschaftlicher Forschung. Hier möchte ich mich insbesondere bei Ana Palacio-Barrera und Dr. rer. nat. Ivan Schlembach für die vielen konstruktiven Diskussionen und die sehr erfolgreiche Projektarbeit bedanken. Heiko Steinhoff und Prof. Dr.-Ing. Alexander Grünberger möchte ich ebenfalls für eine gute Zusammenarbeit danken.

Die tatkräftige Unterstützung von „meinen“ Studierenden möchte ich besonders hervorheben. Ich hatte stets Freude an dem Austausch und der gemeinsamen Arbeit während der verschiedenen Forschungspraktika und Abschlussarbeiten, welche zum erfolgreichen Abschluss dieser Arbeit beigetragen haben. Daher möchte ich mich herzlich bedanken bei: Gereon Fischer, Adrian Faller, Constantin Maaß, Lukas Hartmann, Paul Richter, Eliot Schröder, Carolina Bonerath, Nele von Vegesack, Fabio Sentek, Lluís Coloma de la Fuente, Michelle Peiffer.

Bei meinen ehemaligen Kollegen und Kolleginnen am Lehrstuhl möchte ich mich für die großartige Arbeitsatmosphäre, die fortwährende Hilfsbereitschaft und den starken Zusammenhalt bedanken. Ich kann mich glücklich schätzen über die vielen schönen Freundschaften, die in dieser Zeit entstanden sind. Diesen Freunden und Freundinnen bin ich besonders dankbar und freue mich auf zukünftige gemeinsame Abenteuer.

Meine Familie hat mir stets Rückhalt gegeben und mich in meinen Entscheidungen bestärkt und unterstützt. Danke, dass ihr immer an mich glaubt und für mich da seid. Damit möchte ich mich zuletzt und am allermeisten bei dir, Vanessa, bedanken. Danke, dass du stets an meiner Seite stehst und wir alle Herausforderungen gemeinsam bestreiten.

Zusammenfassung

Der Bedarf an Naturprodukten wie Antibiotika ist größer denn je. Angetrieben durch aufkommende Antibiotikaresistenzen sind neue Produktionsverfahren von besonderem Interesse. Insbesondere filamentöse Ko-Kulturen bieten ein großes Potenzial für die Entdeckung neuer Naturprodukte oder die Intensivierung von Prozessen. Diesen Vorteilen steht jedoch eine im Vergleich zu axenischen Kulturen erhöhte Komplexität gegenüber, die die Nutzung von Ko-Kulturen aufgrund des fehlenden Prozessverständnisses erschwert.

In dieser Arbeit wurde ein filamentöser Ko-Kultivierungsprozess mit dem zellulolytischen Pilz *Trichoderma reesei* RUT-C30 und dem Bodenbakterium *Streptomyces coelicolor* A3(2) für die Produktion von Naturprodukten entwickelt. Durch die Bereitstellung von Zellulose als primäre Kohlenstoffquelle wurde eine Abhängigkeit zwischen den Ko-Kultivierungspartnern geschaffen. Die Zellulose kann durch Zellulasen unter Freisetzung von löslichen Zuckern hydrolysiert werden. Zellulasen werden nur von *T. reesei* gebildet und sekretiert. Die Komplexität dieses Systems wurde durch den Einsatz von Online-Messtechnik mit hohem Durchsatz reduziert. Die Biomassebildung der Ko-Kultivierungspartner wurde individuell durch die Überwachung des Fluoreszenzproteins mNeonGreen in *S. coelicolor* und mCherry in *T. reesei* mit einem 48-Well-Mikrotiterplatten-System verfolgt. In Kombination mit den Informationen über die Sauerstofftransferraten wurde hieraus der Einfluss des Inokulationsverhältnisses, der Osmolalität und des spezifischen Leistungseintrags auf die Populationszusammensetzung erfolgreich abgeleitet. Die Ko-Kultivierung wurde von der Mikrotiterplatte in einen Rührkesselreaktor hochskaliert. Im Rührkesselreaktor wurde mit der Ko-Kultivierung auf Zellulosesubstrat ein mehr als 2-fach erhöhter Titer des pigmentierten Antibiotikums Actinorhodin im Vergleich zu Glukose-limitierten axenischen *S. coelicolor* Kulturen erreicht.

Da die Substrataffinität ein kritischer Parameter in Kohlenstoff-limitierten Ko-Kulturen ist, wurde eine neue respiratorische Methode für die Abschätzung der Affinität entwickelt. Die Methode wurde eingesetzt, um die Affinität von *Corynebacterium glutamicum* und *T. reesei* für Glukose sowie die Affinität eines genetisch veränderten *Gluconobacter oxydans* für Fruktose zu bestimmen. Das Potenzial der Atmungsüberwachung wurde auch für Agar-Kulturen demonstriert. Anstelle einer visuellen Untersuchung wird ein objektiver Atmungsparameter für die Bewertung von Kultivierungen auf festen Medien verwendet. Die Methode wurde erfolgreich für diverse Anwendungen auf Agar demonstriert.

Die vorgestellte Arbeit liefert wertvolle Erkenntnisse und Werkzeuge für die Entwicklung definierter filamentöser Ko-Kulturen, die bei der Herstellung neuartiger Naturprodukte helfen.

Abstract

The demand for novel natural products such as antibiotics is greater than ever. Driven by emerging antibiotic resistances, new production processes are of particular interest. Especially filamentous co-cultivations offer vast potential for the discovery of novel natural products or process intensification. However, these benefits go hand in hand with an inherently increased complexity compared to axenic cultivations, impeding utilization due to the lack of process understanding.

This thesis focused on establishing a model filamentous co-cultivation process with the cellulolytic fungus *Trichoderma reesei* RUT-C30 and the soil bacterium *Streptomyces coelicolor* A3(2) for the production of natural products. By providing cellulose as the primary carbon source, a dependency was created between the co-cultivation partners. The cellulose was hydrolysed by cellulases, releasing soluble sugars. Cellulases were only formed and secreted by *T. reesei*. The complexity of this system was reduced by the utilization of high-throughput online monitoring systems. Biomass formation of the co-cultivation partners was individually tracked by monitoring the fluorescence protein mNeonGreen in *S. coelicolor* and mCherry in *T. reesei* with an in-house built 48-well microtiter plate-based system. In combination with the information on the oxygen transfer rates, the influence of the inoculation ratio, the osmolality and the specific power input on the population composition were successfully derived. The co-cultivation was transferred from the microtiter plate into a stirred tank reactor. In the stirred tank reactor, a more than 2-fold increased titer for the pigmented antibiotic actinorhodin was achieved compared to glucose-limited axenic *S. coelicolor* cultivations.

As substrate affinity is a critical parameter in carbon source limited co-cultivations, a novel respiratory method was developed for the fast initial estimation. The method was utilized to estimate the glucose affinity of *Corynebacterium glutamicum* and *T. reesei* as well as the fructose affinity of a genetically modified *Gluconobacter oxydans*. The potential of respiration monitoring was further demonstrated for agar cultivations. Instead of a visual examination, the respiration represents an objective parameter for evaluating cultivations on solid media. The method was successfully demonstrated for several agar-based applications.

The presented work provides valuable insights and tools for the development of defined filamentous co-cultivations, which assist in the production of novel natural product.

Funding, publications, and contributions

The work reported in this thesis was performed as part of the priority program SPP2170 “InterZell” (Project no. 427899901) funded by the “DFG - Deutsche Forschungsgemeinschaft”. The support and funding are gratefully acknowledged.

Parts of this thesis have been published previously:

- Finger, M.; Sentek, F.; Hartmann, L.; Palacio-Barrera, A. M.; Schlembach, I; Rosenbaum, M. A.; Büchs, J.; *Insights into Streptomyces coelicolor A3(2) growth and pigment formation with high-throughput online monitoring.* Engineering in Life Sciences, 2022, 23, e2100151.*

- [§]Finger, M.; [§]Palacio-Barrera, A. M.; Richter, P.; Schlembach, I.; Büchs, J.; Rosenbaum, M. A.; *Tunable population dynamics in a synthetic filamentous coculture.* MicrobiologyOpen, 2022, 11, e1324.*

- [§]Steinhoff, H.; [§]Finger, M.; Osthege, M.; Golze, C.; Schito, S.; Noack, S.; Büchs, J.; Grünberger, A.; *Experimental k_S estimation: A comparison of methods for Corynebacterium glutamicum from lab to microfluidic scale.* Biotechnology and Bioengineering, 2023, 120, 1288-1302.*

- Finger, M.; Schröder, E.; Berg, C.; Dinger, R.; Büchs, J.; *Towards standardized solid medium cultivations: microbial online monitoring based on respiration activity*. Biotechnology Journal, 2023, 1-12.*

Contributions to further publications during the preparation of this thesis:

- [§]Palacio-Barrera, A. M.; [§]Schlembach, I.; Finger, M.; Büchs, J.; Rosenbaum, M. A.; *Reliable online measurement of population dynamics for filamentous co-cultures.* Microbial Biotechnology, 2022, 1-13.

[§]Both authors contributed equally to the publication

- Miebach, K.; Finger, M.; Büchs, J.; *Parallelized Online Measurement of Hydrogen for Time-Efficient Characterization of Microbial Hydrogen Producers*. Chemie Ingenieur Technik, 2022, 94, 1235-1235.

- Keitel, L.; Finger, M.; Büchs, J.; *Small-scale anaerobic process development: Carbon dioxide and trace oxygen concentrations impact growth and product formation of Bacteroidetes strains*. Chemie Ingenieur Technik, 2022, 94, 1238-1238.

- Berg, C.; Ihling, N.; Finger, M.; Paquet-Durand, O.; Hitzmann, B.; Büchs, J.; *Online 2D Fluorescence Monitoring in Microtiter Plates Allows Prediction of Cultivation Parameters and Considerable Reduction in Sampling Efforts for Parallel Cultivations of Hansenula polymorpha*. Bioengineering, 2022, 9, 438.

- Steinmann, A.; Schullehner, K.; Kohl, A.; Dickmeis, C.; Finger, M.; Hubmann, G.; Jach, G.; Commandeur, U.; Girhard, M.; Urlacher, V. B.; Lütz, S.; *A targeted metabolomics method for extra- and intracellular metabolite quantification covering the complete monolignol and lignan synthesis pathway.* Metabolic engineering communications, 2022, 15, e00205.

- Steinmann, A.; Finger, M.; Nowacki, C.; Decembrino, D.; Hubmann, G.; Girhard, M.; Urlacher, V. B.; Lütz, S.; *Heterologous Lignan Production in Stirred-Tank Reactors—Metabolomics-Assisted Bioprocess Development for an In Vivo Enzyme Cascade.* Catalysts, 2022, 12, 1473.

- Berg, C.; Busch, S.; Alawiyah, M. D.; Finger, M.; Ihling, N.; Paquet-Durand, O.; Hitzmann, B.; Büchs, J.; *Advancing 2D fluorescence online monitoring in microtiter plates by separating scattered light and fluorescence measurement, using a tunable emission monochromator*. Biotechnology and Bioengineering, 2023, 1-15.

- Miebach, K.; Finger, M.; Scherer, A. M. K.; Maaß, C. A.; Büchs, J.; *Hydrogen online monitoring based on thermal conductivity for anaerobic microorganisms*. Biotechnology and Bioengineering, 2023, 1-15.

Contributions to conferences during the preparation of this thesis:

- Finger, M.; Palacio-Barrera, A. M.; Schlembach, I; Rosenbaum, M. A.; Büchs, J.; *High-throughput online-monitoring helps to uncover pigment production mechanisms in Streptomyces coelicolor.* Oral presentation. 6th European Congress of Applied Biotechnology, digital conference, 2021.

- Finger, M.; Palacio-Barrera, A. M.; Schlembach, I; Rosenbaum, M. A.; Büchs, J.; *Development of a filamentous defined co-culture process with high-throughput online-monitoring.* Oral presentation. 7th BioProScale Symposium, Berlin, Germany, 2022.

- Finger, M.; Palacio-Barrera, A. M.; Schlembach, I; Rosenbaum, M. A.; Büchs, J.; *Tuning the population dynamics in a filamentous co-culture for the conversion of cellulose into valuable natural products.* Poster presentation. Himmelfahrtstagung on Bioprocess Engineering, Weimar, Germany, 2023.

Research projects in the area of biochemical engineering require close cooperation with other specialists and experts. Hence, all *Streptomyces* strains and the *Trichoderma reesei* RUT-C30 mCherry strain were kindly provided by the Hans-Knöll-Institute culture collection (Jena, Germany), as well as Ana Palacio-Barrera (Leibniz Institute for Natural Product Research and Infection Biology, Hans-Knöll-Institute, Jena, Germany) and Dr. Ivan Schlembach (Leibniz Institute for Natural Product Research and Infection Biology, Hans-Knöll-Institute, Jena, Germany). Results from this fruitful collaboration were published in Finger and Palacio-Barrera et al. (2022), which is presented partially in chapter 1 and 3. Ana Palacio-Barrera and Maurice Finger contributed equally to this publication. Furthermore, chapter 5 is partially based on the equally shared publication Steinhoff and Finger et al. (2023). For clarity, the experimental results by Heiko Steinhoff (Multiscale Bioengineering, Bielefeld University, Bielefeld, Germany) and other parties presented in the publication were left out of chapter 5. Detailed author contributions are stated before each chapter and in the respective publications and apply to the parts reproduced in this thesis.

Contents

Nomenclature

Abbreviations

Abbreviation	Description
µRAMOS	Micro(µ)-scale respiration activity monitoring system
µTOM	Micro(µ)-scale transfer rate online measurement device
A. wentii	*Aspergillus wentii*
BSA	Bovine serum albumin
CCD	Charge-coupled device
CER	Carbon dioxide evolution rate
C. glutamicum	*Corynebacterium glutamicum*
CTR	Carbon dioxide transfer rate
CTR'	Area specific carbon dioxide transfer rate
DOT	Dissolved oxygen tension
EPDM	Ethylene propylene diene monomer
E. coli	*Escherichia coli*
FDH	Fructose dehydrogenase
GFP	Green fluorescent protein
G. japonicus	*Gluconobacter japonicus*
G. oxydans	*Gluconobacter oxydans*
HPLC	High-performance liquid chromatography
LB	Lysogeny broth
LB-agar	Lysogeny broth agar
LNP	Low nitrogen phosphate medium
MES	2-(N-morpholino)ethanesulfonic acid
mNG	mNeonGreen
MOPS	3-(N-morpholino)propanesulfonic acid

Abbreviation	Description
CDMSS	Circulation Direct Monitoring and Sampling System
MTP	Microtiter plate
OD	Optical density at a wavelength of 600 nm
OTR	Oxygen transfer rate
OTR'	Area specific oxygen transfer rate
OUR	Oxygen uptake rate
PBS	Phosphate-buffered saline
PD-agar	Potato dextrose agar
P. pastoris	*Pichia pastoris*
P. putida	*Pseudomonas putida*
RAMOS	Respiration activity monitoring system
rpm	Revolutions per minute
RQ	Respiratory quotient
S. cerevisiae	*Saccharomyces cerevisiae*
SFM-agar	Soy flour mannitol agar
sl-RA	Substrate-limited respiratory activity
STR	Stirred tank reactor
S. coelicolor	*Streptomyces coelicolor*
T. reesei	*Trichoderma reesei*
WT	Wild type
YPD-agar	Yeast extract peptone dextrose agar

Symbols

Symbol	Description	Unit
Δi	Difference in parameter or variable i	-
μ	Growth rate	h^{-1}
μ_{max}	Maximum growth rate	h^{-1}
A	Area	cm^2
A_λ	Absorption at specific wavelength	a. u.
C	Capacitance	$pF \cdot cm^{-1}$
c_i	Concentration of substance i	$g \cdot L^{-1}$
CTR	Carbon dioxide transfer rate	$mmol \cdot L^{-1} \cdot h^{-1}$
CTR'	Area-specific carbon dioxide transfer rate	$mmol \cdot m^{-2} \cdot h^{-1}$
D	Dilution rate	h^{-1}
d_0	Shaking diameter	mm
d_c	Diameter of cuvette	cm
F_{air}	Gassing rate	$sL \cdot h^{-1}$
I	Intensity of scattered light or fluorescence	a. u.
I_{norm}	Normalized intensity	a. u.
k_S	Affinity constant regarding substrate S	$mg \cdot L^{-1}$
n	Shaking/Stirring frequency	rpm
N	Number of replicates	-
O_L	Dissolved oxygen concentration	$mmol \cdot L^{-1}$
OTR	Oxygen transfer rate	$mmol \cdot L^{-1} \cdot h^{-1}$
OTR'	Area-specific oxygen transfer rate	$mmol \cdot m^{-2} \cdot h^{-1}$
OUR	Oxygen uptake rate	$mmol \cdot L^{-1} \cdot h^{-1}$
p_{CO_2}	Carbon dioxide partial pressure	hPa
p_{O_2}	Oxygen partial pressure	hPa

Symbol	Description	Unit
q_S	Substrate uptake rate	$g \cdot g^{-1} \cdot h^{-1}$
r	Radius	cm
R	Gas constant	$J \cdot K^{-1} \cdot mol^{-1}$
RQ	Respiratory qoutient	-
S	Substrate mass	g
t	Cultivation time	h
T	Temperature	K
V_G	Gas volume	m^3
V_L	Liquid volume	L
X	Biomass	$g \cdot L^{-1}$
X_0	Spore concentration at the beginning of cultivation	$n_{spores} \cdot mL^{-1}$
$Y_{i/j}$	Yield of i on substance j	$g \cdot g^{-1}$
ε_i	Extinction coefficient of substance i	$mol \cdot L^{-1} \cdot cm^{-1}$
$\lambda_{em/ex}$	Wavelength of emission or excitation	nm

List of figures and tables

Parts of the introduction have been published previously in

Finger, M.; Sentek, F.; Hartmann, L.; Palacio-Barrera, A. M.; Schlembach, I; Rosenbaum, M. A.; Büchs, J.; *Insights into Streptomyces coelicolor A3(2) growth and pigment formation with high-throughput online monitoring*. Engineering in Life Sciences, 2022, 1-10.

[§]Finger, M.; [§]Palacio-Barrera, A. M.; Richter, P.; Schlembach, I.; Büchs, J.; Rosenbaum, M. A.; *Tunable population dynamics in a synthetic filamentous coculture.* MicrobiologyOpen, 2022, 11, e1324.

[§]Both authors contributed equally to the publication

1 Introduction

1.1 Natural product formation by the model organism *Streptomyces coelicolor*

Soil-dwelling, filamentous and gram-positive bacteria of the genus *Streptomyces* are intensively studied due to their capability to produce a wide variety of different bioactive natural products. The applications for these natural products range from antibiotics over antivirals to antitumor agents and immunosuppressants [1, 2]. The biosynthesis of these compounds is often tied to complex regulatory mechanisms [3]. Identifying and triggering such mechanisms is a challenging task. The complete genome of the model organism *Streptomyces coelicolor* A3(2) was sequenced as early as 2002, but still, several mechanisms of regulation are yet to be fully elucidated [4]. *S. coelicolor* is a model organism for the genus *Streptomyces* due to the formation of coloured antibiotics. These are the tripyrollic and red-pigmented prodigines, such as undecylprodigiosin and the polyketidic, blue-pigmented actinorhodin [5]. Even for these well-studied compounds, a complete picture of all physiological control mechanisms is missing [6, 7]. It is known that the production is often activated once growth-limiting conditions are reached and hence, tied to an early stationary phase [8]. Growth limitations can either occur due to nutrient limitations such as the carbon, phosphate or nitrogen source or environmental changes like temperature, pH or osmolality. However, the production and yields of the different natural products are affected differently by these limitations [9]. Furthermore, limitations are not always homogenous for all cells in a cultivation. Especially the morphology of filamentous organisms such as *S. coelicolor* affects limitations and, therefore, productivity. The formation of pellets due to the aggregation of hyphae and spores leads to diffusion gradients of nutrients along the pellet radius. The formation and density of pellets, as well as the pellet radius, are dependent on the occurring shear forces [10].

Natural product formation is not only triggered by stress responses or growth cessation but can be stimulated through small diffusible signalling molecules such as γ-butyrolactones [11]. *S. coelicolor* produces various γ-butyrolactones, which have been reported to hold both activating and repressing effects on gene expression for antibiotic production [12, 13]. The signalling process is called quorum sensing and enables cell-cell communication. It is essential for a coordinated initiation of the production in the bacterial population. Hence, these molecules are referenced to as bacterial hormones [14]. Interspecies cell-cell communication is also reported to elicit natural product formation in *S. coelicolor*, indicating a beneficial effect of co-cultivations for the production process [15].

1.2 Cellulolytic, filamentous co-cultivations

For the bioprospecting of compounds and natural product formation, co-cultivations offer great potential [16–18]. This is based on the paradigm that in axenic cultivations with nutrient-rich media, the natural product formation is often not or only triggered to a limited extent [19, 20]. Furthermore, the co-cultivation partners can produce specific metabolites activating natural product formation. The synthesis of several biomolecules can only be triggered by competition with another microbial strain or signalling compounds [21, 22]. Mechanisms triggering synthesis are often examined with filamentous microorganisms, such as bacteria from the genus *Streptomyces*, due to their vast biosynthetic potential [16, 17, 23–26]. Boruta et al. (2021) extensively reviewed the potential of co-cultivation approaches, including *Streptomyces sp*. [27]. The co-cultivation strategy can enable the production of novel natural products. For example, the production of desferrioxamines or the novel antibiotic alchivemycin A could be achieved with a co-cultivation approach [3, 28, 29]. Additionally, it was demonstrated before that co-cultivation can lead to enhanced natural product titers compared to axenic cultivations [30, 31].

In the natural environment of *Streptomyces* sp. and other microorganisms, nutrients are typically not very abundant. Hence, depletion of nutrients can trigger antibiotic production in order to protect the remaining nutrient pool against competing microorganisms [32]. Carbon is often present in the form of recalcitrant lignocellulosic plant material within the natural soil habitat. Therefore, cellulolytic microorganisms are essential in making this lignocellulosic material available to other microorganisms in the community [33]. Thus, fermentation of cellulosic substrates by co-cultivations of cellulolytic microorganisms combined with filamentous soil bacteria represents an interesting strategy to closely mimic the natural situation and induce natural product formation and antibiotic production in a controlled and scalable laboratory environment.

However, control and scaling of filamentous co-cultivations using insoluble cellulosic substrates imposes specific analytical challenges for the evaluation of growth and substrate uptake kinetics. As co-cultivations are highly dynamic and complex, it is difficult to explore their behaviour at sufficient temporal resolution using classical offline sampling techniques. The importance of temporal dynamics in co-cultivations was demonstrated by Bertrand et al. (2014) and Azzollini et al. (2018), who investigated the time-dependent metabolite profiles of solid fungal co-cultivations in miniaturized set-

ups [34, 35]. Thereby, demonstrating that the induction patterns of natural product formation can be very diverse. Many metabolites enhanced over time until the later stages of the co-cultivation, while others appeared only at specific times but did not remain stable until the end of cultivation. While up-scaling their co-cultivations, the authors noticed that the same metabolites could be isolated. Still, the temporal profile of the induction changed, probably caused by the change in population dynamics in the upscaled cultures [34]. Natural product profiles of co-cultivations are directly dependent on the underlying population dynamics, as demonstrated by Zhang and Zhu (2022). Their study revealed that the metabolite profiles for synthetic co-cultivations of gut bacteria could even serve as a fingerprint to track the population dynamics in co-cultivations [36].

1.3 Monitoring and controlling population dynamics in co-cultivations

Most co-cultivation studies are conducted in a rather random approach without in-depth knowledge about the population composition and dynamics. Especially for filamentous organisms growing on cellulosic material, this holds true due to the inherent complexity [16]. However, certain natural products can be produced only under specific conditions, which can be represented by the population composition (Figure 1). The growth and, therewith, the population composition of each co-cultivation partner is affected to a differing extent by the process conditions. Certain process conditions can stress a co-cultivation partner or result in low growth rates leading to a shifted population composition. Simultaneously, these conditions could trigger the production of natural products. Therefore, controlling the population composition in co-cultivation is a valuable tool for investigating product-forming conditions in a more structured manner. Managing population dynamics requires prior monitoring of the respective co-cultivation composition.

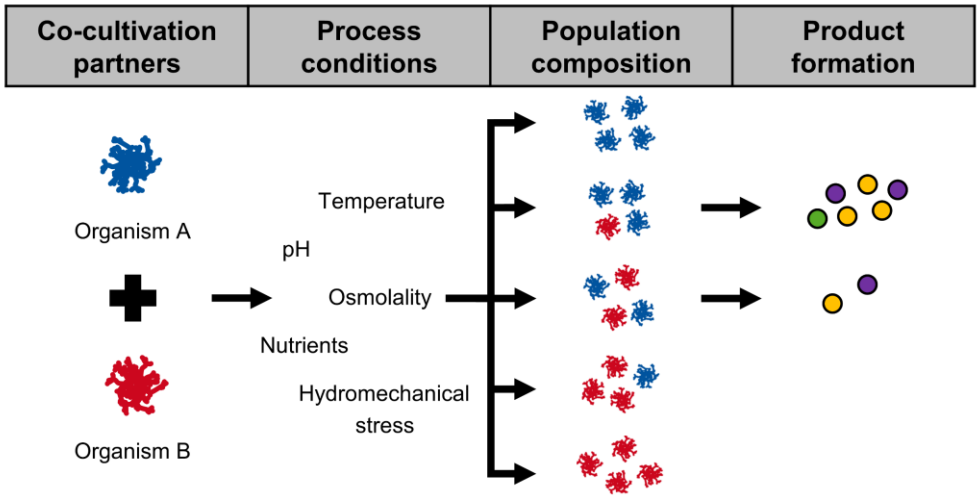

Figure 1. The population composition is dependent on the respective co-cultivation partners and the process conditions. Only under certain conditions stable co-cultivations and product formation are prevalent.

Schlembach et al. (2021) extensively reviewed and summarized measurement techniques for co-cultivation processes [37]. The foundation for all methods is to find an attribute by which one co-cultivation partner can be distinguished from another. The attribute must always be linked to the biomass of the individual co-cultivation partner. This can be attributes such as the DNA or the size of the respective organism [38]. If possible, the attribute measurements should always be conducted non-invasively and online. Thereby, the observed process is not disturbed, and a good timewise resolution can be achieved. Optical methods have a very high capability of gaining real-time data for the control of population dynamics in co-cultivations. Optical methods are mainly comprised of absorbance, scattered light and fluorescence measurements and are broadly applied in the literature [37]. For example, red and green fluorescence monitoring in recombinantly labelled *Escherichia coli* co-cultivations for biosensing of monoaromatics was described by Noonan et al. (2020) [39]. Scattered light strain-specific spectra have been evaluated as well. These different spectra have allowed assessing growth dynamics online without the need for genetic modifications [40].

The adequate monitoring of the population composition in a co-cultivation system enables the establishment of population control mechanisms. The population can be steered by changing initial parameters or parameters throughout the cultivation (Figure 1). However, this holds only valid as long as the change of the respective parameter significantly influences the growth of one co-cultivation

partner compared to the other. The most commonly used parameter to influence population dynamics is the inoculation ratio of co-cultivation partners [41–43]. However, the inoculation ratio does not influence the growth rate directly, and the initial growth rate should be independent of the inoculation ratio. Only due to changing process parameters resulting from the growth of the other co-cultivation partner, the growth rate is indirectly influenced throughout the cultivation. Therefore, the inoculation ratio is an unsuitable parameter to steer the population composition in extended processes. A more direct modulation of the growth rates can be achieved by changing parameters such as the cultivation temperature, pH, osmolality or even the hydromechanical stress [44–47]. These parameters were already used in various studies to control the microbial population compositions in co-cultivations. For example, pH oscillations have enabled the co-existence of *E. coli* and *Saccharomyces cerevisiae* in a chemostat [48]. Also, the temperature has been used for fine-tuning population compositions. Cycles of changing temperatures have been applied in an *E. coli* - *Pseudomonas putida* system. *E. coli* was favoured by a high temperature, and *P. putida* by a low temperature [49].

Although great progress has been achieved in the design of tools for efficient online monitoring and control of population composition in co-cultivations, the primary focus has been on systems with unicellular microorganisms. Monitoring of more complex organisms in co-cultivations has barely been investigated. For instance, a filamentous co-cultivation of *Trichoderma reesei* and *Aspergillus wentii* in a stirred tank reactor (STR) using microcrystalline cellulose has been studied. The online estimation of the growth of each fungal strain was not assessed. Instead, differentiation of strain contributions was made solely based on growth-associated pigments of *A. wentii* [50]. However, it is conceivable that optical process monitoring or respiration monitoring could also be applied to track population compositions for more complex co-cultivations.

1.4 Respiration as a key indicator for biological processes

Respiration data can provide a vast amount of information. Especially for aerobic cultivations, the oxygen uptake rate (OUR) and the carbon dioxide evolution rate (CER) are directly linked to the central metabolism and, therefore, are essential process parameters. The determination of oxygen transfer rate (OTR) and carbon dioxide transfer rate (CTR) is much simpler. It often yields highly similar values to the OUR and CER, as the change in dissolved oxygen or carbon dioxide is neglectable. Hence, over the last two decades, multiple devices have been developed to access respiration across different

cultivation scales. Anderlei et al. (2001 and 2004) developed the first version of the respiration activity monitoring system (RAMOS) to determine the OTR and CTR of shake flask cultivations [51, 52]. For an increased throughput, this principle was adapted by Flitsch et al. (2016) for 48-well microtiter plates (MTP) and by Dinger et al. (2022) for 96-well MTPs [53, 54].

Oxygen serves as the final electron acceptor during oxidative phosphorylation, which is the major pathway for ATP generation for most aerobic organisms [55]. The oxidation of NADH drives ATP formation. Prominent examples of NADH regeneration within some microorganisms include decarboxylation reactions. One decarboxylation reaction is the decarboxylation of pyruvate and the separation of two carboxyl groups in the form of carbon dioxide from isocitrate in the citric acid cycle. Hence, it is no surprise that most mechanisms coupled to energy metabolism can be observed by monitoring oxygen or carbon dioxide respiration. This potential was demonstrated by correlating respiration with substrate uptake, growth, product formation and other process parameters in multiple studies [56–58]. Additionally, respiration monitoring can assist in the scale-up of biological processes [59]. Nonetheless, there is still further potential to exploit the information on respiration and establish methods based on respiration to improve process development and optimization.

1.5 Objectives and overview

The presented work lays the foundation for developing and scaling defined filamentous co-cultivations for producing natural products from cellulosic substrates. A model co-cultivation system was established, and online monitoring methods were further improved and adapted to assist therewith. The co-cultivation consisted of the soil bacterium *S. coelicolor* and the cellulolytic fungus *T. reesei*, explained in detail in chapter 3.1.

Before the co-cultivation could be established, the growth patterns of the co-cultivation partners had to be studied. Previous research extensively examined *T. reesei* growth behaviour in cultivation systems at different scales [60, 61]. However, this information was missing for *S. coelicolor*. Initial experiments indicated a more complex growth and product formation behaviour of *S. coelicolor*. Hence, factors influencing *S. coelicolor* growth and product formation were investigated in detail within a high-throughput MTP system (Chapter 2). As the pigment formation by *S. coelicolor* could pose a challenge for the optical biomass monitoring of the co-cultivation partners, the influence of the pigment on green autofluorescence and scattered light measurements was tested.

With the knowledge from axenic cultivation experiments, co-cultivations could be set-up in MTPs (Chapter 3). The utilization of fluorescence-tagged strains (*T. reesei* mCherry and *S. coelicolor* mNeonGreen (mNG)), in addition to OTR measurements, was tested for the monitoring of population dynamics throughout the cultivation. Thereby, it was further examined how different parameters can be exploited to control the population composition and how this affected pigment formation. The effect of varying inoculation ratios, osmolalities and shaking rates was studied.

The carbon release was further investigated in axenic cultivations of *S. coelicolor* (Chapter 4), as conditions leading to a slow release of soluble sugars were favourable for pigment formation in co-cultivations. Cellulase cocktails of varying concentrations were added to *S. coelicolor* cultivations with cellulose as the main substrate in MTPs. Thereby, the carbon release was selectively examined in a high-throughput format for axenic cultivations. The results were validated in a STR with a low glucose feed to axenic cultivations of *S. coelicolor*. Finally, the co-cultivation process performed in the MTP (Chapter 3) was transferred into a STR.

The second part of this work was focused on establishing respiratory methods to allow for faster bioprocess development. Chapter 5 presents an alternative approach to estimate the affinity of microorganisms towards the main carbon source, as the affinity is a crucial parameter for carbon-limited co-cultivations. Spiking the carbon source of interest to carbon-limited cultivations was tested to determine the affinity by the increase of the OTR. The method was examined for three different organisms.

Furthermore, in chapter 6 and 7, a method for the respiration monitoring of agar cultivations is presented. By modifying the RAMOS for agar cultivations, the area-specific oxygen transfer rate (OTR'), the area-specific carbon dioxide transfer rate (CTR'), as well as the respiratory quotient (RQ) was assessed for several different microorganisms in non-shaken Erlenmeyer flasks. It was investigated whether the respiration data could be useful for deriving information on substrate consumption, growth and product formation of agar cultivations. The method was exemplarily demonstrated for several applications: Determination of colony forming units, antibiotic disk diffusion tests, quality control for spore production or for pre-cultures and investigating the metabolic activity in cultivations on solid media. Further improvement of the handling and measurement precision was attempted by designing an adapter for single-use Petri dishes.

Parts of the following chapter have been published previously in

Finger, M.; Sentek, F.; Hartmann, L.; Palacio-Barrera, A. M.; Schlembach, I; Rosenbaum, M. A.; Büchs, J.; *Insights into Streptomyces coelicolor A3(2) growth and pigment formation with high-throughput online monitoring*. Engineering in Life Sciences, 2022, 1-10.

Fabio Sentek and Lukas Hartmann (AVT - Biochemical Engineering, RWTH Aachen University, Aachen, Germany) assisted with the cultivation experiments presented in chapter 2.3.1, 2.3.2 and 2.3.4.

2 Insights into *Streptomyces coelicolor* growth and pigment formation

2.1 Background

The model organism for the genus *Streptomyces*, *S. coelicolor*, produces a wide variety of natural products. Amongst these are the pigmented antibiotics actinorhodin and undecylprodigiosin. However, even for these well-studied products, conditions leading to product formation are often not wholly recognized. In this chapter, the opportunity to investigate pigment formation and antibiotic production in a high-throughput online monitoring system is demonstrated. The presented methodology paves the way for the examination and validation of influencing factors on product formation. Thereby, the potential is given to increase the speed of bioprocess development significantly. Additionally, the knowledge of pigment formation helps understand and evaluate the complex co-cultivation datasets of *S. coelicolor* and *T. reesei*.

2.2 Material and methods

2.2.1 Microorganisms

S. coelicolor (DSMZ40783) was received from the Hans-Knöll-Institute culture collection (Jena, Germany). All cultivations were inoculated with 10^6 n_{Spores}·mL^{-1}. Spores were prepared similarly to Hobbs et al. (1989) [62]. A spore suspension was spread on soy-flour mannitol agar (SFM-agar) plates, which consisted of 20 g·L^{-1} mannitol, 20 g·L^{-1} soy-flour and 20 g·L^{-1} agar. After ten-day incubation at 30 °C, the spores were harvested by scraping and suspended in deionized water. Mycelium was removed by filtration with a 40 µm cut-off cell strainer (Corning, Corning, USA). Spore concentrations were adjusted in the stock solution to 10^8 n_{Spores}·mL^{-1} using a coulter counter 4 (Beckman Coulter, Brea, USA) and stored at 4 °C. The stock solution was vortexed for 30 s before inoculation of the medium.

2.2.2 Media composition

Cultivations were performed in a low nitrogen phosphate (LNP) minimal medium, similar to the medium previously adapted by Antonov et al. (2017) [63]. If not stated otherwise, this medium consisted of 30 g·L^{-1} glucose, 0.1 M 2-(N-morpholino)ethanesulfonic acid (MES), 3.0 g·L^{-1} $(NH_4)_2SO_4$, 0.5 g·L^{-1} $MgSO_4$·7 H_2O, 0.4 g·L^{-1} KH_2PO_4, 0.3 g·L^{-1} urea, 0.23 g·L^{-1} $CaCl_2$·2 H_2O, 0.05 g·L^{-1} NaCl,

0.25 (v/v) % trace element solution and 0.01 (v/v) % tween 80. The pH of the medium without trace elements was adjusted to 6.7 with 5 M NaOH. The trace element solution contains 180 $g \cdot L^{-1}$ citric acid, 16 $g \cdot L^{-1}$ $ZnSO_4 \cdot 7\ H_2O$, 2.71 $g \cdot L^{-1}$ $CoCl_2 \cdot 6\ H_2O$, 2.29 $g \cdot L^{-1}$ $Fe_2(SO_4)_3$, 2.05 $g \cdot L^{-1}$ $CuSO_4$, 1.60 $g \cdot L^{-1}$ $MnSO_4 \cdot 7\ H_2O$, 0.8 $g \cdot L^{-1}$ H_3BO_3. All stock solutions for the medium were sterile-filtered with a 0.2 µm cut-off filter (MilliporeSigma, Burlington, USA).

2.2.3 Microtiter plate cultivations and online monitoring

For cultivations in MTP, 48-round well plates (MTP-R48-B, m2p-labs GmbH, Baesweiler, Germany) were used. Unless stated otherwise, the filling volume was 1000 µL at a shaking frequency of 800 rpm with a shaking diameter of 3 mm and the temperature set to 30 °C. Well-resolved online monitoring of the OTR was achieved with an in-house built micro(µ)-scale respiration activity monitoring system (µRAMOS) [53]. In intervals of 16 min, microfluidic valves for aeration of the MTP wells were closed for 4 min. During this measurement time, the course of oxygen partial pressure was monitored in the headspace of the sealed wells. The change in oxygen partial pressure over time is approximated by a linear fit, with which the OTR can be calculated.

Autofluorescence wavelength ($\lambda_{ex}/\lambda_{em}$ 483/520 nm) measurements were performed in an in-house built BioLector device coupled to a Fluoromax-4 spectrometer (HORIBA Jobin-Yvon GmbH, Bernsheim, Germany) [64]. The slit size for fluorescence measurements was 8 nm. For the integration time, 900 ms were chosen, which accounts for 12 rotations at 800 rpm. The intensity data of every experiment series was baseline corrected through normalization I_{norm} between 0 and 1 according to equation (1). Additionally, this assisted in better comparability between experiments.

$$I_{norm} = \frac{I - \min(I)}{\max(I) - \min(I)} \quad (1)$$

2.2.4 Shake flask cultivations and online monitoring

For cultivations in shake flasks, unbaffled 250 mL flasks were used. The filling volume was 20 mL at a shaking frequency of 350 rpm with a shaking diameter of 50 mm and the temperature set to 30 °C. The RAMOS was used for online measurements of respiration activities in up to eight parallel shake flasks [51, 52]. For each sampling point, one flask was taken from the system.

2.2.5 Offline measurements

A detailed description of the measurement setup was published by Ladner et al. (2016) [65]. Scattered light intensity scans ($\lambda_{ex}/\lambda_{em}$ 300-700 nm) after cultivation were performed with an excitation step size of 10 nm by an automated monochromator MicroHR Motorized (HORIBA Jobin Yvon GmbH, Unterhaching, Germany) and an emission resolution of the charge-coupled device (CCD) detector Synapse (HORIBA Jobin Yvon GmbH, Unterhaching, Germany) of 0.44 nm. The conditions during measurement were the same as the cultivation conditions. The pH of samples, which were investigated for actinorhodin production, was increased to pH values larger than 12 by the addition of 10 (v/v) % 5 M NaOH. The pH was measured using a pH-meter HI 2211 (HANNA Instruments, Smithfield, USA).

Macroscopic pictures of culture broth samples were scanned using a photo scanner Epson perfection V700 (Epson, Tokyo, Japan). The image analysis of pictures was performed with ImageJ 1.53k [66]. For the determination of the projected pellet area and the maximum Feret diameter, the 8-bit version of the taken pictures was transformed into black and white images using the "Auto threshold" function on the region of interest. The function "Analyze particle" was applied for the same region to measure the projected pellet area and the maximum Feret diameter. Finally, the mode red value of the cultivation broth and pellets was read out with the function "Histogram". Either pellet-free regions or pellets were chosen as regions of interest until the mode red value could be determined from at least 5000 pixels.

2.3 Results and discussion

2.3.1 Correlations of online monitoring signals

For preliminary analysis of pigment formation, initial experiments with *S. coelicolor* were conducted in shake flasks. The cultivations with 30 $g \cdot L^{-1}$ of glucose in LNP medium were red-pigmented after 168 h. Daily sampling from individual shake flasks indicated a rapid change in the production of this red pigment after 96 h (data not shown). Therefore, a detailed investigation implementing spectral online monitoring using an optical system in MTPs was performed to observe whether and how pigment formation can be monitored (Figure 2).

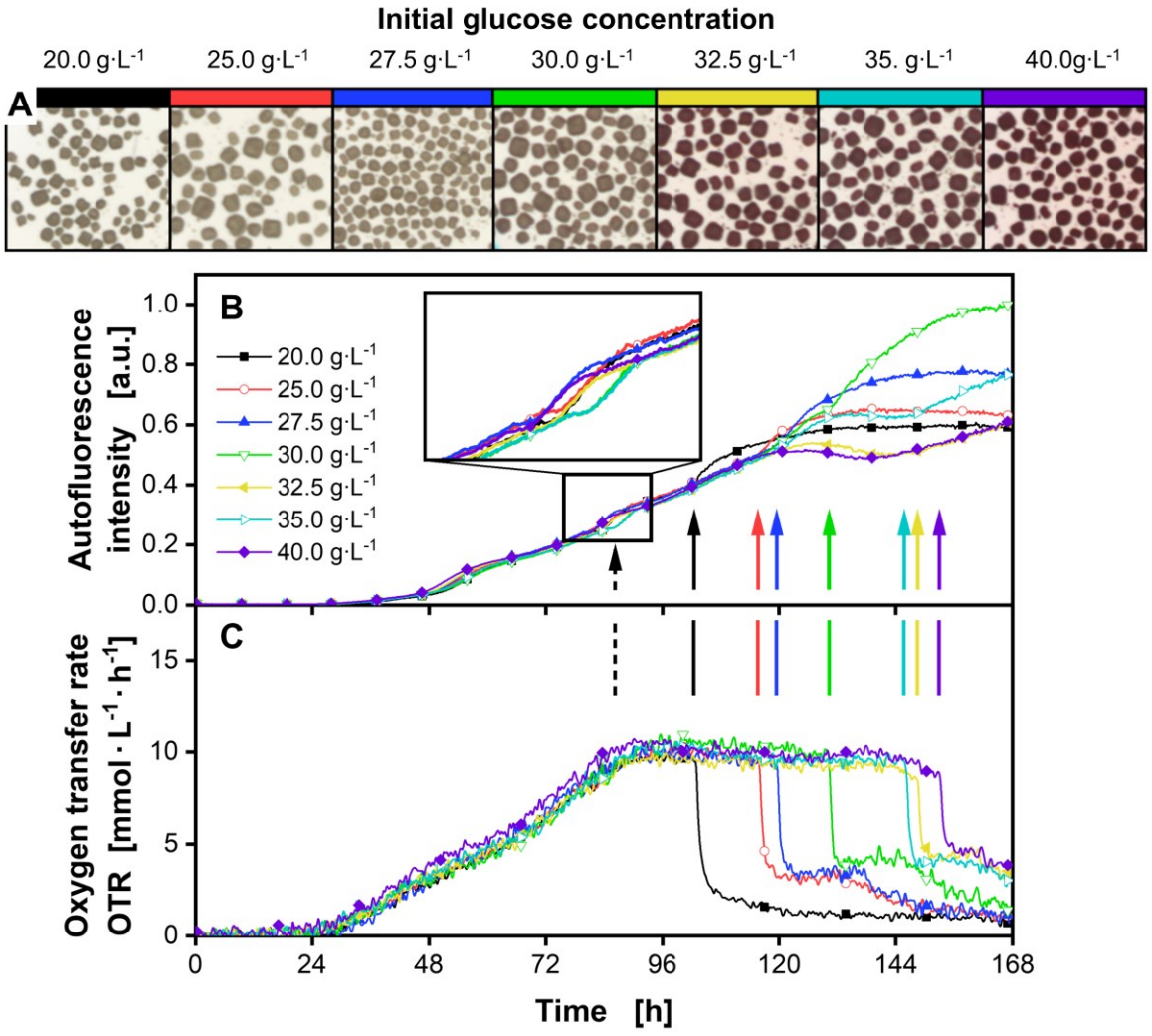

Figure 2. Cultivation of *Streptomyces coelicolor* A3(2) with varying glucose concentrations. (**A**) Macroscopic pictures of pellets after termination of the cultivation. The pellet size was in the order of 300 µm. (**B**) Normalized autofluorescence intensity signals (Excitation: 483 nm; Emission: 520 nm) with an

enlarged view of the stress signal due to phosphate limitation, marked by a dashed arrow. (**C**) Oxygen transfer rates. Solid arrows mark the glucose exhaustion. For clarity, only every 50th data point over time is indicated by the corresponding symbol in (B) and (C). Pictures shown in (A) and data presented in (B) and (C) originate from the same well for each condition, respectively. Culture conditions: 48-well round well plate, V_L = 1000 µL, n = 800 rpm, d_0 = 3 mm, T = 30 °C, $X_0 = 10^6$ spores·mL^{-1}, LNP medium with varying glucose concentrations.

The respiratory activity was tracked by measuring the OTR of each well. As emphasized in the literature, the OTR is linked to growth and can be used to determine growth characteristics as well as limitations [51, 67]. Especially, the depletion of the primary carbon source is distinguishable in most cultivations by a rapid decrease in OTR. Autofluorescence of flavins was monitored at $\lambda_{ex}/\lambda_{em}$ 483/520 nm as an indicator for biomass and as a more precise signal compared to the scattered light signal [68, 69]. The autofluorescence occurrence depends on the organism and the formed metabolites, which can also be traced back to the metabolic state [69]. The duration of glucose availability and the resulting effects on pigmentation were studied by varying glucose concentrations from 20 to 40 g·L^{-1}.

Therefore, different endpoints for the cultivation from 104 to 154 h could be realized. The macroscopic pictures (Figure 2A) displayed a transition towards pigmentation at higher glucose concentrations. First signs of pigmentation were observed for a concentration of 30 g·L^{-1} and higher. The autofluorescence indicates growth starting at 36 h (Figure 2B). However, according to the OTR, initial growth already begins at 24 h (Figure 2C), which can be explained by the higher sensitivity of this measurement technique. The OTR plateau, starting at about 86 h, appears due to a phosphate limitation resulting from the low phosphate content in the LNP medium. This could be proven by sampling and measuring the phosphate concentration as well as by spiking a phosphate solution, which elevated the OTR plateau (Appendix Figure A1). The phosphate limitation can also be seen as a stress signal within the autofluorescence signal at 86 h (Figure 2B). The energy metabolism and, therefore, the ratio of oxidized (fluorescent) to reduced (non-fluorescent) flavins are drastically changing. Similar observations were made by Surre et al. (2018). They showed that stressing agents led to changes in NAD and FAD fluorescence [70]. Once respiratory activity drastically decreased due to the depletion of glucose, an increase in autofluorescence at precisely the same point in time is observed (Figure 2B-C solid arrows). The reason for this increase was not investigated in this chapter. However, for cultivations without phosphate limitation due to phosphate spiking (Appendix Figure A1) or the use of even lower amounts

of glucose (Appendix Figure A2A), no increase after carbon source depletion was noted. The progression until glucose depletion is similar for the different glucose concentrations tested. This indicates good reproducibility and a low effect of osmolality differences resulting from different glucose concentrations. At higher glucose concentrations, the OTR plateau is prolonged, and, therefore, the increase of autofluorescence appeared later. However, all pigmented samples exhibited a different trajectory, only visible in the autofluorescence and not in the OTR. At around 130 h, the autofluorescence intensities of all pigmented cultivations started dropping until the glucose was depleted and the autofluorescence rose again. Explanations for the decrease in autofluorescence at 130 h could be either a change in the energy metabolism, as explained before, or a reduction in excitation or emission intensity resulting from light absorption by the produced red pigment. This will be further evaluated in chapter 2.3.3.

2.3.2 The influence of volumetric power input on growth kinetics and pigment production

Cultivations of *Streptomyces* are subject to inherent complexity. Due to their filamentous nature and morphology, slight differences in cultivation conditions lead to significant changes in fermentation performance and especially in product formation [71]. Therefore, literature data is often hardly comparable, and results differ in orders of magnitude. A parameter frequently not considered in small-scale cultivations is the volumetric power input. This parameter directly influences morphology, growth trajectories and, therefore, alters product formation, such as pigmentation [72]. The volumetric power input in MTP systems can mainly be influenced by shaking diameter, shaking frequency, or filling volume. Sohoni et al. (2012) as well as Koepff et al. (2017) studied how small-scale cultivations of *Streptomyces* could be made more robust and reliable [73, 74]. Besides the investigation of the inoculum, the addition of glass beads and the increase in shaking frequency were studied, respectively. Glass beads and a higher shaking frequency led to more homogenous and reproducible conditions. In this chapter, it is additionally shown that the choice of filling volume has a drastic effect on growth and pigment production (Figure 3). It is observed that with increasing filling volume, the slope of the OTR after 24 hours of cultivation is decreasing. This can be explained by the concomitant reduction in volumetric power input and its impact on pelleting behaviour (Figure 3A). The power input in 48-well plates has not yet been characterized. However, Montes-Serano et al. (2022) showed that for increasing filling volumes in 6-, 24- and 96-well plates a decrease in volumetric power input due to the change of surface-to-volume ratio can be noted [75]. The same effect holds true for 48-well plates. The volumetric power input in 48-well plates was roughly estimated with three different models (Appendix Figure A3)

for shake flasks as well as for cylindrical shaken bioreactors [76–78]. With the increase in filling volume from 1000 µL to 2000 µL, a decrease of the volumetric power input of about 25 – 37 % was calculated with all models. The change in volumetric power input affects the morphology. Fewer and bigger pellets resulted of the decrease in volumetric power. The pellet size was evaluated by the determination of the projected area (Appendix Figure A4A) and maximum Feret diameter (Appendix Figure A4B) of pellets within the macroscopic images taken after the cultivation ended (Figure 3A). Both, the projected pellet area as well as the maximum Feret diameter increase with increasing filling volumes. The median projected pellet area at the highest filling volume of 2000 µL is more than doubled with 0.19 mm^2 compared to the median at the lowest filling volume condition of 1000 µL with 0.08 mm^2. It is hypothesized that in the early growth phase, several seed pellets are formed by spore aggregation depending on the power input, which later only grow in size but not in number. Similar results of an inversely related pellet number to pellet size were also previously reported by Tough and Prosser for varying impeller speeds and, therefore, varying power input [10].

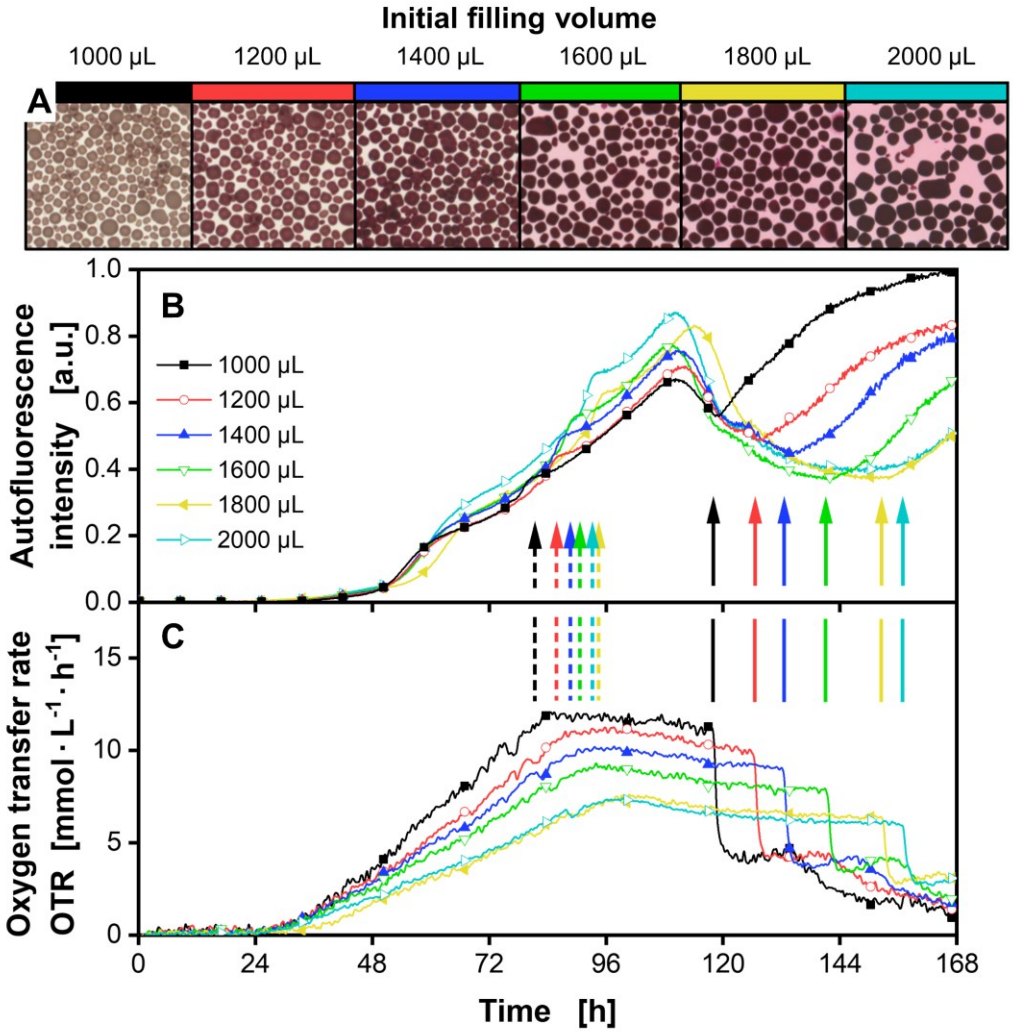

Figure 3. Cultivation of *Streptomyces coelicolor* A3(2) with varying filling volumes. (**A**) Macroscopic pictures of pellets after termination of the cultivation. The pellet size was in the order of 300 µm. (**B**) Normalized autofluorescence intensity signals (Excitation: 483 nm; Emission: 520 nm). (**C**) Oxygen transfer rates. Dashed arrows mark the stress signal due to phosphate limitation and solid arrows mark glucose exhaustion. For clarity, only every 50th data point over time is indicated by the corresponding symbol in (B) and (C). Pictures shown in (A) and data presented in (B) and (C) originate from the same well for each condition, respectively. Culture conditions: 48-well round well plate, V_L = 1000 - 2000 µL, n = 800 rpm, d_0 = 3 mm, T = 30 °C, $X_0 = 10^6$ spores·mL^{-1}, LNP medium with 30 g·L^{-1} glucose.

The linear OTR increase qualitatively indicates growth in pellet size. Thereby, the slope of the OTR increase represents the seed pellet concentration. Interestingly, the effect is more pronounced with the addition of microparticles such as talc or α-cellulose (Appendix Figure A5A). The resulting change in growth culminated in different OTR plateau heights as soon as the phosphate was depleted (Figure 3B dashed arrows). Hence, the OTR drop due to glucose depletion (Figure 3B solid arrows) for the lowest tested filling volume of 1000 µL occurred around 40 h earlier than for the highest of 2000 µL. The general autofluorescence trajectory is comparable to Figure 2. When phosphate becomes limiting, a stress signal is visible in the autofluorescence and the autofluorescence increases after glucose depletion (Appendix Figure A2B) in contrast to cultivations without phosphate limitation (Appendix Figure A2A). Furthermore, for pigmented cultivations, a drop in the autofluorescence is visible (Appendix Figure A2C). With varying filling volumes, the phosphate is depleted at different time points according to the OTR. Therefore, the stress signal in the autofluorescence is also shifted in time (Figure 3B and Appendix Figure A6 dashed arrows). The same holds true for the time point of glucose depletion. Interestingly, regardless of these nutritional effects, the start of pigment formation was highly synchronized under all conditions at around 110 h and was coincident with an apparent decrease in the autofluorescence signal. Additionally, it is observed that the autofluorescence drops further down for higher filling volumes, where pigment formation was increased. This correlation is also indicated by image analysis of the macroscopic images taken at the end of cultivation (Appendix Figure A7). The mode red value, which represents the red pigmentation level, of the cultivation broth (Appendix Figure A7A) as well as of the pellets (Appendix Figure A7B) correlates well ($R^2 = 0.91$ and $R^2 = 0.97$) with the autofluorescence value at the local minimum after the drop. A correlation with the autofluorescence at the end of cultivation (t = 168 h) is also given (Appendix Figure A7). However, as the autofluorescence was still rising for the higher filling volume conditions at this time, the coefficient of determination was lower ($R^2 = 0.80$ and $R^2 = 0.89$). The increased pigmentation with an increase in filling volume can be explained by the extended time of glucose availability, which prolonged the pigment production phase. In conclusion, it can be stated that a higher filling volume and, therewith, volumetric power input, directly leads to higher pigmentation levels (Figure 3A). The reason and factors affecting the synchronized pigmentation onset have yet to be determined but will be further discussed in chapter 2.3.4.

2.3.3 Light absorption effects caused by pigment formation

A requirement of optical online measurements is that there should be little to no interference of the monitored variable or compound with others. Kunze et al. (2014) showed this is not the case for many observed systems. For instance, an interference of mCherry fluorescent protein on the scattered light signal could be noted [79]. Therefore, to test whether the impact of pigmentation on autofluorescence is the result of a metabolic change or light absorption effects, pigmentation was investigated by spectrally resolved scattered light measurements at the end of the cultivation displayed in Figure 3. The scattered light spectra from 300 – 700 nm show a dip in the signal forming near the maximum absorption wavelength for undecylprodigiosin at 535 nm (Figure 4B) [80]. This decreased intensity around the absorption maximum is systematically increasing with stronger pigmentation.

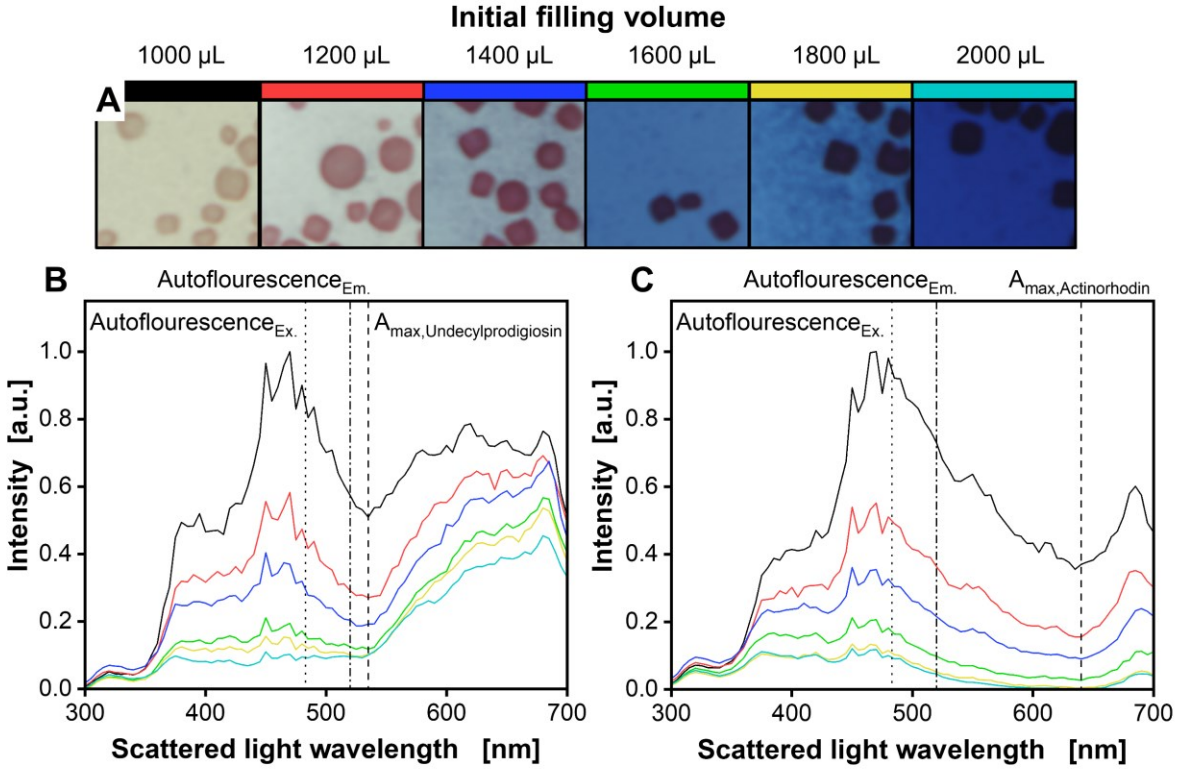

Figure 4. Pigmentation and resulting scattered light absorption of *Streptomyces coelicolor* A3(2) cultures with varying filling volumes. (**A**) Macroscopic pictures of pellets after pH was increased above pH 12. The pellet size was in the order of 300 µm. (**B**) Normalized scattered light intensity signals without pH adjustments. (**C**) Normalized scattered light intensity signals after pH was increased above pH 12. Dotted lines represent the excitation wavelength and dash-dotted lines the emission wavelength for all autofluorescence measurements. Dashed lines indicate the maximum absorption wavelength of

undecylprodigiosin and actinorhodin, respectively [80, 81]. Culture conditions: 48-well round well plate, V_L = 1000 - 2000 µL, n = 800 rpm, d_0 = 3 mm, T = 30 °C, $X_0 = 10^6$ spores·mL^{-1}, LNP medium with 30 g·L^{-1} glucose.

The difference in the trajectory of the scattered light spectra becomes even more evident in comparison with entirely unpigmented biomass (Appendix Figure A8). Since the autofluorescence is measured at an excitation wavelength of 483 nm (Figure 4B dotted line) and an emission wavelength of 520 nm (Figure 4B dash-dotted line), the influence of pigmentation on autofluorescence can be deduced from the decreased scattered light intensity at this wavelength. Therefore, the decrease in autofluorescence noted in Figure 2B and 3B is clearly correlated to the light-absorbing effects resulting from increasing pigmentation levels. Besides undecylprodigiosin, *S. coelicolor* also produces actinorhodin. However, this compound only turns to its characteristic blue colour at alkaline conditions [81]. Hence, the pH of the samples taken after cultivation was increased to a pH > 12 by the addition of 10 (v/v) % 5 M NaOH solution. In the macroscopic pictures (Figure 4A), an increase in blue pigmentation with an increase in filling volumes and, consequently, a similar production pattern as for undecylprodigiosin can be perceived. Measurements of the scattered light spectra of these samples revealed a local minimum due to absorption at around 640 nm, which corresponds to the reported maximum absorption wavelength of actinorhodin (Figure 4C) [81].

2.3.4 Investigation of pigmentation onset

For future investigations and optimization of space-time yields of secondary metabolite production, it is crucial to understand how and when production is triggered. Here, signalling molecules play a pivotal role. The addition of purified γ-butyrolactones to *S. coelicolor* was shown to trigger the precocious production of actinorhodin and undecylprodigiosin [82]. The different γ-butyrolactone derivatives are majorly produced under limiting conditions, such as in the early stationary phase. The presented online monitoring approach would be beneficial to investigate precocious pigment production and could assist in other studies regarding the control mechanisms [83]. The onset time and intensities of the pigment formation could be accurately determined. As a proof of concept, it was tested whether the addition of supernatant from previous cultivations could manipulate the synchronized pigmentation onset observed in chapter 2.3.2. Therefore, shake flask cultivations were performed and stopped before as well as after pigmentation occurred (Appendix Figure A9). The supernatants of these cultivations were sterile

filtered and different amounts (1, 5, 10 (v/v) %) were added to new cultivations (Figure 5 and Appendix Figure A10). For reference, 10 (v/v) % deionized water was also added. Since γ-butyrolactone concentrations should only be increased in the pigmented supernatants, an earlier pigmentation onset should be observable for these additions. Following the previous findings, the onset of pigmentation is assessed by the declining autofluorescence. The pigmentation for the reference started at approximately the same cultivation time as the preceding results at 115.8 ± 6.0 h (Figure 5 and Appendix Figure A10 solid black arrow). The addition of increasing amounts of unpigmented supernatant (Figure 5) did not influence the pigmentation onset, accordingly. In contrast, the cultures supplemented with pigmented supernatant showed a shortened time until the onset of pigmentation, which is notable in the unedited data in Appendix Figure A10. The addition of the highest amount of pigmented supernatant with 10 (v/v) % led to a 27.3 ± 6.6 h precocious pigmentation, compared to the reference. Depending on the type and added amount of supernatant, the autofluorescence increased differently after glucose depletion. Although the autofluorescence increase was not quantitatively investigated in this chapter, the results indicate a link to the occurring phosphate limitation (Appendix Figure A1 and Appendix Figure A2). Hence, varying amounts of phosphate and metabolites added with the supernatant could explain this pattern. For precocious pigmentation, Takano et al. (2000) discovered a similar result in agar plate tests [82]. Only the addition of transition and stationary phase culture supernatants elicited pigment production in a confluent *S. coelicolor* lawn on agar plates.

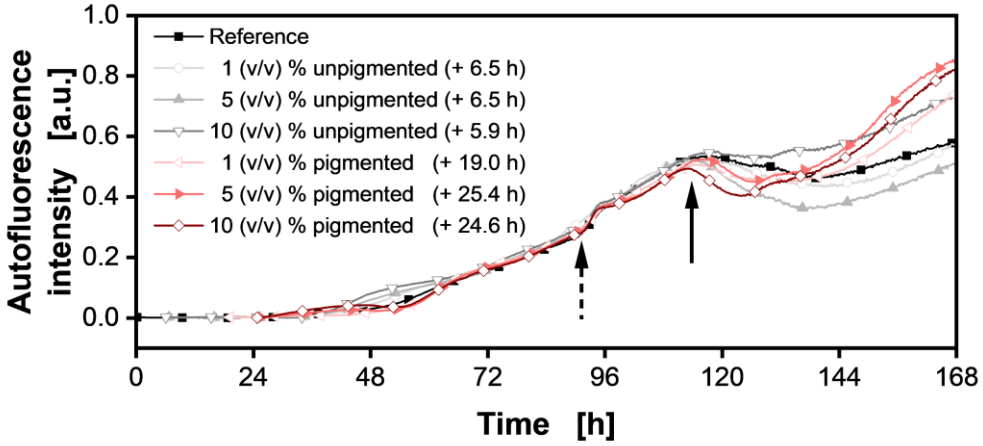

Figure 5. Cultivation of *Streptomyces coelicolor* A3(2) supplemented with different amounts of supernatants from unpigmented (grey scale) and pigmented (red scale) cultures. Normalized autofluorescence intensity signals (Excitation: 483 nm; Emission: 520 nm). Data was shifted according to the occurrence of the stress signal to the reference. For the unedited graph compare Appendix Figure A10.

The dashed arrow marks the stress signal due to phosphate limitation and the solid arrow marks the pigmentation onset. For clarity, only every 50th data point over time is indicated by the corresponding symbol. Data are mean values and originate from technical triplicates for each condition, respectively. Culture conditions: 48-well round well plate, V_L = 1000 µL, n = 800 rpm, d_0 = 3 mm, T = 30 °C, $X_0 = 10^6$ spores·mL^{-1}, LNP medium with 30 g·L^{-1} glucose.

By testing spent culture supernatant from different media as well as agar types, they also concluded that nutrient availability had a subordinate role compared to the signalling effect of γ-butyrolactones. However, in the here presented results, the earlier pigmentation goes along with faster growth. This might be due to the presence of metabolites and building blocks within the added supernatants, which boosted the initial growth of new cultures. The stress signal due to phosphate limitation (Figure 5 and Appendix Figure A10) is reached earlier, similarly to the pigmentation onset. Therefore, the difference between these time points remains similar for all conditions. This could be visualized by shifting the data of each condition to align with the stress signal (Figure 5). Aligning the stress signal also resulted in an alignment of the pigmentation onset of each condition. Hence, these findings are not an indication of quorum sensing activities but of a pigmentation onset, which is growth-dependent. These results showcase the importance of online monitoring since these patterns of growth and pigment formation would have been missed by sampling or endpoint determination. The next step would be the addition and testing of purified γ-butyrolactones to fully elucidate the influence on growth and pigmentation behaviour by employing the presented online monitoring system.

2.4 Conclusion

This chapter presented small-scale online monitoring as a tool to investigate the growth and pigment production of complex microbial systems such as *S. coelicolor*. It was demonstrated that the OTR and the autofluorescence signals provide a multitude of information. The autofluorescence, used as a proxy for biomass, also indicates phosphate and glucose depletion as well as pigmentation onset and intensity. It was proven by spectral scattered light measurements that pigment formation led to a clear signal decrease at the respective absorption maximum of the pigments. This allowed for precisely timing the onset of pigment formation and estimating pigment quantity non-invasively, either by scattered light or autofluorescence measurements. Under the tested conditions, a rapid change in autofluorescence comparing unpigmented to pigmented cultivations was observed during cultivations. It could be clearly

shown that the rapid change resulted from the pigmentation starting at a fixed time after the phosphate limitation. The pigmentation intensity depended mainly on the time frame of carbon availability after the onset of pigmentation. This was additionally substantiated by the investigation of different filling volumes. The filling volume affected the specific power input and, therewith, morphological development. The resulting different carbon consumption rates led to differing times of carbon availability and, therefore, differing pigmentation intensities. A potential quorum sensing was also investigated by the addition of supernatant from previous cultivations. Although precocious pigment formation was observed up to 27.3 ± 6.6 h earlier, compared to the reference, it could be demonstrated that this was mainly caused by a faster initial growth rather than quorum sensing effects. The cultivation time after phosphate limitation remained the key factor controlling pigmentation onset. In conclusion, the combination of respiratory and spectral online monitoring in high throughput experiments enabled the investigation of these effects and interactions, which would otherwise have been missed. As a promising next step, the addition of purified γ-butyrolactones should be studied with this system.

Parts of the following chapter have been published previously in

[§]Finger, M.; [§]Palacio-Barrera, A. M.; Richter, P.; Schlembach, I.; Büchs, J.; Rosenbaum, M. A.; *Tunable population dynamics in a synthetic filamentous coculture*. MicrobiologyOpen, 2022, 11, e1324.

[§]Both authors contributed equally to the publication

Ana M. Palacio-Barrera (Leibniz Institute for Natural Product Research and Infection Biology, Hans-Knöll-Institute, Jena, Germany) performed parts of the cultivations and the evaluation of the experiments presented in chapter 3.3.2 and 3.3.4. Paul Richter (AVT - Biochemical Engineering, RWTH Aachen University, Aachen, Germany) conducted the co-cultivation experiments with varying osmolalities presented in chapter 3.3.3.

3 Tuning population dynamics of the filamentous co-cultivation process

3.1 Background

Microbial co-cultivations are used as a tool to stimulate natural product biosynthesis. However, studies often empirically combine different organisms without a deeper understanding of the population dynamics. Hence, this chapter highlights how high-throughput online monitoring allows for handling the arising complexity of these systems. Thereby, control strategies for tuning population dynamics were established to find conditions which favour the formation of specialized metabolites. This is showcased for a model co-cultivation system composed of the fungi *T. reesei* and *S. coelicolor* (Figure 6).

The visible pigments produced by *S. coelicolor* serve as easily observable target products to follow the kinetics of natural compound formation. By growing this co-cultivation on a mineral medium containing α-cellulose as the primary carbon source, a dependency of *S. coelicolor* on *T. reesei* is imposed, as *S. coelicolor* is unable to consume cellulose. A small amount of glucose with 5 $g \cdot L^{-1}$ is included in the medium to act as a common booster for the initial growth of both organisms. After initial non-limited growth, further growth on cellulose is only possible with a successful expression of cellulase enzymes by *T. reesei*. This results in a fed-batch process with carbon-limited conditions throughout the fermentation, which is known to stimulate antibiotic production [84]. Similar interactions occur in nature and are reported to lead to specialized metabolite formation, e.g. antibiotics and pigments, by *S. coelicolor* [85, 86].

In this complex system, the initial population dynamics during non-limited growth on glucose will affect the nutrient partition for cellulase formation and, thus, strongly affect the subsequent population dynamics and natural product formation during growth on cellulose. It is, therefore, of great interest to learn 1) how population dynamics affect natural product formation and 2) how population dynamics can be tuned to maximize natural product formation.

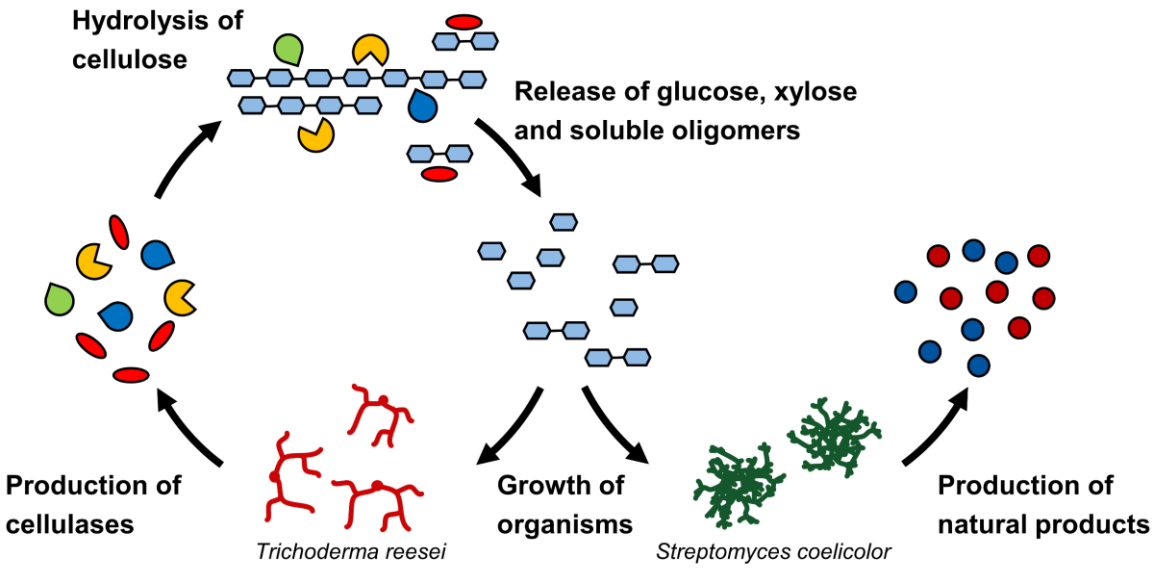

Figure 6. Concept of a bacterial-fungal dependency in a model co-cultivation consisting of the cellulolytic fungus *Trichoderma reesei* and the non-cellulolytic bacterium *Streptomyces coelicolor* for the production of natural products from renewable cellulosic material.

High-throughput online monitoring of OTR and fluorescence are combined to investigate how biotic and abiotic factors influence the population dynamics and production profiles of the model co-cultivation. The OTR monitoring has been proven a reliable method for evaluating cellulase formation and cellulose consumption in axenic cultures, as well as defined co-cultivations [63, 87, 88]. Although the OTR only delivers a sum-signal of the co-cultivation respiration activity, the metabolic contribution of each partner can be estimated by comparison to axenic cultures. Further, a fluorescence-based procedure was developed for online monitoring of population dynamics in filamentous co-cultivations [89]. Additionally, previously it was shown that fluorescence monitoring could help estimate the onset of pigment biosynthesis for *S. coelicolor* (Chapter 2) [90].

Deploying these methods, the influence of inoculation ratio, osmolality and shaking frequency on the co-cultivation dynamics was studied. Different population ratios are found in natural environments and greatly impact metabolic capabilities [41]. Hence, different inoculation ratios were investigated at first, to understand which growth kinetics and initial population ratios lead to beneficial interaction between the microorganisms. Then it was analyzed how the population dynamics can be tuned using different

osmolalities and shaking frequencies. Osmolality can alter the growth kinetics and productivity of filamentous organisms [91, 92]. Furthermore, shaking frequency and, thereby, power input is a crucial parameter for filamentous microorganisms, as was demonstrated in chapter 2 for *S. coelicolor*. The power input can affect the growth and morphology of shear-sensitive filamentous microbes, as well as oxygen availability and physical contact in co-cultivations.

3.2 Material and methods

3.2.1 Microorganisms

Three different organisms were used in this chapter. *T. reesei* mCherry as well as *S. coelicolor* (DSMZ 40783) and *S. coelicolor* mNG. The construction of tagged strains was previously reported [89]. Unless stated otherwise, cultivations were inoculated with 10^6 n_{Spores}·mL^{-1}. *S. coelicolor* spores were prepared similarly to Hobbs et al. (1989) and as mentioned in previous works [62, 89, 90]. The procedure is described in chapter 2.2.1. Deionized water or phosphate-buffered saline was used as storage solution for spores. The spores of *T. reesei* mCherry were produced by cultivation in shake flasks with LNP medium with 30 g·L^{-1} α-cellulose. After seven days, spore formation was indicated by a green colouration. The mycelium of all spore solutions was removed by filtration with a 40 µm cut-off cell strainer (Corning, Corning, USA). Spore concentrations were adjusted in the stock solutions to 10^8 n_{Spores}·mL^{-1} using a coulter counter 4 (Beckman Coulter, Brea, USA). *S. coelicolor* spore solutions were stored at 4 °C and -80 °C with the addition of glycerol. *T. reesei* mCherry spore solutions were stored at -80 °C. The stock solutions were vortexed for 30 s before inoculation of the medium.

3.2.2 Media composition

The medium for all cultivations was LNP medium with 5 g·L^{-1} glucose and 30 g·L^{-1} α-cellulose, as described in chapter 2.2.2.

3.2.3 Cultivations in microtiter plates

Cultivations were performed as described in chapter 2.2.3, if not stated otherwise. The different factors for the control of the co-cultivation composition were evaluated in the following manner: For inoculation ratio, the spore concentrations of the strains were varied, ranging from one to four orders

of magnitude below the base spore concentration with $1 = 10^6\ n_{Spores} \cdot mL^{-1}$. Sodium chloride was added with 150 mM, 300 mM and 600 mM to the media for the osmolality experiments. The inoculation ratio was set as 1:1. For shaking frequency, parallel co-cultivations were performed at a shaking frequency of 800 rpm or 1200 rpm. In these last experiments, inoculation ratios were kept within the same order of magnitude.

The µRAMOS, in combination with an in-house built BioLector system [53, 65], was used for OTR determination and mCherry fluorescence (Excitation: 587 nm; Emission: 610 nm) as well as green fluorescence (Excitation: 483 nm; Emission: 520 nm) measurements. The slit size was 8 nm, and the integration time was 900 ms.

Additionally, a commercial BioLector I (Beckman Coulter, Brea, USA) was used. Filter modules were used for the monitoring of the mCherry signal (Excitation: 580 nm; Emission; 610 nm) and green fluorescence signal (Excitation: 480 nm; Emission: 520 nm) [93]. The fluorescence measurements were performed with a gain of 100.

3.2.4 Offline measurements

Macroscopic pictures of the culture broth were taken after the cultivations were ended with an Epson perfection V700 photo scanner (Epson, Tokyo, Japan), or with an EOS 700D photo camera (Canon, Tokyo, Japan). The pH measurements were performed either with a pH-meter HI 2211 (HANNA Instruments, Smithfield, USA) or MA 235 pH/Ion Analyzer (Mettler Toledo, Columbus, USA). Extracellular protein quantification was conducted according to the Bradford method, using Bovine Serum Albumin (BSA) as standard [94].

3.3 Results and discussion

3.3.1 Characterization of the axenic culture behaviour of the co-cultivation partners

As a first step, the growth profiles of the axenic cultures of the partner organisms *T. reesei* mCherry and *S. coelicolor* are described. The *T. reesei* mCherry strain expresses mCherry fluorescent protein under the control of a synthetic constitutive promoter. This allows precise online monitoring of *T. reesei* mCherry biomass in the co-cultivation. The robust correlation of the fluorescence signal to biomass was demonstrated previously [89]. The experiment (Figure 7) was undertaken in an in-house built µRAMOS combined with an in-house built BioLector system [53, 65]. For a better understanding of interactions in the co-cultivation, especially in regards to cellulose hydrolysis, a chemically defined medium with 5 $g \cdot L^{-1}$ of glucose and 30 $g \cdot L^{-1}$ of α-cellulose as carbon source was used.

The macroscopic pictures (Figure 7A), taken of the broth at the end of cultivation, indicate a red hue for the axenic *T. reesei* mCherry cultivation (Figure 7A, black boxes). The broth of axenic *S. coelicolor* cultivations (Figure 7A, turquoise boxes) presents a white to grey hue. The colouring of the *S. coelicolor* cultivation can be attributed to unconsumed cellulose. Here, only small pellets of the *Streptomyces* strain can be seen, resulting from the sole consumption of the initially provided glucose. In contrast, *T. reesei* mCherry can produce and secrete cellulases to consume the cellulose in addition to the glucose. Furthermore, *T. reesei* mCherry grows in dispersed form and expresses the red-coloured mCherry fluorescent protein.

The online monitoring signals underline these observations. The metabolic activity, represented by the OTR (Figure 7B), indicates the growth of the axenic culture of *S. coelicolor* (turquoise line, hexagons) until 62 h. After this time, the signal sharply drops because of the complete consumption of soluble carbon sources. The actinomycete *S. coelicolor* has at least eight genes encoding cellulases, which thus theoretically allow growth on cellulose [4]. However, Lim et al. (2016) suggest that due to tight expression regulation, no cellulase production and, therefore, no growth can be seen for *S. coelicolor* in a minimal medium with cellulose [95]. Hence, this first OTR peak (turquoise line, hexagons) corresponds solely to the consumption of the initially provided glucose in the medium. In contrast, for *T. reesei* mCherry (black line, squares), after the first peak is reached at 40 h, there is a transition to cellulose consumption. This can be concluded from the OTR integral of approximately 0.92 $mol \cdot L^{-1}$,

which clearly exceeds the theoretical value achieved by the complete combustion of the initial glucose with 0.17 mol·L^{-1}. As no carbon source other than glucose and cellulose is present in the medium, the second oxygen consumption peak must be caused by cellulose consumption.

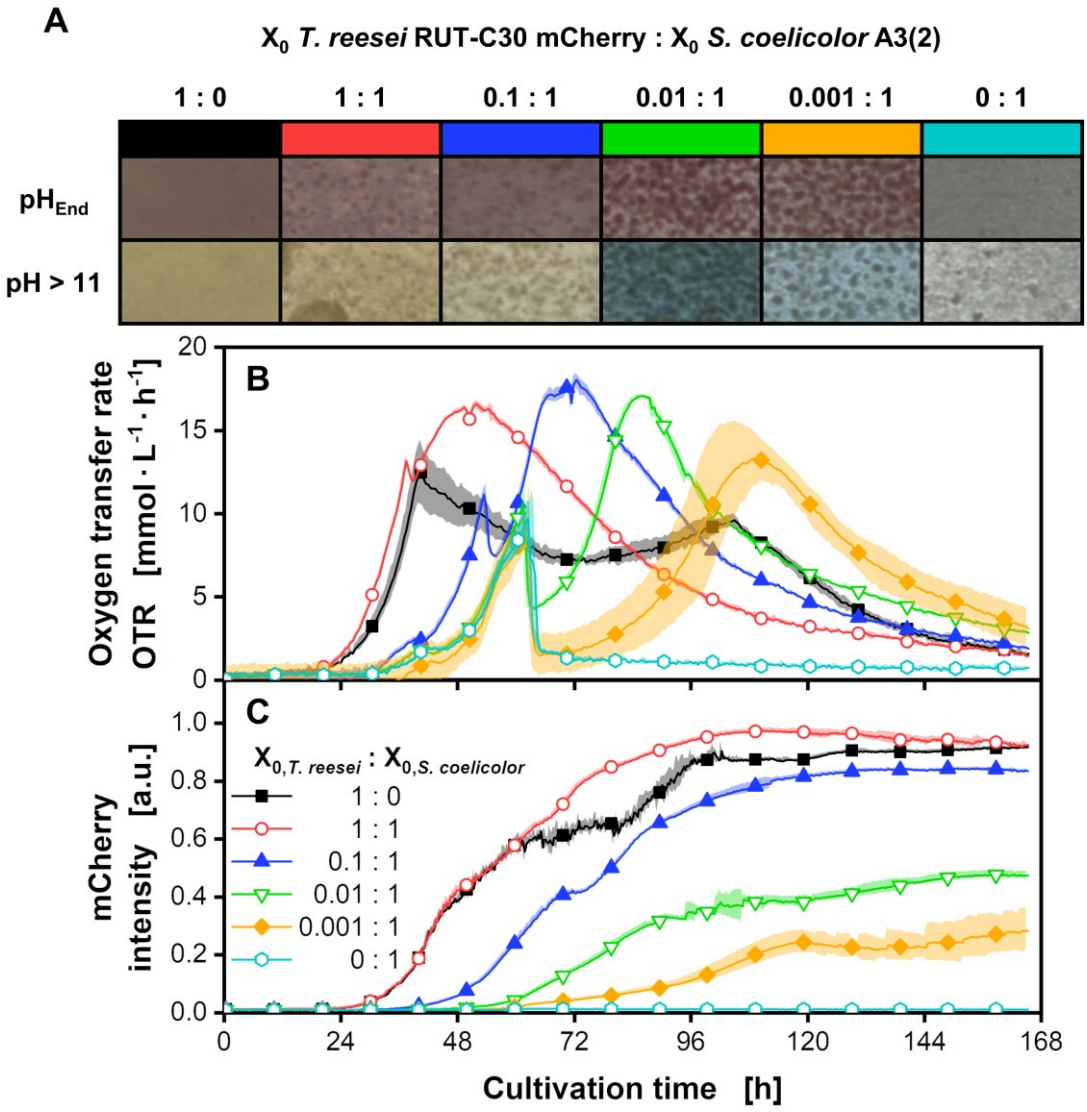

Figure 7. Co-cultivations of *Trichoderma reesei* RUT-C30 mCherry and *Streptomyces coelicolor* A3(2). Inoculation ratios were varied, as given, relating to the standard inoculation size of $X_0 = 10^6$ spores·mL^{-1}. The spore stock of *S. coelicolor* was prepared with deionized water. (**A**) Macroscopic pictures of the culture broth after termination of the cultivation. The pH was changed to a value above 11 to determine production of the blue pigment actinorhodin (second row in (A)). (**B**) Oxygen transfer rates. (**C**) mCherry intensity signals (Excitation: 587 nm; Emission: 610 nm).

For clarity, only a representative amount of data points is indicated by the corresponding symbols in (B) and (C). Culture conditions: 48-well round well plate, N = 3, V_L = 1000 µL, n = 800 rpm, d_0 = 3 mm, T = 30 °C, LNP medium with 5 g·L^{-1} glucose and 30 g·L^{-1} α-cellulose.

3.3.2 Controlling co-cultivation composition with a variation of the inoculation ratio

With the information on axenic cultivations, the influence of different inoculation ratios on OTR profiles and *T. reesei* mCherry growth was examined in co-cultivations. Because the axenic *T. reesei* mCherry culture grew faster than the axenic *S. coelicolor* culture, the inoculation density of the faster-growing fungus was lowered in comparison to *S. coelicolor* to achieve varying co-cultivation compositions. With a highly reduced inoculation ratio for *T. reesei* mCherry of 0.01:1 (green line, inverted triangles) and 0.001:1 (yellow line, diamonds), it can be observed that the initial OTR peaks resemble the OTR peak of the axenic *S. coelicolor* cultivation. However, later, there was an additional increase in the OTR compared to the axenic culture of *S. coelicolor*. These cultures also exceed the OTR integral of 0.17 mol·L^{-1} for the combustion of the initial glucose, as mentioned in chapter 3.3.1. This implies that *T. reesei* mCherry successfully produced cellulases for cellulose hydrolysis and the release of additional free sugars in these co-cultivations. For these conditions, the presence of the pigment actinorhodin was detected, based on a hue change to blue in the final culture broth after the pH was increased to basic values (Figure 7A, green and yellow boxes) [81]. Therefore, it can be suggested that the co-cultivation composition favouring *S. coelicolor* in combination with the slow release of soluble sugars (glucose, cellobiose, xylose) could trigger pigment biosynthesis in comparison to the other conditions (Figure 7A) [9].

According to the mCherry intensity signal (Figure 7C), *T. reesei* mCherry biomass formation occurred in all conditions except for the axenic *S. coelicolor* culture (turquoise line, hexagons). However, due to nutrient competition between *T. reesei* mCherry and *S. coelicolor*, different final biomass and, thus, mCherry fluorescence values were reached, depending on the inoculation ratio. The 1:1 and 0.1:1 co-cultivations reached similar biomass levels of *T. reesei* mCherry as the axenic *T. reesei* mCherry culture. The slightly lower mCherry signal in the axenic *T. reesei* mCherry cultivation (black line, squares) compared to the 1:1 condition (red line, circles) can be explained by enhanced growth on the MTP wall. This also leads to a slight scattering in the mCherry signal after 60 h due to biomass resuspension. In contrast, the 0.01:1 and 0.001:1 cultures show strongly decreased final biomass of *T. reesei* mCherry.

Therefore, even though the growth of *S. coelicolor*, indicated by pellet formation in macroscopic pictures (Figure 7A), took place in all co-cultivations, more nutrient uptake and biomass formation of *S. coelicolor* were achieved for the 0.01:1 and 0.001:1 conditions. It can be concluded that a substantial advantage has to be given to *S. coelicolor* utilizing inoculation density to compete with the faster-growing *T. reesei* mCherry successfully and to induce pigment production in these co-cultivations.

To validate the conclusions, similar co-cultivations were conducted with a *S. coelicolor* strain tagged with a mNG fluorescent protein, as reported by Palacio-Barrera et al. (2022) [89]. The work of Palacio-Barrera et al. (2022) demonstrates a good correlation of the mNG fluorescence intensity to the dry biomass of *S. coelicolor* and hence, enables more direct monitoring of individual population dynamics of both organisms. In contrast to the previous co-cultivation experiment, *T. reesei* mCherry grew slower than *S. coelicolor* mNG. This can be recognized by comparison of the respective mCherry and green fluorescence signals (Figure 8B and 8C) of the axenic cultures. The signals (*T. reesei* mCherry - magenta line, squares and *S. coelicolor* mNG - maroon line, cross marks) indicate the onset of the exponential growth phase for *S. coelicolor* mNG occurred earlier. The shorter lag phase is also reflected in co-cultivations ranging from 0.0001:1 to 0.1:1 (Figure 8B and 8C, red to yellow lines). The faster growth of *S. coelicolor* mNG is caused by a change in the spore storage solution from water to phosphate-buffered saline (PBS). The spore viability in the PBS buffered spore stocks is higher and therefore, the OTR increases faster. It was also confirmed that the *S. coelicolor* mNG strain behaves identically to the untagged *S. coelicolor* strain when both are stored in PBS (Appendix Figure A11). The faster growth of *S. coelicolor* mNG led to a strong suppression of *T. reesei* mCherry growth due to nutrient competition for the initially available glucose. Hence, lower *T. reesei* mCherry biomass, as indicated by mCherry signals, and subsequently less cellulases were produced in co-cultivations with inoculation ratios ranging from 0.0001:1 to 1:0.01. This also becomes evident by comparing extracellular protein content in co-cultivations (Figure 8D). However, at inoculation ratios of 1:0.001 and 1:0.0001 (blue and purple bar), similar extracellular protein levels were reached as in axenic *T. reesei* mCherry cultures. This indicates efficient cellulase production in these co-cultivations. For the conditions with 1:0.001 and 1:0.0001, *T. reesei* mCherry was able to access the nutrients before *S. coelicolor* mNG and thereby, the initial growth of *S. coelicolor* mNG was suppressed. The latter becomes evident by the low green fluorescence in the early growth phase of these cultures (Figure 8C, blue line, triangles and purple line, circles). Hence, an interesting switch from competition in the early stage to commensalism in the later stage of cultivation can be noticed. Because of the cellulases

supplied by *T. reesei* mCherry, *S. coelicolor* mNG could access hydrolysate sugars from the cellulose. Thereby, even higher green fluorescence and, hence, biomass levels than in the axenic cultures of *S. coelicolor* mNG were reached. This was also reflected in the stimulation of pigment production (Figure 8A).

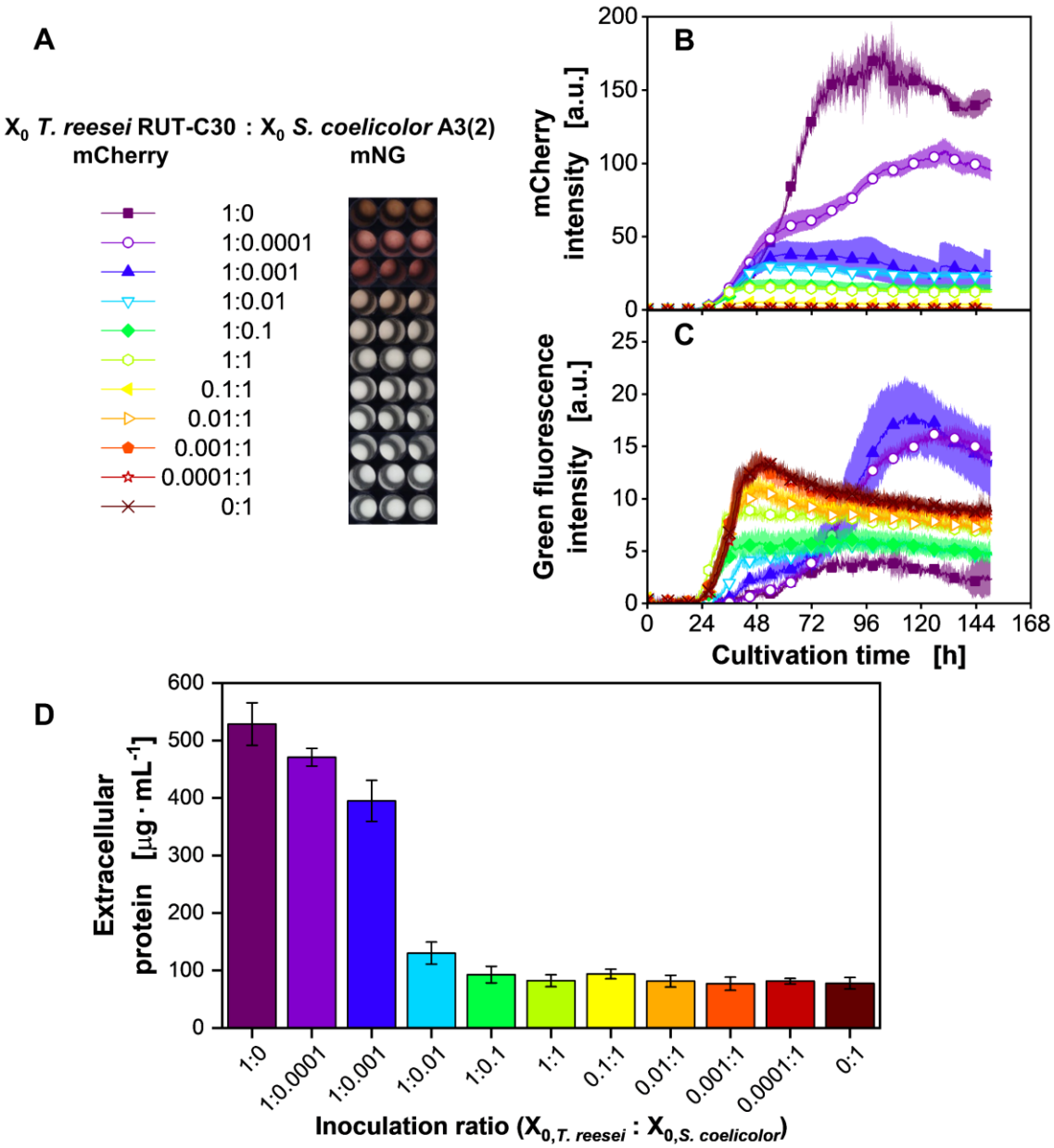

Figure 8. Co-cultivations of *Trichoderma reesei* RUT-C30 mCherry and *Streptomyces coelicolor* A3(2) mNG. Inoculation ratios were varied, as given, relating to the standard inoculation size of $X_0 = 10^6$ spores·mL^{-1}. The spore stock of *S. coelicolor* mNG was prepared with phosphate-buffered saline. (**A**) Macroscopic pictures of the culture broth after termination of the cultivation. (**B**) mCherry

intensity signals (Excitation: 580 nm; Emission: 610 nm). (**C**) Green fluorescence intensity signals (Excitation: 480 nm; Emission: 520 nm). (D) Extracellular protein concentration at the end of cultivation. For clarity, only a representative amount of data points is indicated by the corresponding symbols in (B) and (C). Culture conditions: 48-well round well plate, N = 3, V_L = 1000 µL, n = 800 rpm, d_0 = 3 mm, T = 30 °C, LNP medium with 5 g·L^{-1} glucose and 30 g·L^{-1} α-cellulose.

It can be observed that the *T. reesei* mCherry axenic cultivation displays a low-intensity green fluorescence signal (Figure 8C, magenta line, squares). The recorded green fluorescence is a mixed signal, which partly corresponds to biogenic fluorophores that are found in both partners and, secondly, to the mNG green fluorescent protein that is expressed in *S. coelicolor* mNG. Both signals have emissions in the green wavelength region (520 nm). Yet, the mNG labelling strongly enhances the signal and confers a bias towards *S. coelicolor* mNG biomass. Therefore, there is a remarkable difference in the signal from the axenic *T. reesei* mCherry cultivation, compared to the axenic cultivation with *S. coelicolor* mNG (maroon line, cross marks). Thus, despite the effect of autofluorescence, the biomass of the *S. coelicolor* mNG strain in co-cultivations can already be evaluated from the uncorrected green fluorescence signal.

To confirm this interpretation, the autofluorescence bias of the green fluorescence signal was exemplarily separated from the mNG fluorescence through signal unmixing, as proposed by Palacio-Barrera et al. (2022) (Appendix Figure A12) [89]. Thereby, the green fluorescence that arises from naturally occurring fluorophores was uncoupled from the overall green fluorescence signal. In this manner, a signal exclusively attributed to the mNG fluorescent protein was obtained. Trajectories of the green fluorescence mNG signal (Figure 8C) look very similar to the unmixed signal (Appendix Figure A12B) for all cultures with the presence of *S. coelicolor* mNG. In contrast, the trajectory is flattened for axenic *T. reesei* mCherry cultivations when the signal is corrected for autofluorescence.

Overall, successful cellulose-based co-cultivations are possible if inoculation ratios are adjusted to allow synchronous growth of the two partners. In contrast, out competition is observed when inoculation ratios are mismatched. Hence, the population dynamics highly depend on the timing of the onset of growth, which is not only dependent on inoculum density but also on inoculum viability.

3.3.3 Controlling co-cultivation composition with a variation of the osmolality

In the first approach, the timing of growth onset was varied via inoculation densities and viability of the used spore stock. Another approach is a direct change of growth rates for each partner for steering the population dynamics in a co-cultivation. For example, increased osmolality and water activity are reported to negatively influence the growth rates of fungi such as *T. reesei* [96]. However, according to the literature, *Streptomyces* are less affected by increased salt concentrations [97].

For a suitable steering strategy, a parameter, which mainly affects one of the co-cultivation partners, is favourable to reduce the complexity of the system. Therefore, axenic cultivations of *T. reesei* mCherry and *S. coelicolor* mNG were performed with increasing amounts of sodium chloride, resulting in a variation of osmolality (Figure 9).

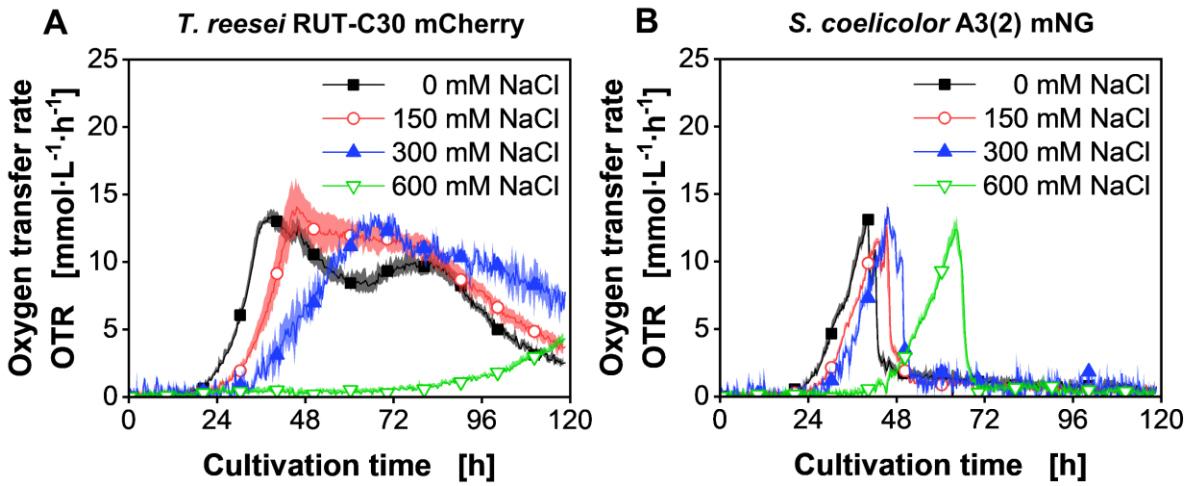

Figure 9. Oxygen transfer rates for axenic cultivations of (**A**) *Trichoderma reesei* RUT-C30 mCherry and (**B**) *Streptomyces coelicolor* A3(2) mNG with varying amounts of added sodium chloride. For clarity, only a representative amount of data points is indicated by the corresponding symbols. Culture conditions: 48-well round well plate, N = 3, $X_0 = 10^6$ spores·mL^{-1}, $V_L = 1000$ µL, n = 800 rpm, $d_0 = 3$ mm, T = 30 °C, LNP medium with 5 g·L^{-1} glucose and 30 g·L^{-1} α-cellulose.

Generally, with higher sodium chloride concentrations, the start of the increase in the OTR is delayed. Especially for *T. reesei* mCherry (Figure 9A), the time until the OTR starts increasing for the culture with 600 mM sodium chloride (green line, inverted triangles) is quadrupled, with approximately 72 h compared to 18 h for the control (black line, squares). In contrast, for *S. coelicolor* mNG (Figure 9B), only a delay from 22 h to 40 h can be noted. Overall, the growth rates of *T. reesei* mCherry are more affected in comparison to *S. coelicolor* mNG, as indicated by the substantial drop in OTR increase with higher osmolality. For *S. coelicolor* mNG, the increase remains similar, despite the increase in the sodium chloride concentration. The same effect and OTR trajectory could also be seen for the untagged *S. coelicolor* strain (Appendix Figure A13). Thus, higher osmolality provided a growth advantage to *S. coelicolor* compared to *T. reesei* mCherry.

The co-cultivations were conducted with a spore inoculation ratio of 1:1 and with the same concentrations of sodium chloride (0 – 600 mM) as tested before (Figure 10). The macroscopic pictures, taken after cultivation (Figure 10A), are similar to the co-cultivation pictures in Figure 7A.

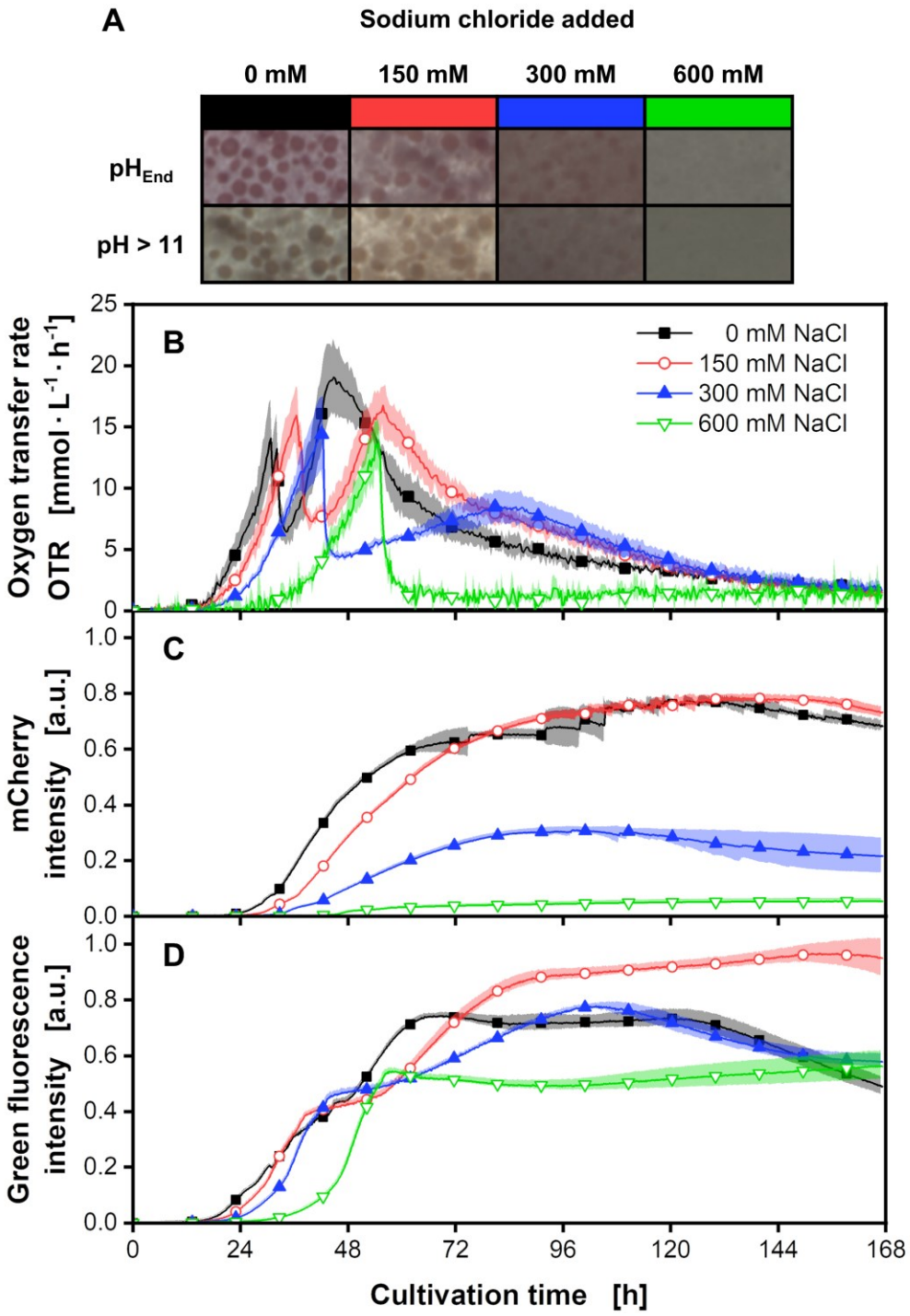

Figure 10. Co-cultivations of *Trichoderma reesei* RUT-C30 mCherry and *Streptomyces coelicolor* A3(2) mNG with varying amounts of added sodium chloride. (**A**) Macroscopic pictures of the culture broth after termination of the cultivation. The pH was changed to a value above 11 to determine production of the blue pigment actinorhodin (second row in (A)). (**B**) Oxygen transfer rates. (**C**) mCherry intensity signals (Excitation: 587 nm; Emission: 610 nm). (**D**) Green fluorescence intensity signals (Excitation:

483 nm; Emission: 520 nm). For clarity, only a representative amount of data points is indicated by the corresponding symbols in (B) - (D). Culture conditions: 48-well round well plate, N = 3, $X_0 = 10^6$ spores·mL^{-1}, V_L = 1000 µL, n = 800 rpm, d_0 = 3 mm, T = 30 °C, LNP medium with 5 g·L^{-1} glucose and 30 g·L^{-1} α-cellulose.

However, besides the red colouration, which appeared in pH untreated samples due to undecylprodigiosin produced by *S. coelicolor* mNG or mCherry of *T. reesei* mCherry, no blue pigmentation was observed after a pH increase above 11. A similar effect was reported by Sevcikova and Kormanec, who observed that the production of actinorhodin and undecyprodigiosin was differentially affected at high salt concentrations [98]. Due to unconsumed cellulose, the picture of the condition with 600 mM sodium chloride (Figure 10A, green boxes) remains white-greyish. For this condition, very low hydrolysis of cellulose and uptake of soluble sugars is indicated by the OTR (Figure 10B). The initial OTR peak (green line, inverted triangles) resembles the axenic OTR peak of *S. coelicolor* mNG in Figure 9B. The slow rise of the OTR afterwards is due to the slow growth of *T. reesei* mCherry (Figure 10C), along with the production and secretion of cellulases. Overall, a clear and comparable trend to axenic cultures is visible for the change in osmolality. The time until the onset of growth is noticeably prolonged with increasing osmolality (Figure 10B). Additionally, the period between the first and second OTR peaks increases until no second peak is visible for the condition with 600 mM sodium chloride. This can be explained by the co-cultivation composition, similar as described in chapter 3.3.2. With the increase of added sodium chloride, less *T. reesei* mCherry biomass is formed, which is also evident in the mCherry intensity data (Figure 10C). The increase in mCherry fluorescence and, thus, biomass formation for *T. reesei* mCherry halts after the initial glucose is depleted and rises with the increase in OTR due to cellulose consumption.

The same effect also becomes visible in the green fluorescence signal (Figure 10D), which partly represents the whole co-cultivation growth. However, as explained in chapter 3.3.2, the mNG labelling confers a bias of this signal for mainly representing the *S. coelicolor* mNG biomass. This was also confirmed when comparing these data with the data of the same experiment conducted with the untagged *S. coelicolor* strain (Appendix Figure A14D). Here, the green fluorescence signals show the same trend but at much lower magnitudes due to the lack of mNG. Overall, these results demonstrate

that osmolality is a suitable factor for steering population dynamics by tuning the activity of *T. reesei* mCherry.

3.3.4 Controlling co-cultivation composition with a variation of the shaking frequency

In the third approach, shaking frequency and, therefore, power input was evaluated as a factor that can influence population dynamics. The effect of power input on the growth of *S. coelicolor* was previously reported as leading to a change in spore agglomeration [10, 90]. Hence, the influence of two different shaking frequencies was tested first on axenic cultivations of *T. reesei* mCherry and *S. coelicolor* mNG (Figure 11).

The mCherry intensity signal of both conditions for *T. reesei* mCherry (Figure 11A) indicated no effect on the onset of the exponential phase and growth. Therefore, *T. reesei* mCherry is mostly unaffected by the tested shaking frequency. In contrast, for *S. coelicolor* mNG (Figure 11B) and the untagged *S. coelicolor* strain (Appendix Figure A15), an apparent delay in the onset of the exponential phase for cultures shaken at 1200 rpm, compared to 800 rpm, could be noted. Similar to chapter 3.3.3, one co-cultivation partner is mainly affected, which qualifies the shaking frequency as a suitable control parameter. However, here the role is reversed, with *S. coelicolor* growth being more responsive.

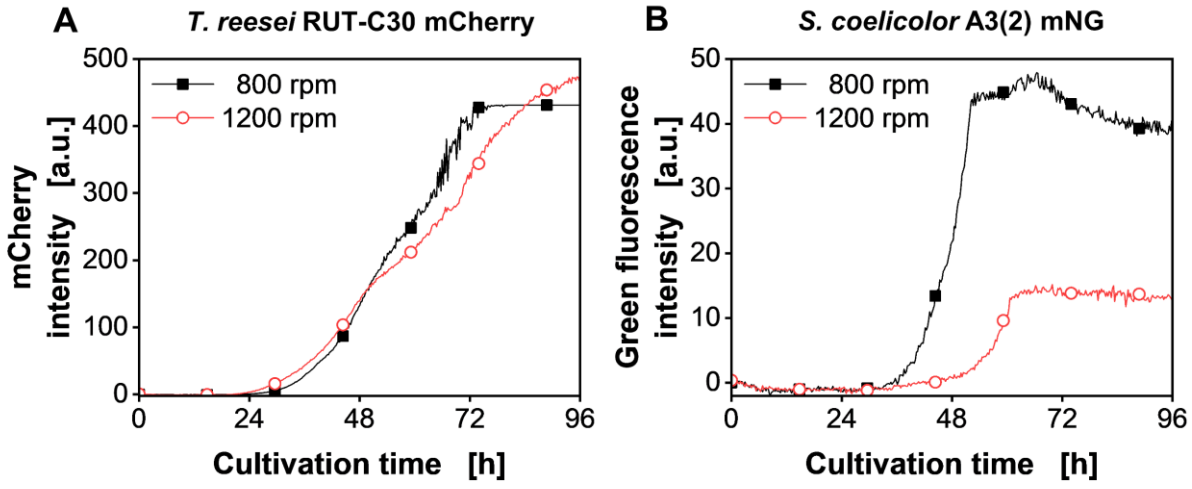

Figure 11. Biomass signal for axenic cultivations of (**A**) *Trichoderma reesei* RUT-C30 mCherry and (**B**) *Streptomyces coelicolor* A3(2) mNG with shaking frequencies of 800 and 1200 rpm. The mCherry intensity signals (Excitation: 580 nm; Emission: 610 nm) and green fluorescence intensity signals (Excitation: 480 nm; Emission: 520 nm) were monitored. For clarity, only a representative

amount of data points is indicated by the corresponding symbols. Culture conditions: 48-well round well plate, $X_0 = 10^6$ spores·mL^{-1}, $V_L = 1000$ µL, n = 800 rpm, $d_0 = 3$ mm, T = 30 °C, LNP medium with 5 g·L^{-1} glucose and 30 g·L^{-1} α-cellulose.

Whether this parameter can be further used to modulate the co-cultivation composition was tested in parallel co-cultivations at 800 rpm or 1200 rpm. Both partners are expressing fluorescent proteins under the control of a constitutive promoter. A narrow range of inoculation ratios of 9:1, 6:1, 3:1, 1:2, 1:4 and 1:6 within the same order of magnitude from fungi to bacterium were analyzed (Figure 12).

The macroscopic pictures (Figure 12A) indicate colouration, especially with an increased colour intensity for the 800 rpm conditions with an inoculation ratio favouring *T. reesei* mCherry (3:1, 6:1 and 9:1). In addition, it can be observed that at 800 rpm (Figure 12C), there is a late increase in the green fluorescence signal for the co-cultivations with highest *T. reesei* mCherry to *S. coelicolor* mNG inoculation ratio. Hence, additional biomass formation of *S. coelicolor* mNG is indicated. For the conditions at 1200 rpm, the picture is different. Despite the gradual increase of green fluorescence (Figure 12E) until 70 h, the total intensity values remained very low. It can be hypothesized that the higher specific power input under these conditions exerted a growth disadvantage to *S. coelicolor* mNG. Contrasting to the co-cultivation at 800 rpm, for which *S. coelicolor* mNG could compete with *T. reesei* mCherry, at 1200 rpm, the data suggests no considerable competition of *S. coelicolor* mNG for the limiting nutrients (soluble carbon source or nitrogen).

With the results obtained by means of OTR and fluorescence online monitoring, it can be proposed that in order to sustain and control the growth of both partners, two prerequisites must be fulfilled: 1. The axenic growth behaviour has to be well characterized before the co-cultivations are conducted. 2. The co-cultivation partner with slower growth should be given an advantage in the co-cultivation, as was presented by utilizing inoculation ratio, osmolality and shaking frequency. The fact that both, biotic and abiotic parameters, can be used to control the co-cultivation partner activity and that both partners can be independently influenced, opens the avenues towards controlled co-cultivation bioprocesses.

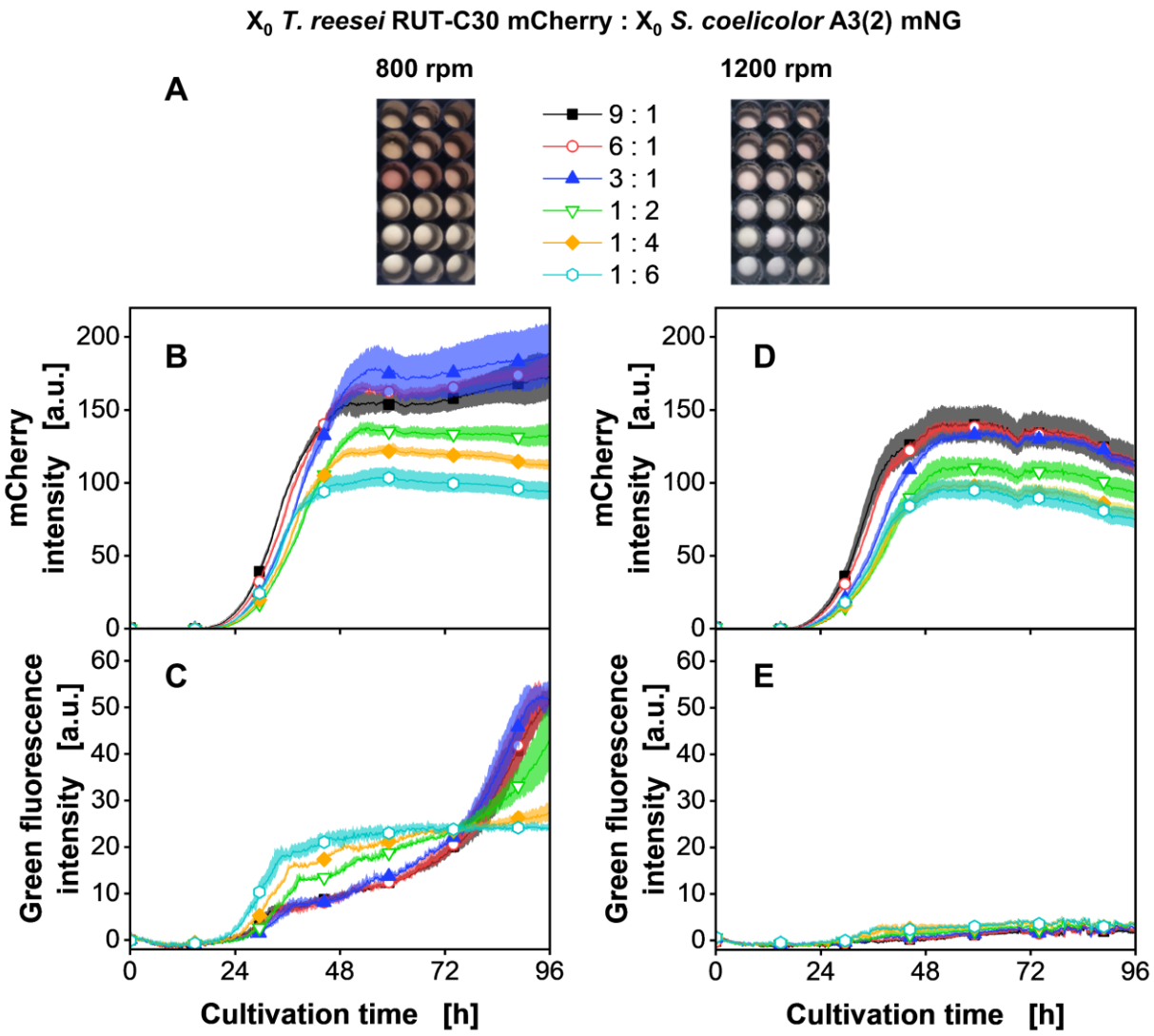

Figure 12. Co-cultivations of *Trichoderma reesei* RUT-C30 mCherry and *Streptomyces coelicolor* A3(2) mNG with shaking frequencies of 800 and 1200 rpm. Inoculation ratios were varied, as given, relating to the standard inoculation size of $X_0 = 10^6$ spores·mL^{-1}. (**A**) Macroscopic pictures of the culture broth after termination of the cultivation. (**B** and **D**) mCherry intensity signals (Excitation: 580 nm; Emission: 610 nm) for cultivations at 800 and 1200 rpm, respectively. (**C** and **E**) Green fluorescence intensity signals (Excitation: 480 nm; Emission: 520 nm) for cultivations at 800 and 1200 rpm, respectively. For clarity, only a representative amount of data points is indicated by the corresponding symbols in (B) - (E). Culture conditions: 48-well round well plate, N = 3, V_L = 1000 µL, n = 800 rpm, d_0 = 3 mm, T = 30 °C, LNP medium with 5 g·L^{-1} glucose and 30 g·L^{-1} α-cellulose.

3.4 Conclusion

In this chapter, a filamentous co-cultivation between the cellulolytic fungus *T. reesei* mCherry and the bacterium *S. coelicolor* was successfully demonstrated and established. Highly different factors, such as inoculation ratio, osmolality and shaking frequency, were presented to affect co-cultivation population dynamics. Furthermore, it was shown that after gathering knowledge with high-throughput online monitoring, the mentioned influencing parameters can be utilized to control the envisioned co-cultivation. Monitoring and estimating biomass development with the fluorescent proteins mCherry and mNG were used to effectively determine suitable conditions for the growth of both co-cultivation partners. In addition, the OTR data provided valuable information on metabolic activity, co-cultivation growth and consumption of cellulose. Slow hydrolysis of cellulose and a co-cultivation advantage for *S. coelicolor* was connected to pigment formation and has to be investigated in further studies. Additionally, the presented approach could be utilized for the co-cultivation of *T. reesei* mCherry with other *Streptomyces sp*., using cellulose as a carbon source. These *Streptomyces* strains do not necessarily need to be tagged since the OTR was shown to provide deep insights into the population dynamics with the combination of a tagged *T. reesei* strain. Thereby, the proposed cellulose-based co-cultivation platform could be explored to unlock the production of novel natural products systematically. Furthermore, analyzing the broth from cultivations with variable population compositions with mass spectrometry could reveal correlations to metabolite profiles and lead to the identification of interesting new natural products, which might require very specific co-cultivation settings to be induced.

Paul Richter (AVT - Biochemical Engineering, RWTH Aachen University, Aachen, Germany) assisted with the cultivations presented in chapter 4.3.1. Lukas Hartmann (AVT - Biochemical Engineering, RWTH Aachen University, Aachen, Germany) performed the experiments presented in chapter 4.3.2 and 4.3.3.

4 Substrate-limited pigment formation and scale-up of the filamentous co-cultivation process

4.1 Background

In the envisioned co-cultivation, the production and secretion of cellulases by *T. reesei* mCherry leads to the release of soluble sugars through the hydrolysis of cellulose. The presented results in chapter 3 indicate that the pigment formation by *S. coelicolor* depends on this release of carbon sources. In such a carbon-limited process, low release rates lead to the production of undecylprodigiosin and actinorhodin by *S. coelicolor*. Similar findings are described in the literature [9]. However, the information on suitable feed rates for pigment formation varies in the literature, which can be explained by the different media and cultivation conditions used [99]. In this study, the media and cultivation conditions were chosen to meet the requirements for appropriate growth of both co-cultivation partners. Hence, the glucose-dependent pigment formation is expected to vary from the literature and was assessed for axenic *S. coelicolor* cultivations within this chapter. Additionally, the successful pigment production is showcased for co-cultivations of *S. coelicolor* and *T. reesei* mCherry in a STR.

4.2 Material and methods

4.2.1 Microorganisms

In this chapter, *T. reesei* mCherry as well as *S. coelicolor* (DSMZ 40783) were used as stated in chapter 3.2.1. Cultivations were either inoculated by spores with 10^6 n_{Spores}·mL^{-1} or with 1 (v/v) % of a pre-culture. Pre-cultures were centrifuged for 10 min at 4000 rpm, the supernatant was discarded, and the cells were washed with a 9 $g·L^{-1}$ NaCl solution to avoid a medium transfer into the main culture. The cell pellet was resuspended with medium after washing.

4.2.2 Media composition

The medium used for the pre-cultivation of *T. reesei* mCherry was potato extract glucose broth. The medium was mixed from powder (Carl Roth, Karlsruhe, Germany) with 26.5 $g·L^{-1}$. Pre-cultivations of *S. coelicolor* were performed with tryptone soy broth consisting of 17 $g·L^{-1}$ peptone from casein, 3 $g·L^{-1}$ peptone from soy meal, 5 $g·L^{-1}$ NaCl, 2.5 $g·L^{-1}$ KH_2PO_4 and 2.5 $g·L^{-1}$ glucose. All other cultivations were done with LNP minimal medium, as described in chapter 2.2.2. If not stated otherwise, 5 $g·L^{-1}$

glucose and 30 $g \cdot L^{-1}$ α-cellulose were added as carbon sources. The complex media were autoclaved and the LNP medium as well as the trace element solution were sterile-filtered with a 0.2 µm cut-off filter (MilliporeSigma, Burlington, USA). For cultivations in MTPs, a commercial cellulase cocktail from *T. reesei* (MilliporeSigma, Burlington, USA) was diluted in water and sterile-filtered. A volume of 100 µL of the different dilutions and a reference with pure, sterile water was added to the cultivations after 72 h.

4.2.3 Cultivations in microtiter plates

Cultivations in MTPs were performed, as described in chapter 2.2.3.

4.2.4 Cultivations in shake flasks

Shake flask cultivations were performed in 250 mL shake flasks, and the respiration was monitored with an in-house built RAMOS device [51, 52]. Cultivation conditions were a filling volume of 20 mL, a temperature of 30 °C, a shaking diameter of 50 mm and a shaking frequency of 320 or 350 rpm, stated for each cultivation. All pre-cultivations were conducted in shake flasks. For *S. coelicolor* pre-cultures, 30 $g \cdot L^{-1}$ of autoclaved glass beads were added to the shake flasks. The glass beads lead to the formation of smaller pellets and more homogenous inoculum for main cultivations.

4.2.5 Cultivations in stirred tank reactors

Cultivations in STRs were performed in Biostat B Plus 2 L reactor (Sartorius AG, Göttingen, Germany). The reactor was autoclaved with water before cultivation. The exhaust gas composition was monitored with a DASGIP gas analyser (Eppendorf SE, Hamburg, Germany). Calibration was conducted with air and a mixture of 2 % oxygen and 10 % carbon dioxide. OTR data were partially omitted due to faulty oxygen measurements in the exhaust gas. For dissolved oxygen tension (DOT) measurements, an optical probe VisiFerm DO ECS 225 (Hamilton Company, Reno, United States) was used. The DOT was calibrated with pure air and nitrogen. All pH measurements were done with the Easyferm plus PHI K8 200 (Hamilton Company, Reno, United States) probe. The pH measurement was calibrated with pH 4 and 7 buffers. Capacitance was measured with a TCNK 12410 (ABER instruments, Aberystwyth, United Kingdom) probe at 580 and 15,650 kHz with a moving average filter option of 90 and polarisation correction. Cultivations were conducted with an agitation rate of either 600 rpm or

1000 rpm and with a gassing rate of 60 $sL \cdot h^{-1}$. If necessary, antifoam Plurafac LF1300 (BASF, Ludwigshafen, Germany) was added to the cultivations.

4.2.6 Offline measurements

Samples for offline analysis were taken at the end of cultivations in MTP and during fermentations in STR. Due to small sampling volumes, not all analysis methods were applied for each sample.

Glucose concentrations were measured with high-performance liquid chromatography (HPLC) UltiMate3000 (Dionex, Sunnyvale, USA). The mobile phase was sulfuric acid with 5 mM, and an organic-acid-resin column (CS-Chromatographie Service, Langerwehe, Germany) was used. The temperature was set to 60 °C and the volumetric flow to 0.8 $mL \cdot min^{-1}$. Ammonium and phosphate content was quantified photometrically (Ammonium test kit, phosphate test kit, Supelco, MilliporeSigma, Burlington, USA). For dry weight measurements, 1-2 mL culture broth was filled into dried and weighed 2 mL reaction tubes. The reaction tubes were centrifuged at 14,000 rpm for 10 min and the supernatant was used for other offline analytics. After drying for at least 48 h at 80 °C, the tubes were weighed again, and the dry weight concentration was determined. Fluorescence measurements of offline samples with a volume of 1 mL were conducted in an in-house built BioLector device, as stated in chapter 3.2.3.

The pH measurements were performed with a pH-meter HI 2211 (HANNA Instruments, Smithfield, USA). For osmolality measurements, the Osmomat 3000 (Gonotec, Berlin, Germany) was used. Macroscopic pictures of the culture broth were taken with an Epson perfection V700 photo scanner (Epson, Tokyo, Japan) after the cultivations were ended. Scans for qualitative analysis of blue pigment formation were taken after the addition of 10 (v/v) % of 1 M NaOH to the culture broth.

As indicated in chapter 2, the autofluorescence measurement is heavily influenced by pigmentation due to light absorption. Therefore, the decrease in autofluorescence can be utilized for semi-quantitative evaluation of pigment formation. This was tested for the axenic cultivations of *S. coeliolor* in MTP with the addition of cellulase cocktails. According to equation (2), the autofluorescence decrease

$\Delta I_{Autofluorescence}$ was defined as the difference between the maximal autofluorescence value after the addition of cellulases $I_{Autofluorescence,max}$ and the autofluorescence value at the end of the cultivation $I_{Autofluorescence,end}$. The results were normalized similarly to equation (1) to yield the relative autofluorescence decrease.

$$\Delta I_{Autofluorescence} = I_{Autofluorescence,max} - I_{Autofluorescence,end} \quad (2)$$

Quantitative analysis of pigment formation was achieved by measurement of the absorption of actinorhodin and prodigiosin after alkalinisation and acidification. For the determination of actinorhodin concentrations, 50 (v/v) % 3 M KOH and 50 (v/v) % methanol was added to the samples. After vortexing and incubating for 10 min at room temperature, the sample was centrifuged for 10 min at 14,000 rpm. The absorbance of the supernatant was measured at 640 nm with a photometer Genesys 20 (Thermo Fisher Scientific, Waltham, United States). For the determination of undecylprodigiosin concentrations, 50 (v/v) % 3 M HCl and 50 (v/v) % methanol were added to the samples. After vortexing, the sample was incubated for 48 h at 900 rpm and at room temperature. Then, the mixture is centrifuged for 10 min at 14,000 rpm. The absorbance of the supernatant was measured at 530 nm. LNP medium with 50 (v/v) % 3 M KOH or 3 M HCl and 50 (v/v) % methanol is used as a reference for absorbance measurements. For both pigments, samples were diluted with the respective reference solutions for absorbance beyond the linear range of the photometer at 0.3. The pigment concentration $c_{Pigment}$ was calculated according to equation (3) based on the absorbance at the specific wavelength A_λ, the cuvette diameter d_c and the molar extinction coefficient $\varepsilon_{Pigment}$ ($\varepsilon_{Actinorhodin}$ = 25,320 $mol \cdot L^{-1} \cdot cm^{-1}$, $\varepsilon_{Undecylprodigiosin}$ = 100,150 $mol \cdot L^{-1} \cdot cm^{-1}$) [9, 81].

$$c_{Pigment} = \frac{A_\lambda}{\varepsilon_{Pigment} \cdot d_c} \quad (3)$$

4.3 Results and discussion

4.3.1 Carbon-limited pigment formation by *Streptomyces coelicolor*

In cellulolytic cultivations, the carbon supply is often a limiting factor due to the hydrolysis process. Either insufficient cellulases are produced, or the cellulose digestibility becomes limiting [63]. Hence, to understand the final co-cultivation process, it is necessary to examine how *S. coelicolor* reacts upon carbon-limited conditions. To this extent, an axenic *S. coelicolor* cultivation was performed with 5 $g \cdot L^{-1}$ glucose and 30 $g \cdot L^{-1}$ α-cellulose. After 72 h, different dilutions of a commercial cellulase cocktail from *T. reesei* were spiked into the cultivations as well as a reference with distilled water (Figure 13). Initially, *S. coelicolor* consumed the supplied glucose. This results in standard batch trajectories for the OTR, scattered light and autofluorescence. The OTR (Figure 13A) gradually increases until a sudden drop occurs at approximately 52 h due to glucose depletion, in accordance with the results presented in chapter 2 and 3. The scattered light and autofluorescence (Figure 13B and Figure 13C) indicate a sigmoidal pattern due to biomass formation. *S. coelicolor* is not able to produce cellulases to hydrolyse the cellulose. Due to the carbon source depletion, all signals (Figure 13A-C) remained constant until the cellulase cocktails were spiked in.

The different dilution levels are noticeable in the online monitoring signals after the spike at 72 h. In the OTR, an initial peak after the spike and a plateau is formed at around 88 h with a decreasing height depending on the cellulase cocktail dilution. The cellulase concentration defines the amount of glucose released by cellulose hydrolysis in the cultivations. The glucose release leads to the growth of *S. coelicolor* and, therewith, an increase in the OTR. Hence, the OTR plateau height correlates with the cellulase cocktail dilution. The OTR of the dilutions with 1:1000 and 1:2000 (blue line, inverted triangles and red line, triangles) does not increase considerably compared to the reference (black line, circles). Biomass formation is indicated by an initial increase of the scattered light and autofluorescence signals (Figure 13B and Figure 13C). However, the signals drop after the initial short increase. The drop is explained by cellulose hydrolysis as well as pigment formation. As the insoluble cellulose is degraded, less light is scattered, leading to a signal decrease [100]. Additionally, more light is absorbed if the pigment is formed, resulting in a decline of the scattered light and autofluorescence signal (Chapter 2.3.2 and 2.3.3) [90]. Interestingly, the decrease was also detected for the dilutions with 1:1000 and 1:2000 despite the non-differentiable OTR signals. Noticeable is a change in the order of signal intensities for autofluorescence compared to scattered light intensities (Figure 13B and

Figure 13C). The final intensity of the scattered light signals is lower with an increased amount of cellulase cocktail added. However, this does hold true for the autofluorescence signal. The highest final intensity is reached for the cultivation with the most cellulases (brown line, pentagons) spiked in.

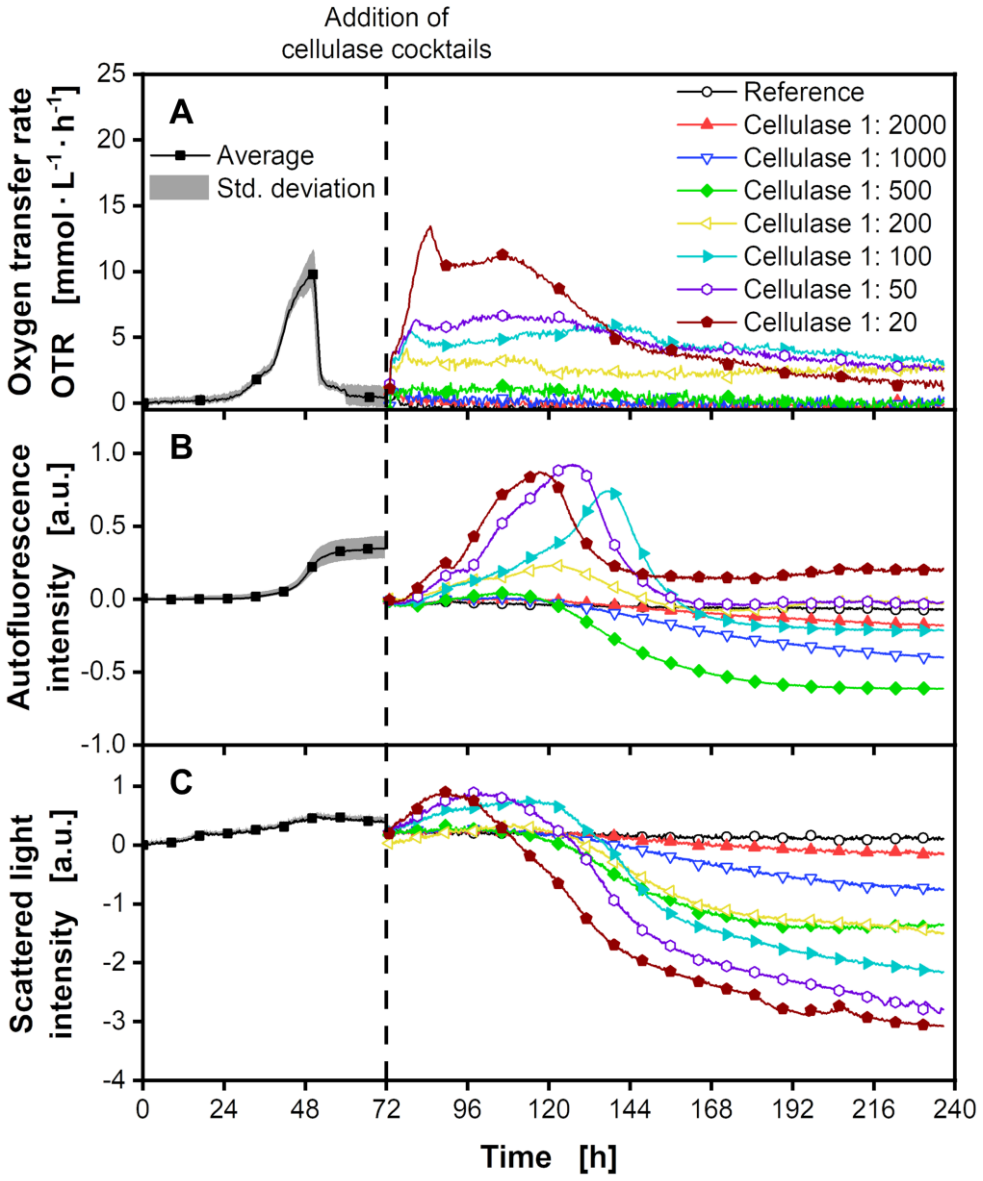

Figure 13. Cultivation of *Streptomyces coelicolor* A3(2) with 30 g·L^{-1} α-cellulose. After 72 h Sigma cellulase cocktails in varying dilutions or demineralized water for reference were added (Dashed line). (**A**) Oxygen transfer rates. (**B**) Autofluorescence intensity signals (Excitation: 483 nm; Emission: 520 nm). (**C**) Scattered light intensity signals (Excitation: 535 nm; Emission: 535 nm). All intensity signals were subtracted with the initial values at the start of cultivation and after the addition. For clarity, only every 50th data point over time is indicated by the corresponding symbol. Before

addition of cellulase cocktails, the average and standard deviation of all 48 wells is presented. After 72 h, only one representative dataset for each condition, tested in triplicates, is represented. Culture conditions: 48-well round well plate, V_L = 1000 µL + 100 µL after addition, n = 800 rpm, d_0 = 3 mm, T = 30 °C, $X_0 = 10^6$ spores·mL^{-1}, LNP medium with 5 g·L^{-1} glucose and 30 g·L^{-1} α-cellulose.

Scattered light and autofluorescence are optical sum signals representing biomass formation, cellulose hydrolysis and pigment formation. However, the signals are affected to different extents. The autofluorescence of cellulose is very low, and therefore, the signal is affected too little extent by cellulose hydrolysis. This can also be noticed by comparing all three signals (Figure 13A-C) for the cellulase dilution of 1:20 (brown line, pentagons) after 168 h. The OTR indicates low respiratory activity, and the scattered light gradually decreases due to cellulose hydrolysis. However, this decrease cannot be seen in the autofluorescence as the signal remains on a constant level. Hence, the autofluorescence decrease might serve as an estimate for the amount of pigment formed under different conditions.

Therefore, the relative autofluorescence decrease was calculated according to chapter 4.2.6 and compared with macroscopic pictures taken at the end of the cultivation as well as the photometrically determined actinorhodin concentrations (Figure 14). According to the autofluorescence decrease, the highest pigment formation is expected for the dilution with 1:100. Furthermore, all approaches except for the reference should indicate pigmentation. A qualitative comparison with the macroscopic pictures supports this observation. The trend is also observable for the determined actinorhodin concentrations except for the condition with a cellulase cocktail dilution of 1:200. However, the high standard deviation for this condition, especially for the relative autofluorescence drop, could indicate that the cultivations were not comparable. At a cellulase cocktail dilution of 1:100, the highest concentration was measured at approximately 143 ± 2 µmol·L^{-1}. The actinorhodin concentrations decreased gradually with a decrease or further increase of added cellulases. Hence, this indicates that the pigment formation was directly dependent on the amount of added Sigma cellulases and, therefore, on the respective glucose release rate from cellulose hydrolysis. Furthermore, the range of glucose release rates for pigment formation by *S. coelicolor* appears to be very narrow, which has to be accounted for within the envisioned co-cultivation.

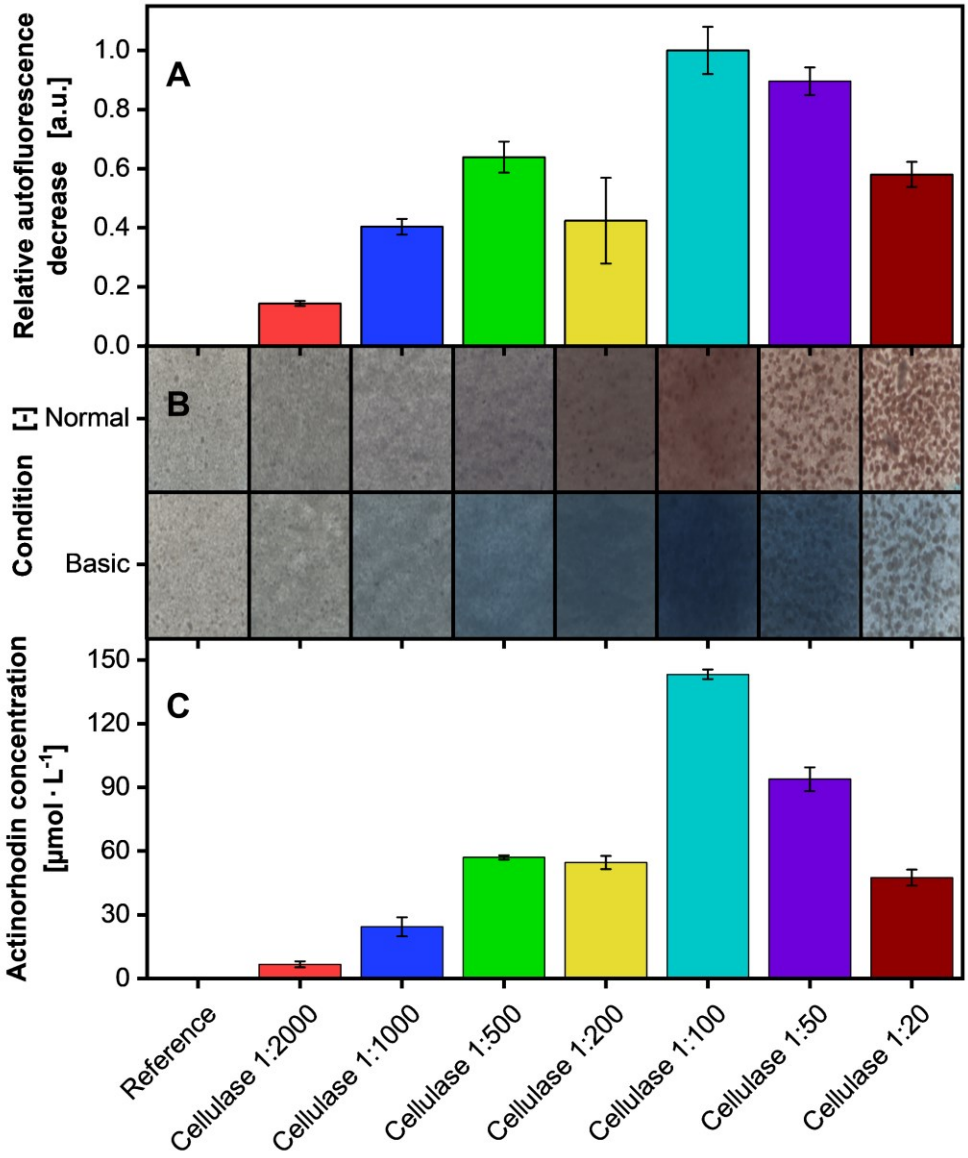

Figure 14. Evaluation of the pigment formation in the cultivation of *Streptomyces coelicolor* A3(2) depicted in Figure 13. The average and standard deviation of triplicates is presented. (**A**) Relative autofluorescence decrease (Excitation: 483 nm; Emission: 520 nm) as explained in chapter 4.2.6. (**B**) Macroscopic pictures after the termination of cultivation (Normal) and with addition of 10 (v/v) % 1 M NaOH (Basic). (**C**) Actinorhodin concentration determined by measuring the absorption of an extract of the cultivation broth.

4.3.2 Pigment production by axenic cultivations of *Streptomyces coelicolor* in a stirred tank reactor

For the validation of the results presented in chapter 4.3.1, additional axenic cultivations of *S. coelicolor* were performed in a STR (Figure 15). Instead of a slow glucose release through cellulose hydrolysis, glucose was fed with a constant amount after the initial batch phase. The glucose feed was approximated based on the OTR of the condition with a cellulase cocktail dilution of 1:100. In order to provide comparable cultivation conditions, no DOT or pH control was enabled, and the same MES buffer as for MTP experiments was used. During the initial batch phase, the trajectories of all determined signals for both cultivations (black line, squares and red line, circles) were highly similar. Additionally, the CTR (Figure 15A) indicates a similar growth trajectory as can be derived from the OTR of the previous MTP experiment (Chapter 4.3.1). After consumption of the initial 5 $g \cdot L^{-1}$ glucose, the CTR dropped likewise to the increase in DOT (Figure 15B) at 43 h (red line, circles) and 47 h (black line, squares). Furthermore, the capacitance signal (Figure 15C) was decreasing, likely due to cell lysis and, therefore, a reduction of the membrane-enclosed area, which was also reported previously [101, 102]. The pH (Figure 15E) increased during this period. During the batch phase, no pigment formation of actinorhodin and undecylprodigiosin (Figure 15F and Figure 15G) was measurable.

After the start of the glucose feed at approximately 66 h, the CTR increased, and the DOT decreased rapidly due to the added glucose. The different feed rates are noticeable by the different plateau heights in the CTR. The higher feed rate of 0.12 $g \cdot h^{-1}$ compared to the lower feed rate of 0.08 $g \cdot h^{-1}$ resulted in an elevated CTR plateau, a faster increase of the capacitance signal and a decrease of the pH. The information obtained by dry weight measurements is limited due to the high measurement noise, which could be attributed to the low sampling volume combined with the pelleted morphology of *S. coelicolor*. After 128 h, which accounts for a feeding time of 62 h, pigment formation was visible in the STR and could also be measured. Thereafter, actinorhodin and undecylprodigiosin concentrations (Figure 15F and Figure 15G) increased almost linearly until a plateau was reached. Final titers of 70 $\mu mol \cdot L^{-1}$ and 109 $\mu mol \cdot L^{-1}$ of actinorhodin and 1.9 $\mu mol \cdot L^{-1}$ and 2.3 $\mu mol \cdot L^{-1}$ of undecylprodigiosin were measured for the high and low glucose feed rate, respectively. The actinorhodin titer is comparable to the titer (94 ± 6 $\mu mol \cdot L^{-1}$) achieved for the condition with a cellulase cocktail dilution of 1:50 in the MTP experiment (Chapter 4.3.1). These results further validate that a specific glucose release rate is favourable within co-cultivations for pigment production. However, it has to be noted that the pigment formation could also be linked to the growth rate rather than the prevalent glucose. Therefore, the

optimal glucose release rate for pigment formation depends on the biomass concentration of *S. coelicolor*.

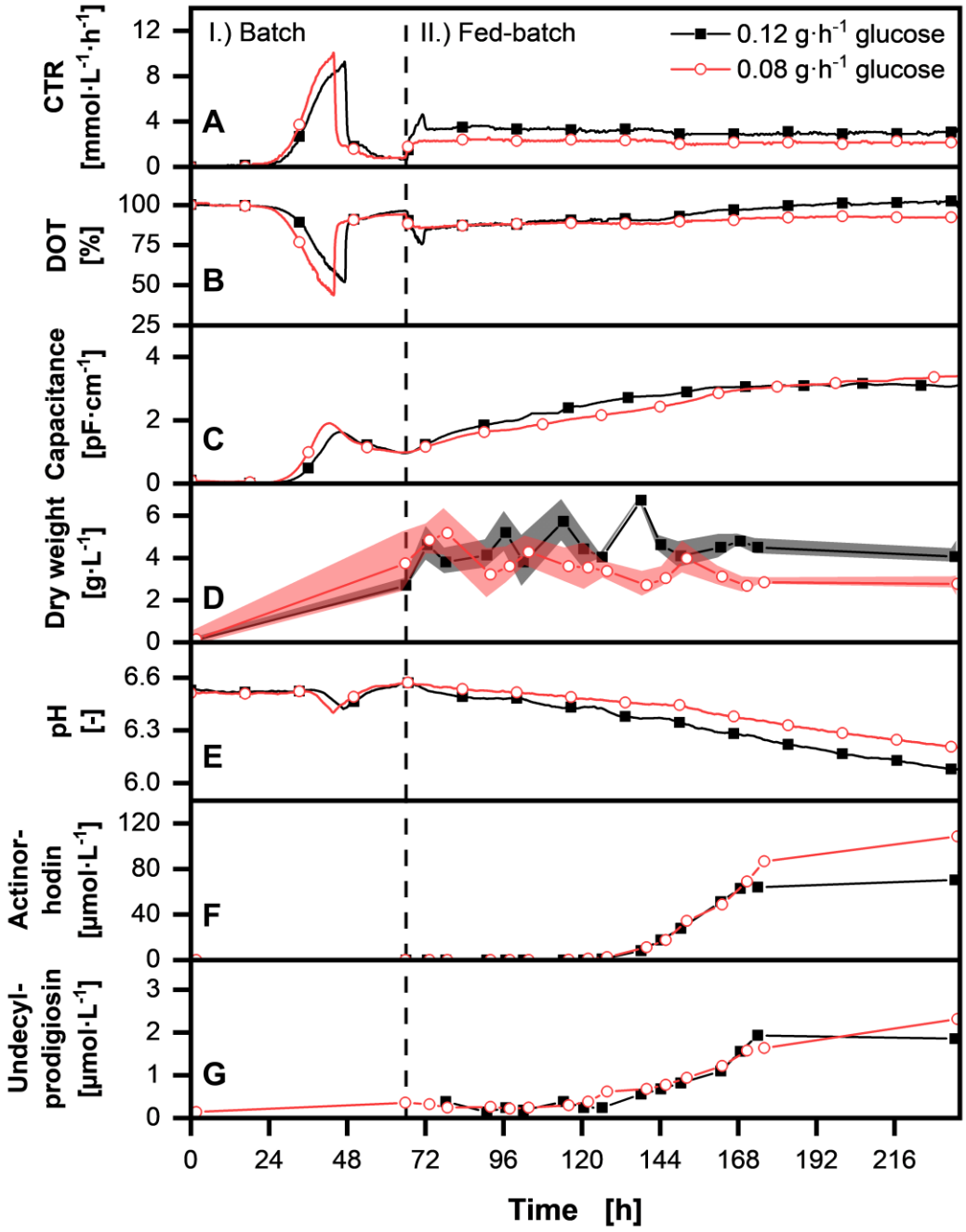

Figure 15. Fed-batch cultivations of *Streptomyces coelicolor* A3(2) with varying feed rates in a stirred tank reactor. The feed of 0.08 or 0.12 g·h^{-1} glucose was started after the batch phase (Dashed line) at 62 h. (**A**) Carbon dioxide transfer rate (CTR). (**B**) Dissolved oxygen tension (DOT). (**C**) Capacitance.

(**D**) Dry weight (N=3). (**E**) pH. (**F**) Actinorhodin concentration. (**G**) Undecylprodigiosin concentration. In (A-C) and (E), only a representative amount of data points are indicated by the corresponding symbols. Data points in (D), (F) and (G) indicate sampling. Culture conditions: 2 L stirred tank reactor, $V_{L,initial} = 1$ L, n = 600 rpm, T = 30 °C, $X_{0,S.\ coelicolor} = 10^6$ spores·mL^{-1}, $F_{air} = 60$ sL·h^{-1}, $pH_0 = 6.5$, $F_{glucose} = 5$ mL·h^{-1}, LNP medium with 5 g·L^{-1} initial glucose.

4.3.3 Pigment production by co-cultivations of *Streptomyces coelicolor* and *Trichoderma reesei* mCherry in a stirred tank reactor

Prior to scaling up the co-cultivation process, axenic cultivations were tested in the STR beforehand (Appendix Figure A16 and Appendix Figure A17). Simultaneous cultivations in shake flasks and STR indicated comparable but shifted trajectories across the different scales. These shifts can be attributed to the increased volumetric power input in the fermenter and, thereby, influenced growth similar as described in chapter 2.3.2 and 3.3.4. Hence, a different trajectory has to be expected for the co-cultivation in the STR compared to shake flask or MTP.

Due to the expected differences for the co-cultivation across scales, four different inoculation ratios were tested in a STR (Figure 16) similar to the MTP experiment presented in chapter 3.3.2. Conditions were kept comparable by utilization of MES buffer instead of active pH control. In contrast to the MTP experiment, the population dynamics were clearly shifted in the STR. This can be noted primarily for the conditions with inoculation ratios favouring *S. coelicolor* with 1:0.001 (black line, squares) and 1:0.01 (red line, circles). The CTR and the DOT (Figure 16A and Figure 16B) only indicate the depletion of the initial glucose, but no subsequent consumption of glucose released by cellulose hydrolysis. This was proven by glucose measurements, which remained at 0 g·L^{-1} (data not shown) after the initial CTR peak. Furthermore, the dry weight measurements (Figure 16D) stayed at the same level. If insoluble cellulose were to be hydrolysed, this should result in a decreasing trend of the dry weight. Hence, under these co-cultivation conditions, *T. reesei* mCherry did not produce sufficient amounts of cellulases. This is in accordance with the low formation of *T. reesei* mCherry biomass, represented by the constantly low mCherry fluorescence intensity (Figure 16F). As the initial glucose is entirely consumed by *S. coelicolor*, the carbon is too limited to support *T. reesei* mCherry growth and, thereby, cellulase formation. In accordance with the findings presented in chapter 4.3.2, no pigment was produced (Figure 16G).

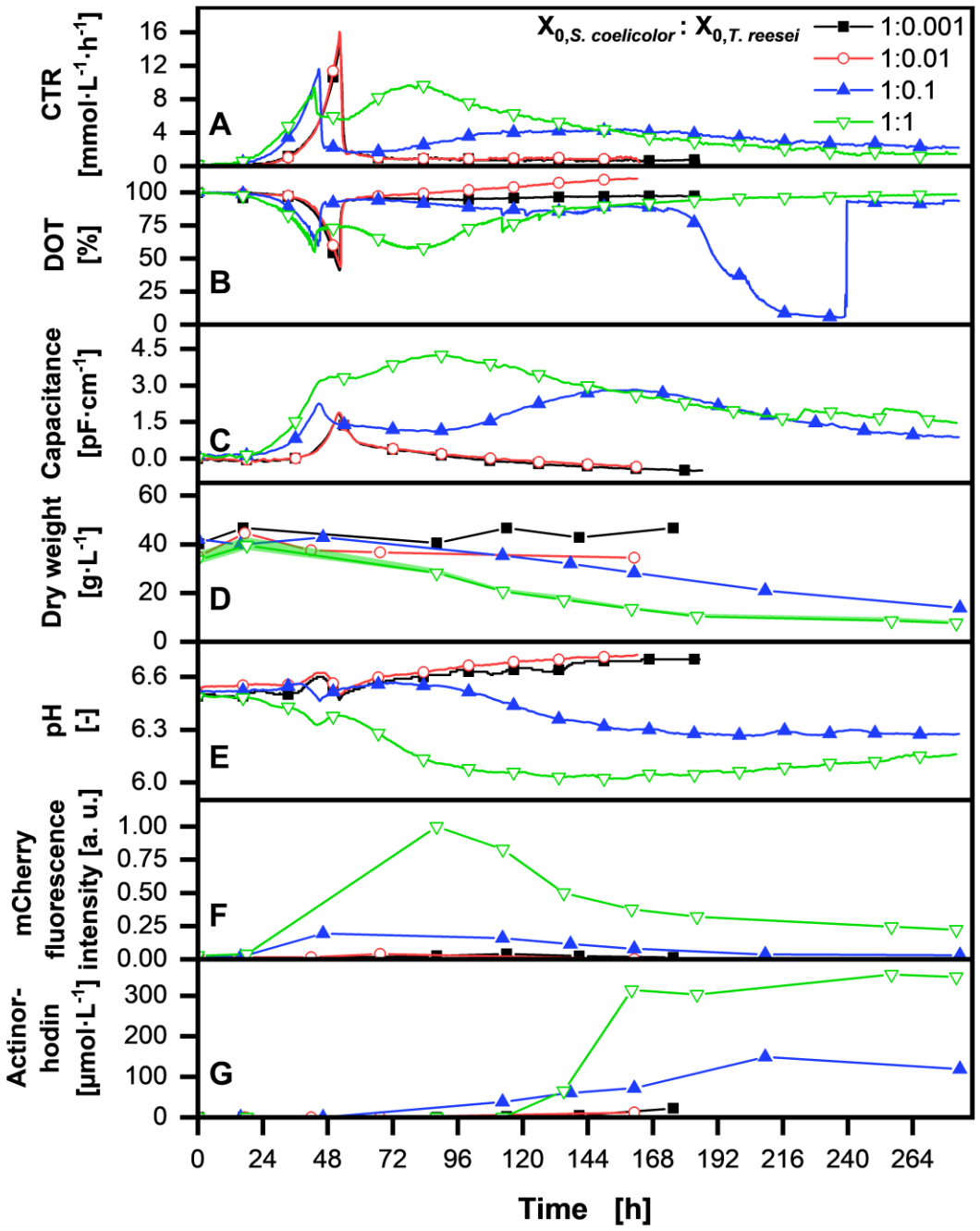

Figure 16. Co-cultivation of *Streptomyces coelicolor* A3(2) and *Trichoderma reesei* RUT-C30 mCherry with varying inoculation ratios in a stirred tank reactor. (**A**) Carbon dioxide transfer rate (CTR). (**B**) Dissolved oxygen tension (DOT). The rapid decrease in the signal for the condition with 1:0.1 at about 168 h was caused by biofilm formation on the probe, which is removed at about 240 h. (**C**) Capacitance. (**D**) Dry weight (N=3). (**E**) pH. (**F**) mCherry fluorescence intensity (Excitation: 587 nm; Emission: 610 nm). (**G**) Actinorhodin concentration. In (A-C) and (E), only a representative amount of data points are indicated by the corresponding symbols. Data points in (D), (F) and (G)

indicate sampling. Culture conditions: 2 L stirred tank reactor, V_L = 1 L, n = 600 rpm, T = 30 °C, $X_{0,S.\ coelicolor}$ = 10^6 spores·mL^{-1}, $X_{0,T.\ reesei}$ = 10^3 - 10^6 spores·mL^{-1}, F_{air} = 60 sL·h^{-1}, pH_0 = 6.5, $t_{end,1:0.001}$ = 186 h, $t_{end,1:0.01}$ = 163 h, $t_{end,1:0.1}$ = 281 h, $t_{end,1:1}$ = 280 h, LNP medium with 5 g·L^{-1} glucose and 30 g·L^{-1} α-cellulose.

In contrast to these co-cultivations, *T. reesei* mCherry growth in combination with cellulase production could be observed in co-cultivations with more equal inoculation ratios of 1:0.1 (blue line, triangles) and 1:1 (green line, inverted triangles). These observations are supported especially by the mCherry fluorescence intensity data (Figure 16F) as well as the second peak in CTR and DOT (Figure 16A and Figure 16B) due to the utilization of released glucose from cellulose hydrolysis. Additionally, it can be stated that the cellulose hydrolysis led to decreasing dry weights (Figure 16D), while the capacitance signal (Figure 16C) further increased as more biomass was produced. This also resulted in decreased pH values (Figure 16E). Glucose measurements (data not shown) indicated limiting conditions after the initial glucose was consumed, and a measurement of glucose release rates was not possible. However, pigment formation was recorded for these co-cultivations, in which cellulases were formed by *T. reesei* mCherry. For the co-cultivation with an inoculation ratio of 1:1 (green line, inverted triangles), actinorhodin formation began after approximately 113 h, increased very fast and indicated a saturation with a maximum titer of 352 µmol·L^{-1}. The pigment formation for the condition with an inoculation ratio of 1:0.1 (blue line, triangles) was more linear and began earlier. For the sample taken at 113 h, 39 µmol·L^{-1} actinorhodin was already produced. However, after that, the titer only increased slowly compared to the condition with an inoculation ratio of 1:1. Finally, at 210 h, the maximum titer of 149 µmol·L^{-1} was reached.

Based on the results obtained in chapter 4.3.1 and 4.3.2, it is known that only a certain ratio of prevalent carbon source to *S. coelicolor* biomass results in successful pigment formation. However, the titer with 352 µmol·L^{-1} achieved for the co-cultivation with an inoculation ratio of 1:1 was more than 2-fold higher compared to the highest titers reached in axenic cultivations of 143 ± 2 µmol·L^{-1} in chapter 4.3.1 and 109 µmol·L^{-1} in chapter 4.3.2. It can be hypnotized that this increased titer could be attributed to an additional interaction with *T. reesei* mCherry in the co-cultivation. However, to prove this, the feeding rate in the co-cultivations has to be precisely mimicked in axenic cultivation. Comparing the titer of this work with literature is only helpful to a limited extent. No actinorhodin standard for

quantification was available and is used in literature, leading to highly different values depending on the used photometer.

4.4 Conclusion

In this chapter, the glucose-dependent pigment formation by *S. coelicolor* was thoroughly investigated in different scales. It was showcased that a certain glucose release rate is required for a natural product formation in the form of pigments. The evaluation of MTP experiments with cellulose hydrolysis in axenic cultivations of *S. coelicolor* was validated with data from STR fed-batch investigations. These experiments successfully mimicked the carbon release in the co-cultivation with the cellulolytic fungus *T. reesei* mCherry. Based on the obtained data, a theoretical model of this co-cultivation can be established in future studies for the elaboration of the glucose release-dependent pigment formation. Furthermore, the samples of the presented co-cultivations could also be analysed for other natural products. Therewith, a time-resolved investigation of the natural product profile could be performed for different population compositions in the co-cultivations.

Parts of the following chapter have been published previously in

[§]Steinhoff, H.; [§]Finger, M.; Osthege, M.; Golze, C.; Schito, S.; Noack, S.; Büchs, J.; Grünberger, A.; *Experimental k_S estimation: A comparison of methods for Corynebacterium glutamicum from lab to microfluidic scale.* Biotechnology and Bioengineering, 2023, 120, 1288-1302.

[§]Both authors contributed equally to the publication

For clarity, experimental results of this publication obtained by Heiko Steinhoff (Multiscale Bioengineering, Bielefeld University, Bielefeld, Germany) and other parties were excluded from this thesis.

Lukas Hartmann (AVT - Biochemical Engineering, RWTH Aachen University, Aachen, Germany) assisted in the experiments conducted for the k_S estimation of *T. reesei* in chapter 5.3.3. Svenja Battling (AVT - Biochemical Engineering, RWTH Aachen University, Aachen, Germany) performed the cultivations for the k_S estimation of *Gluconobacter oxydans* presented in chapter 5.3.3. These parts have not been published previously.

5 Respiratory estimation of the substrate affinity

5.1 Background

The growth rate μ is a central parameter for population dynamics in co-cultivation processes. In order to predict microbial growth behaviour, Monod [103] established the first growth kinetic model in 1949, while considering the bioavailability of the substrate according to equation (4). Within this empirical relationship, k_S denotes the affinity of a bacterium towards a corresponding substrate *S* with the concentration c_s and marks the concentration where half of the specific maximum growth rate μ_{max} is reached [104].

$$\mu = \mu_{max} \cdot \frac{c_s}{c_s + k_S} \tag{4}$$

The growth of cells in bioprocesses is affected by biological, chemical and physical factors [105]. In large-scale bioreactors, gradients of the substrate, dissolved gases and pH occur through limiting capacities of motors, resulting in reduced input of power per volume, increased mixing times, and reduced k_La values [106–109]. Hence, if the consumption rates of components required by the cells are higher than their supply, limiting conditions are present. This can lead to stress responses, which have a substantial impact on the yield and quality of the target product [107]. Therefore, the access to precise k_S values is urgently required to model complex substrate gradients occurring within bioreactors by computational fluid dynamics. Additionally, k_S values are necessary to adjust the steady-state concentration of a carbon source, especially in bioprocesses operated in chemostat mode, to secure an efficient conversion of substrate into biomass [110].

State-of-the-art estimation of k_S is based on measuring specific substrate uptake rates q_s within the exponential growth phase [111]. Uptake rates q_s are determined as a function of substrate concentration c_s and correspond to the ratio of growth rate μ to the biomass yield $Y_{X/S}$ in accordance with equation (5). This lays the foundation to estimate k_S by incorporating the Monod expression (4) and rearranging for k_S (6) [112]. The approach can be extended for chemostat cultivations under the condition that no residual concentration is present in the effluent by replacing the substrate concentration c_s with the feed concentration $c_{s,feed}$, as well as the growth rate with the set dilution rate *D* (7) [113].

$$q_s = \frac{\mu}{Y_{X/S}} \tag{5}$$

$$k_s = c_s \cdot \left(\frac{\mu_{max}}{q_s \cdot Y_{X/S}} - 1\right) \tag{6}$$

$$k_s = c_{s,feed} \cdot \left(\frac{\mu_{max}}{D} - 1\right) \tag{7}$$

Mainly three methods are reported in the literature to determine uptake rates q_s, including HPLC [114], enzymatic assays [113] or liquid scintillation counting [115]. However, liquid scintillation counting is only applicable if a labelled substrate such as ^{14}C glucose is used. Alternative approaches to estimate the k_S value are to measure the oxygen uptake rate *OUR* or the oxygen transfer rate *OTR* of aerobic growing cells, which correlates to growth [58, 116]. With the biomass concentration c_X and the biomass yield on oxygen $Y_{X/O2}$ the k_S can be estimated according to equation (8).

$$k_s = c_s \cdot \left(\frac{\mu_{max} \cdot c_X}{OUR \cdot Y_{X/O_2}} - 1\right) \tag{8}$$

Respirometry methods for the estimation of kinetic parameters have been used more frequently and can deliver similarly precise k_S estimations in comparison to established chemostat methods [117, 118]. These methods often rely on experiments in a respirometer but can also be conducted *in situ* through pulse respirometry [119, 120].

Reported k_S values are scarce even for prominently used organisms. *Corynebacterium. glutamicum* is recognized as a model organism in bioprocess engineering and industrial microbiology for its broad capabilities as a producer of value-added goods like amino acids [121], organic acids [122], polymer precursors [123], aromatic chemicals [124], and proteins [125]. Moreover, *C. glutamicum* stands out for its robustness in large-scale applications [113, 126]. However, even for this industrial-relevant organism, only a few published k_S values are available regarding glucose [113, 115, 127]. As stated by Kovárová-Kovar and Egli, this is due to analytical difficulty in monitoring substrates at growth-controlling concentrations [128]. The applied state-of-the-art methods for a high precision k_S estimation are technically very complex, and they primarily provide merely extrapolated values if liquid scintillation counting was not used.

Hence, a fast and straightforward respiratory method is presented for the estimations of k_S values using *C. glutamicum* as a model organism. The newly developed micro(µ)-scale Transfer rate Online Measurement (µTOM) [54] device for high-throughput respiratory activity measurements is utilized. The substrate-limited respiratory activity (sl-RA) monitoring method determines the change in the OTR after spiking a defined glucose concentration, which correlates with the growth rate for aerobic-growing cells. The estimated k_S values are compared with literature values. Additionally, k_S estimations for the filamentous growing fungi *T. reesei* on glucose as well as for a modified *Gluconobacter oxydans* strain on fructose, are provided. Due to an incorporated plasmid, the *G. oxydans* strain can convert fructose to 5-ketofructose by oxidation with the membrane-bound fructose dehydrogenase (FDH) enzymes originally from *Gluconobacter japonicus* [129]. It was tested whether this oxidation reaction could also be examined with the proposed method and whether an affinity for fructose can be determined.

5.2 Material and methods

The strains *C. glutamicum* ATCC 13032, *T. reesei* RUT-C30 and *G. oxydans* 621H Δ*hsdR*, containing the plasmid p264-FDH-ST (*G. oxydans fdh*) developed by Siemen et al. (2018), were used for experiments presented in this chapter [129]. The *G. oxydans fdh* strain has genes on the plasmid encoding for the membrane-bound FDH and a kanamycin resistance [129–131].

Main cultivations of *C. glutamicum* were performed with modified CGXII medium [132], containing 20 $g \cdot L^{-1}$ $(NH_4)_2SO_4$, 1 $g \cdot L^{-1}$ K_2HPO_4, 1 $g \cdot L^{-1}$ KH_2PO_4, 5 $g \cdot L^{-1}$ urea, 13.25 $mg \cdot L^{-1}$ $CaCl_2 \cdot 2H_2O$, 0.25 $g \cdot L^{-1}$ $MgSO_4 \cdot 7H_2O$, 10 $mg \cdot L^{-1}$ $FeSO_4 \cdot 7H_2O$, 10 $mg \cdot L^{-1}$ $MnSO_4 \cdot H_2O$, 0.02 $mg \cdot L^{-1}$ $NiCl_2 \cdot 6H_2O$, 0.313 $mg \cdot L^{-1}$ $CuSO_4 \cdot 5H_2O$, 1 $mg \cdot L^{-1}$ $ZnSO_4 \cdot 7H_2O$, 0.2 $mg \cdot L^{-1}$ biotin, 37.5 $mg \cdot L^{-1}$ citrate, 42 $g \cdot L^{-1}$ 3-(N-morpholino)propanesulfonic acid (MOPS) and 10 $g \cdot L^{-1}$ glucose, unless stated otherwise. Similar to previous studies, PCA was replaced by citrate as an iron chelator [133]. Citrate as a potential available carbon source can only be metabolized by *C. glutamicum* if the saline concentration of NaCl is at least 1 $g \cdot L^{-1}$ [134, 135]. For the *T. reesei* main cultivations, LNP medium, as described in 2.2.2, was used with 5 $g \cdot L^{-1}$ glucose and without α-cellulose. The *G. oxydans fdh* main cultivations were conducted with a complex medium containing 5 $g \cdot L^{-1}$ yeast extract, 2.5 $g \cdot L^{-1}$ $MgSO_4 \cdot 7H_2O$, 1 $g \cdot L^{-1}$ $(NH_4)_2SO_4$, 1 $g \cdot L^{-1}$ KH_2PO_4 similar to Richhardt et al. (2013) [136]. The medium was supplemented with 50 $\mu g \cdot mL^{-1}$ kanamycin.

Pre-cultures for inoculation with *C. glutamicum* were performed with CGXII medium containing 10 $g \cdot L^{-1}$ glucose as the sole carbon source. The main culture was inoculated with 5 (v/v) % from the stationary phase pre-culture. The *T. reesei* cultivation was inoculated with 10^6 $spores \cdot mL^{-1}$. For *G. oxydans fdh* pre-cultures, the same medium as for the main culture was used with additional 80 $g \cdot L^{-1}$ mannitol and 50 $\mu g \cdot mL^{-1}$ cefoxitin supplemented. The main culture was inoculated with centrifuged pre-culture cells to an OD_{600} of 1. All pre-cultures were performed in 250 mL shake flasks within a RAMOS device at a temperature of 30 °C, a shaking speed of 350 rpm and a shaking diameter of 50 mm.

For the respiratory estimation of the k_S values, deepwell MTPs Riplate RW (Ritter GmbH, Schwabmünchen, Germany) with 96 wells were used. The OTR of every well was monitored online with the µTOM (Figure 17A) [54]. All wells were filled with 1 mL of inoculated culture. Cultivations for *C. glutamicum* and *G. oxydans fdh* were performed at a temperature of 30 °C, a shaking speed of 800 rpm and a shaking diameter of 3 mm. The *T. reesei* cultivation was conducted with a temperature of 30 °C, a shaking speed of 350 rpm and a shaking diameter of 50 mm. After the initial batch cultivations, 100 µL of the glucose or fructose solutions with different concentrations were spiked into each well of the MTP (Figure 17B). This resulted in a theoretical filling volume of 1.1 ml per well with initially set glucose and fructose concentrations. A multi-channel multi-stepper pipette Eppendorf Research pro (Eppendorf, Hamburg, Germany) was used to spike all wells 2 min before the next OTR measurement phase started. The first 30 s of the measurement phase of the µTOM device were cut-off, and OTRs were determined by the oxygen partial pressure decrease within the next 2 min. The end of the initial batch and depletion of the main carbon source was indicated by a rapid decrease in the OTRs (Figure 17C). In contrast, the glucose or fructose spike resulted in a concentration-dependent fast increase of the OTR. The resulting OTRs after the spike with 0.0 $mg \cdot L^{-1}$ of glucose or fructose were subtracted from all other resulting OTRs. A regression of these values to the Monod equation was performed with OriginPro (OriginPro 2020 9.7.0.188; OriginLab Corporation) to estimate the k_S value.

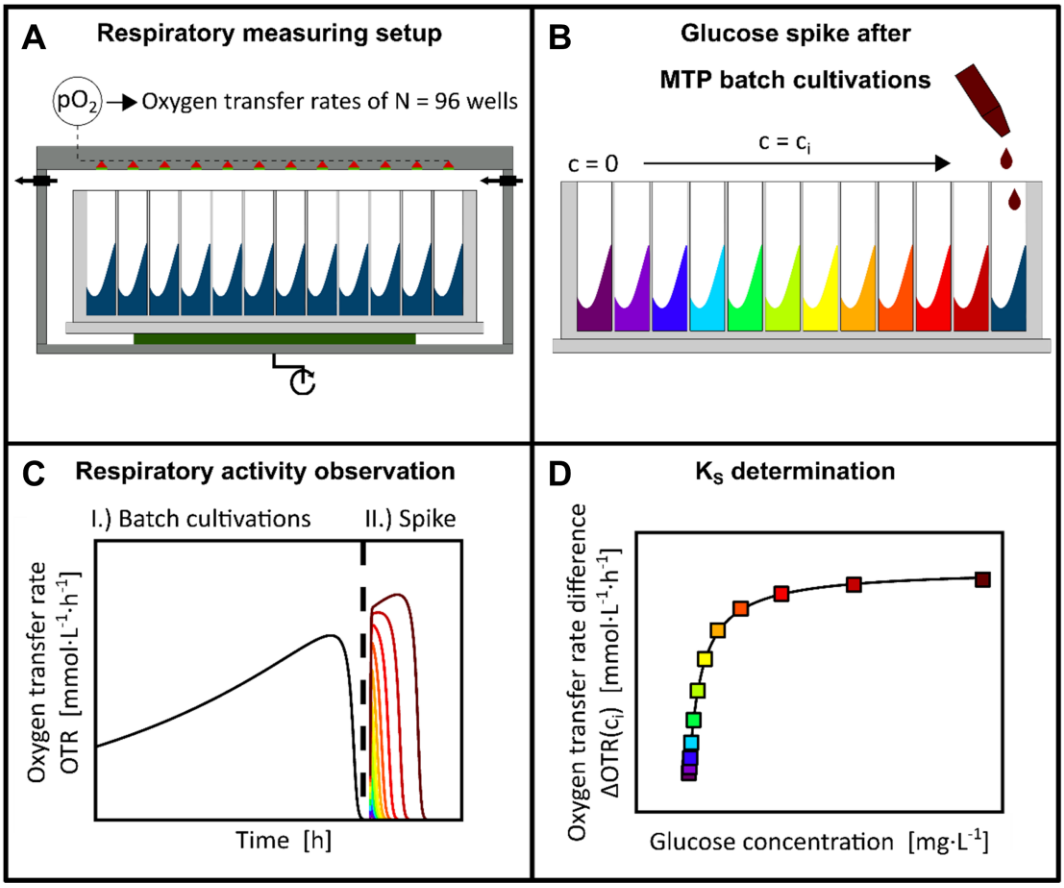

Figure 17. Experimental setup and workflow for estimating the k_S of microbial cells with substrate-limited respiratory activity monitoring (sl-RA). (**A**) Micro(µ)-scale Transfer rate Online Measurement device (µTOM) for 96-deepwell microtiter plates. The figure for the µTOM device was adapted from Dinger et al. (2022) [54]. (**B**) Spike of varying substrate concentrations after the termination of the batch cultivations with 96 replicates. (**C**) Observation of the substrate-dependent oxygen transfer rates. (**D**) K_S determination based on Monod-type respiratory response.

5.3 Results and discussion

5.3.1 Theoretical background and k_S estimation for *Corynebacterium glutamicum*

For k_S estimations, biomass growth has to be monitored, and information on substrate concentrations is required. With the time-resolved data, the Monod equation (4) can be fitted and k_S estimated. However, high-quality time-resolved biomass concentration, as well as substrate concentration data, are not easily obtained. Therefore, for the proposed sl-RA method, the substrate concentration is initially set by spiking with a substrate solution. Instead of the time-resolved biomass concentration, the oxygen transfer rate *OTR* is observed. The change in dissolved oxygen dO_L/dt is assumed to be negligible compared to the oxygen uptake rate *OUR,* similar to Mühlmann et al. (2018) and Ihling et al. (2021) [137, 138]. Hence, the *OTR* is used equivalently to the *OUR* according to equation (9). Data by Graf et al. (2020) indicate a linear correlation between growth rates (0.2-0.4 h^{-1}) and oxygen uptake rates and, therefore, a constant $Y_{X/O2}$ [113]. However, this assumption is not necessarily valid at very low growth rates. Growth rates can be quantified only due to this simplified linearity assumption of the growth rate and the OTR, as well as a negligible change of the biomass concentration c_X within the observed time frame of 2 min (10). Thereby, the k_S value can be estimated directly with the glucose concentration-dependent OTR and using a regression of the Monod equation.

$$OTR = OUR \quad s.t.\ OUR \gg \frac{dO_L}{dt} \tag{9}$$

$$\mu = \frac{OTR \cdot Y_{X/O_2}}{c_X} \tag{10}$$

The respiratory estimation of the k_S was tested for the model organism *C. glutamicum* at first. Initially, 96 batch cultivations were performed simultaneously in a 96-deepwell plate. The online monitored OTR of these cultivations shows an increase and, therefore, the initial growth of *C. glutamicum* for the first 3 h (Figure 18A). The rapid decrease of the OTR afterwards points to the depletion of the main carbon source glucose, which was only supplied with 1 $g \cdot L^{-1}$. The utilization of alternative carbon sources leads to a low OTR of around 1 $mmol \cdot L^{-1} \cdot h^{-1}$, which is also progressively decreasing after 3.5 h (Figure 18A). As soon as glucose is spiked into the wells, growth, according to Monod, sets in.

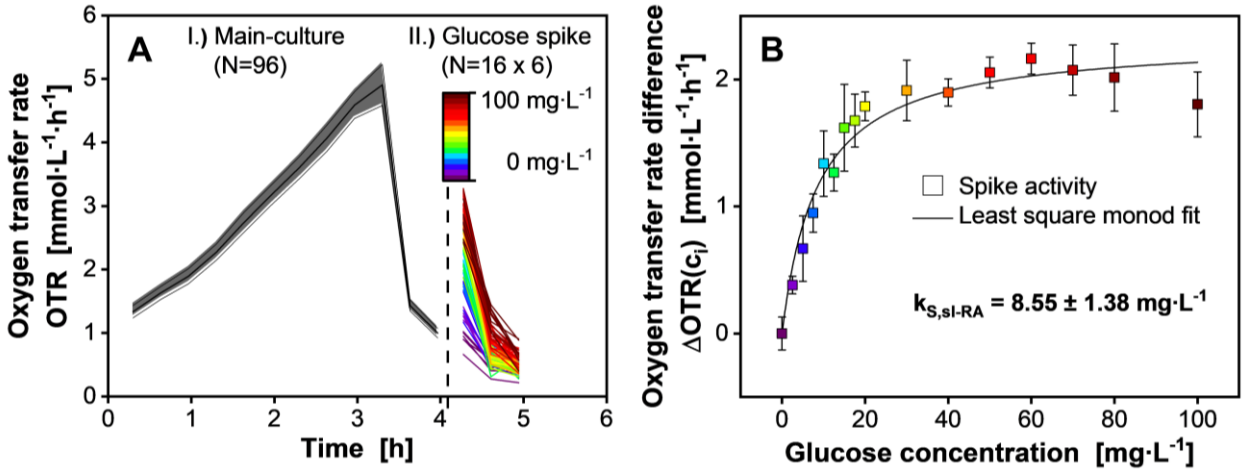

Figure 18. Substrate-limited respiratory activity estimation (sl-RA) of the k_S for *Corynebacterium glutamicum* with glucose spiked batch cultivations. (**A**) Oxygen transfer rates of *C. glutamicum* cultivations (N=96) spiked with 16 different glucose concentrations (N=6) after glucose depletion of the main culture. (**B**) Correlation of the resulting oxygen transfer rate difference after the spike to the respective glucose concentrations with N=6. Culture conditions: 96-deepwell microtiter plate, V_L = 1/1.1 mL, n = 800 rpm, d_0 = 3 mm, T = 30 °C, CGXII medium without PCA, spike with 100 µL of 16 different glucose concentrations.

Only for the glucose spike concentration of 0 mg·L^{-1} a lower OTR after spiking was measured with 0.9 ± 0.1 mmol·L^{-1}·h^{-1}. The differences between the OTR reference value at 0 mg·L^{-1} and all other OTRs were calculated (Figure 18B). For spiked glucose concentrations of at least 20 mg·L^{-1}, a constant ΔOTR of 2 mmol·L^{-1}·h^{-1} is noticeable. The decreased ΔOTR value for the condition with a glucose concentration of 100 mg·L^{-1} could be subject to measurement variance or caused by a physiological explanation due to overflow metabolism. However, as this chapter focuses on the k_S value, this trend was not further investigated here. For glucose concentrations of 20 mg·L^{-1} to 0 mg·L^{-1}, the ΔOTR is decreasing. With the regression to the Monod equation, a k_S of 8.55 ± 1.38 mg·L^{-1} was obtained with a coefficient of determination of R^2 = 0.95.

5.3.2 Comparison with the literature

The presented method within this chapter yielded a logical k_S value for *C. glutamicum*. However, the value has to be compared with the literature to make a qualitative statement about the respiratory method. Already published k_S values (Table 1) for *C. glutamicum* on glucose range from

0.52 - 7.68 $mg \cdot L^{-1}$, including given standard deviations. Lindner et al. (2011) [115] obtained a value of 2.52 $mg \cdot L^{-1}$, and Uhde et al. (2013) [127] 2.17-2.70 $mg \cdot L^{-1}$ by applying liquid scintillation counting. Both values match very well. However, the used protocol of both was highly similar. In these studies, different concentrations of ^{14}C labelled glucose were supplied to previously washed *C. glutamicum* cells. After defined time intervals, cell samples are collected and analyzed with a scintillation counter. The data indicate a high reproducibility and very precise monitoring of glucose uptake rates. Nonetheless, the required equipment and components impede a broad and fast application of this method. In contrast, Graf et al. (2020) [113] utilized enzymatic assays to determine glucose concentrations and deduct glucose consumption rates in batch and chemostat cultivations. Based on a mathematical fit, a k_S of 4.39 ± 3.20 $mg \cdot L^{-1}$ in batch and 0.97 ± 0.45 $mg \cdot L^{-1}$ in chemostat cultivation has been estimated.

While an enzymatic assay for glucose has a detection limit of 400 $\mu g \cdot L^{-1}$, it provides an accurate and fast estimation of residual glucose concentration. However, if the expected affinity towards glucose is higher and consequently below the detection limit, liquid scintillation counting or HPLC is necessary. Interestingly, the authors note different k_S values for batch and chemostat cultivations but do not elaborate on the reason because the work had a different focus. This differentiation of batch and continuous cultivation for k_S value estimation is often neglected. However, the k_S value is subject to the cell state, duration of cultivation as well as environmental conditions and, therefore, can vary between batch and chemostat cultivations. Reasons for the deviations could include the washout of slower-growing cells due to the set dilution rate or the continuous supply of PCA as a secondary carbon source during chemostat cultivation [139].

In addition to the aforementioned established methods, sl-RA provides a benefit due to the fast and straightforward estimation approach. The drawback is a rather low accuracy of the k_S estimation (8.55 ± 1.38 $mg \cdot L^{-1}$) and suggests that the method is not advisable for investigations below concentrations of 10 $mg \cdot L^{-1}$. The slightly increased k_S value for the sl-RA compared to literature values is partially explained by an inherent overestimation due to the measurement principle. Oxygen partial pressure values are averaged within the required measurement time frame for OTR determination. However, for the k_S estimation, the initial glucose concentrations are assumed. This effect becomes more prominent with further increased lengths of the measurement phase (Appendix Figure A18). This

overestimation depends on the sharpness of the switch from exponential to stationary phase and, therefore, on the k_S value. Nonetheless, for initial estimations or situations where the k_S value is expected to be somewhat in the higher $mg \cdot L^{-1}$ range, sl-RA can be taken into consideration due to the reduced labour intensity.

Table 1. Overview of substrate affinities of *Corynebacterium glutamicum* towards glucose.

Method	Analytics	k_S [$mg \cdot L^{-1}$]	Mode	Reference
^{14}C uptake rate	Liquid Scintillation counting	2.52	Batch	Lindner et al. (2011) [115]
^{14}C uptake rate	Liquid Scintillation counting	2.17 – 2.70	Batch	Uhde et al. (2013) [127]
Consumption rate	Enzymatic assay	4.39 ± 3.20	Batch	Graf et al. (2020) [113]
Consumption rate	Enzymatic assay	0.97 ± 0.45	Chemostat	Graf et al. (2020) [113]
sl-RA	µTOM	8.55 ± 1.38	Batch	This work

5.3.3 Application for other organisms and enzymatic systems

The validity of the proposed method was further tested with experiments for the organisms *T. reesei* RUT-C30 and *G. oxydans fdh* (Figure 19). However, as the modified *G. oxydans fdh* can oxidize fructose to 5-ketofructose, rather the k_S of the enzymatic system was evaluated regarding fructose.

The filamentous fungus *T. reesei* grows in a dispersed form at the given conditions. Hence, an exponential growth pattern can be assumed. Cell pellet formation was not observed, which could lead to nutrient gradients across the pellet radius as well as in a resulting cubic growth pattern [140]. This has to be considered if pellet-forming organisms were to be tested. Nonetheless, for *T. reesei,* a substrate-dependent increase of the OTR was noticeable (Figure 19A), similar to the *C. glutamicum* experiment. The different heights resulted from the different amounts of biomass before the glucose spike. For some cultivations of *T. reesei*, a slightly longer batch phase could be noticed. This led to varying final biomass and high standard deviations. Therefore, the results for 12.5, 60, 70 and 80 $mg \cdot L^{-1}$ were excluded entirely from the k_S estimation based on a standard deviation exceeding 0.35 $mmol \cdot L^{-1} \cdot h^{-1}$. A k_S of 12.69 ± 3.25 $mg \cdot L^{-1}$ for *T. reesei* on glucose was estimated. The information in the literature is limited, and for comparison, only a k_S value of 24 ± 19 $mg \cdot L^{-1}$ measured in chemostat

cultivation by Minty et al. (2013) can be stated [141]. The comparable result proves the validity and showcases the sl-RA method's good accuracy. In the test of *G. oxydans fdh* with fructose for k_S estimation (Figure 19B), the determined OTR only represents microbial growth to a very limited extent, as the majority of oxygen is utilized for fructose oxidation. This becomes especially evident considering the approximate biomass yield on oxygen $Y_{X/O2}$ (0.226 mol·mol^{-1}) as well as the product yield on oxygen $Y_{P/O2}$ (1.532 mol·mol^{-1}) [142]. Hence, the estimated k_S value of 1.00 ± 0.10 g·L^{-1} represents the oxidation reaction and is multifold higher compared to values for glucose and microbial growth. In comparison, for the purified FDH, which originates from *G. japonicus* NBRC3260 (formerly *G. industrius* IFO3260), a Michaelis-Menten constant of approximately 1.8 g·L^{-1} determined at a pH of 4.5 is stated [130]. The results are in good agreement considering the completely different systems and chosen parameters.

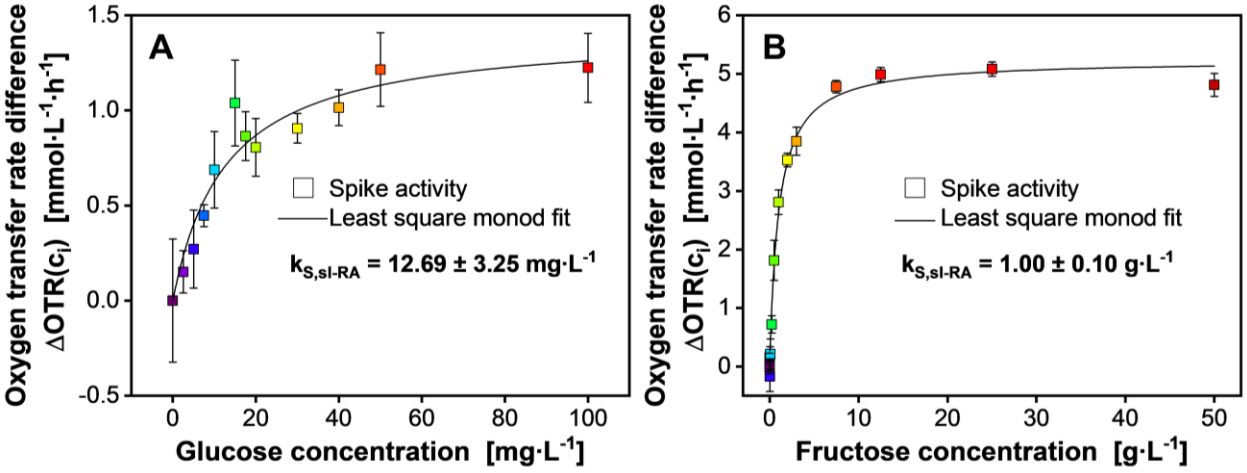

Figure 19. Results for the respiratory k_S estimation for (**A**) *Trichoderma reesei* RUT-C30 on glucose and (**B**) *Gluconobacter oxydans fdh* on fructose. Each experiment was spiked with 16 different glucose or fructose concentrations (N=6) after carbon depletion of the main culture. Due to high standard deviations greater than 0.35 mmol·L^{-1}·h^{-1}, the results for the glucose concentrations of 12.5, 60, 70 and 80 mg·L^{-1} were excluded for the *T. reesei* experiment. Results for the fructose concentrations of 4 and 5 g·L^{-1} were excluded for the *G. oxydans fdh* experiments since no increase in oxygen transfer rates were monitored after the spike. Culture conditions: 96-deepwell microtiter plate, V_L = 1 mL, n = 800 rpm, d_0 = 3 mm, T = 30 °C, spike with 100 µL of 16 different glucose or fructose concentrations.

5.4 Conclusion

In this chapter, sl-RA was presented as a new respiratory method for the estimation of k_S values. The value obtained for the model organism *C. glutamicum* with glucose as a limiting substrate was compared to literature values. Although the method is not as precise and accurate as some conventional methods, sl-RA is an innovative method providing simple and fast initial k_S values. Further, sl-RA was demonstrated to be applicable for filamentous growing organisms such as *T. reesei*. Additionally, the experiment with *G. oxydans fdh* and fructose highlights the utilization of this method for other substrates and incorporated enzymatic systems depending on oxidation reactions. However, it has to be further investigated, whether the method can be utilized if the concerning substrate is not the primary carbon source and is not as tightly linked to oxygen consumption. Made assumptions might become invalid if the biomass yield on oxygen drastically changes. Nonetheless, if the k_S value for the main carbon source has to be estimated and no established procedure is suitable for the tested substrate, sl-RA could provide a useful alternative.

Parts of the following chapter have been published previously in

Finger, M.; Schröder, E.; Berg, C.; Dinger, R.; Büchs, J.; *Towards standardized solid medium cultivations: microbial online monitoring based on respiration activity*. Biotechnology Journal, 2023, 1-12.

Eliot Schröder (AVT - Biochemical Engineering, RWTH Aachen University, Aachen, Germany) assisted in the cultivations presented in chapter 6.3.3-6.3.5.

6 Respiration monitoring of cultivations on solid media

6.1 Background

Frequently, cultivations are conducted on solid and, especially, on agar media. These types of cultivations can be exploited, if liquid media are unsuitable for the organisms. Furthermore, agar cultivations are used for pre-cultures, the production of spores or other applications, such as antibiotic susceptibility testing. Nonetheless, in contrast to liquid cultivations, information about the details of these agar cultivations is scarce. Typically, a subjective examination of the macroscopic appearance of cultivations on an agar surface is carried out. A more objective evaluation can be achieved by different automated optical methods. These optical methods and the applied image analysis tools, such as OpenCFU, ScanLag or ColTapp, depend on distinguishable single colonies contrasting the background [143–145]. The fast determination of colony counts, positions, sizes and growth kinetics are advantages of the optical methods. Additional information can be obtained by utilizing the PreSens USB-microscope "VisiSens" in combination with fluorescent sensor foils. These foils are available for monitoring the oxygen and pH value. Two-dimensional distributions and temporal changes can be visualized. Therewith, Tschiersch et al. (2012) determined the oxygen consumption for *E. coli* colonies on lysogeny broth agar (LB-agar) [146]. The application is very suitable for determining oxygen gradients developing around colonies. Thereby, the heterogeneity of the oxygen distribution across a single colony can be elucidated, which leads, in combination with the heterogeneous substrate availability, to different phenotypes. However, due to the fluorophore used, the foil is limited to the detection of oxygen and is not broadly applicable for regular respiration quantification in agar cultivations. Carbon dioxide cannot be monitored, which negates an application for e.g. anaerobic cultivations.

For cultivations in liquid media, the gas consumption and production are typically monitored in the off-gas of the respective cultivation vessel. In Erlenmeyer flasks, the monitoring can be conducted, for example, with the Circulation Direct Monitoring and Sampling System (CDMSS), the BCpreFerm system (BlueSens, Herten, Germany), the Transfer-rate Online Measurement (TOM) system (Kuhner Shaker, Herzogenrath, Germany) or the Respiration Activity MOnitoring System (RAMOS) [51, 52, 147]. The RAMOS monitors the changes in the partial pressure of a gas within a defined cultivation vessel's gas phase. The changes in the partial pressures allow for the calculation of mass transfer rates between the gas and the liquid phase for the respective gases. The RAMOS was continuously adapted

to allow for the online monitoring of several gases, such as oxygen, carbon dioxide, and ethylene, as well as total gas production [52, 148, 149]. The system was extensively utilized for cultivations in liquid media while correlating gas transfer rates with substrate uptake, growth patterns, and product formation [45, 150, 151].

To the best of our knowledge, the RAMOS technology has never been used for respiration monitoring of cultivations on solid media. Potential reasons for this could be lower gas consumption and production rate, in contrast to liquid cultivations, as well as diffusion gradients forming in the gas phase leading to inaccurate measurements. A circulation of the gas phase, as introduced by Takahashi et al. (2017) for the CDMSS, could prevent the formation of gradients [147]. Hence, in a proof-of-concept, this chapter showcases that a modified version of the RAMOS technology with gas circulation by a microfluidic piezo-membrane pump enables the respiration monitoring of agar cultivations. Furthermore, the system allows for reliable measurements even for cultures forming large films or lawns at which conventional optical methods are less applicable. To highlight potential application scenarios, four different exemplary use cases are demonstrated in this chapter (Figure 20): The respiration monitoring of agar cultivations enables the determination of colony forming units (Figure 20A), the evaluation of antibiotic disk diffusion tests (Figure 20B), quality control for spore production or for pre-cultures (Figure 20C), and an assessment of the metabolic activity (Figure 20D). In addition, references from the literature are given to outline how respiration monitoring can benefit research using solid media.

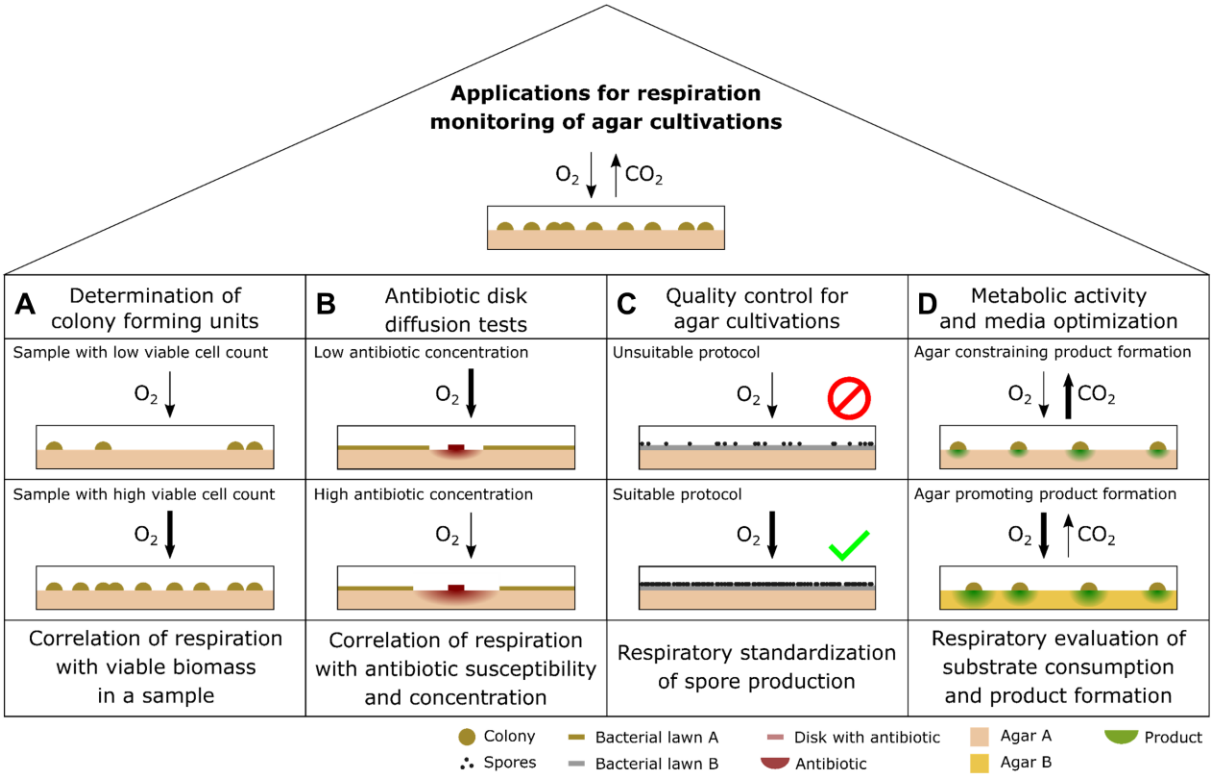

Figure 20. Exemplary fields of application, in which respiration monitoring of agar cultivations may be advantageous. (**A**) Oxygen uptake increases with the viable biomass and, thereby, the colony forming units in a sample. (**B**) Oxygen uptake decreases with the antibiotic concentration due to the diffusion of the respective antibiotic into the adjacent agar (red zone). (**C**) Oxygen uptake patterns can be utilized as a quality indicator to secure reproducible cultivations, for example, for the production of spores on solid medium. (**D**) The ratio of oxygen uptake and carbon dioxide evolution can indicate formation of certain products (green zone).

6.2 Material and methods

6.2.1 Microorganisms

The applicability of respiration monitoring for agar cultivations was tested with the following microorganisms: *E. coli* BL21, *Pseudomonas putida* KT2440, *S. coelicolor* A3(2), *Saccharomyces cerevisiae* WT, *Pichia pastoris* WT and *T. reesei* RUT-C30.

6.2.2 Media composition and cultivation procedures

LB-agar was used for cultivations with *E. coli* and *P. putida*. It consisted of 20 $g \cdot L^{-1}$ agar (Kobe I, Carl Roth, Karlsruhe, Germany), 10 $g \cdot L^{-1}$ tryptone (Pancreatic digest from casein, Carl Roth, Karlsruhe, Germany), 10 $g \cdot L^{-1}$ sodium chloride (MilliporeSigma, Burlington, USA) and 5 $g \cdot L^{-1}$ yeast extract (Carl Roth, Karlsruhe, Germany). To compare the respiratory trajectory, *E. coli* cultivations were also performed in 250 mL Erlenmeyer flasks with liquid LB-medium, for which no agar was added. Liquid cultivations were performed with a filling volume of 20 mL, a shaking frequency of 250 rpm and a shaking diameter of 50 mm. Additionally, *E. coli* cultivations were performed on a modified Wilms-MOPS medium with 20 $g \cdot L^{-1}$ agar (Kobe I, Carl Roth, Karlsruhe, Germany) [152, 153]. The mineral medium was supplemented with 1 $g \cdot L^{-1}$ glucose, 2 $g \cdot L^{-1}$ lactose and 4 $g \cdot L^{-1}$ glycerol as carbon source, and the pH was adjusted to a pH of 7.4 with 5 M NaOH. Experiments for *S. coelicolor* were conducted with SFM-agar, as stated in chapter 2.2.1. Yeast extract peptone dextrose agar (YPD-agar) consisted of 20 $g \cdot L^{-1}$ peptone (Tryptic digest from casein, Carl Roth, Karlsruhe, Germany), 20 $g \cdot L^{-1}$ glucose (Carl Roth, Karlsruhe, Germany), 15 $g \cdot L^{-1}$ agar as well as 10 $g \cdot L^{-1}$ yeast extract (Carl Roth, Karlsruhe, Germany) and was used for cultivations with *S. cerevisiae* and *P. pastoris*. For *T. reesei* cultivations, 39 $g \cdot L^{-1}$ of potato dextrose agar (PD-agar) (Carl Roth, Karlsruhe, Germany) powder was used. The pH of the complex media was not adjusted. All media were autoclaved at 121 °C for 20 minutes. After autoclaving, the agar medium was liquid. While liquid, 20 mL of the respective agar medium was carefully pipetted into 250 mL Erlenmeyer flasks. Occurring bubbles were removed by manual punctuation with a sterile needle to prevent an uneven agar surface. The agar was cooled at room temperature and, therefore, solidified. For the inoculation, 200 µL of the respective organism stock solution was spread on the solidified agar with a Drigalski spatula. For the optical density (OD) corresponding to the viable cell count within a sample, the absorbance of the inoculum was measured at a wavelength of 600 nm and is stated in arbitrary units (a.u.). These measurements were either conducted with a Genesys 20 photometer (Thermo Scientific, Darmstadt, Germany) or with an Ultraspec 2100 UV-Visible spectrophotometer (biochrom, Holiston USA). Cultivations for *E. coli* were performed at 30, 33.5 and 37 °C. All other organisms were cultivated at 30 °C.

After the cultivations were conducted, water was added to the agar within the Erlenmeyer flasks. The Erlenmeyer flasks were then autoclaved at 121 °C for 20 minutes to inactivate the biological material. The temperature increase resulted in liquifying of the agar and mixing with the water. Due to the

reduced agar concentration, the mixture did not solidify any more after cooling, and the Erlenmeyer flasks were cleaned similarly to liquid cultivations.

For the agar diffusion tests, Whatman No 1 filter paper (Whatman plc, Little Chalfont, United Kingdom) was stamped to receive filter disks with a diameter of 6 mm. The antibiotic tetracycline (Fluka, Buchs, Switzerland) was dissolved with 10 $g \cdot L^{-1}$ in water, sterile filtered and a tetracycline dilution series was prepared. The required amount of tetracycline was applied by pipetting 10 µL of the respective concentration from the dilution series on top of the filter disk. For comparison, the agar diffusion tests were also perfomed in Petri dishes without respiration monitoring, which were sealed with parafilm (Bemis, Neenah, USA).

6.2.3 Respiration monitoring of agar cultivations

All cultivations were monitored with modified versions of the Respiration Activity MOnitoring System (RAMOS) depicted in Appendix Figure A19 [51, 52]. Similar to Schulte et al. (2018), Munch et al. (2020) and Mann et al. (2021), a measurement loop is used to monitor the gas transfer rates in Erlenmeyer flasks [148, 149, 154]. The gas phase of each flask is continuously circulated through the respective measurement loop with approximately 20 $smL \cdot min^{-1}$, using microfluidic piezo-membrane pumps mp6-gas (Bartels Mikrotechnik, Dortmund, Germany). The measurement loop is equipped with an electrochemical oxygen sensor Max-250+ (Maxtec, Salt Lake City, USA), an infrared carbon dioxide sensor MSH-P-CO_2 (Dynament, Mansfield, England) and a differential pressure sensor type 26PCA (Maxwell Technologies, San Diego, USA). For the intermittently occurring measurement phases, the gas content of each flask is sealed by closing the in- and outlet 3/2-way flipper solenoid valves (Bürkert, Ingelfingen, Germany). Oxygen and carbon dioxide partial pressure $\frac{\Delta p_i}{\Delta t}$ changes were fitted linearly during the measurement phase. Thereby, with the available information about the total gas phase volume V_G, the agar surface area A, the temperature T and the gas constant R, the OTR' and CTR' could be calculated according to equations (11) and (12). The agar area was assumed to be equal to the inner area of the Erlenmeyer flask with 51.9 cm^2. In contrast, the respiration of cultivations with a liquid medium is calculated, as usual, as the volume-specific oxygen and carbon dioxide transfer rates [51, 52]. The respiratory quotient (RQ) was quantified by dividing the CTR' by the OTR' according to

equation (13). The measurement technique was described in detail by Anderlei et al. (2001, 2004) [51, 52].

$$OTR' = \frac{\Delta p_{O_2}}{\Delta t} \cdot \frac{V_G}{R \cdot T \cdot A} \quad (11)$$

$$CTR' = \frac{\Delta p_{CO_2}}{\Delta t} \cdot \frac{V_G}{R \cdot T \cdot A} \quad (12)$$

$$RQ = \frac{CTR'}{OTR'} \quad (13)$$

Additionally, oxygen sensor spots (PyroScience, Aachen, Germany) were utilized in combination with the RAMOS. Thereby, the potential heterogeneity in the gas phase and formation of an oxygen partial pressure gradient above the agar cultivations was studied. Sensor spots were glued to the Erlenmeyer flask wall at 2, 4 and 6 cm above the agar surface (Appendix Figure A20). The oxygen partial pressure was measured after a 2-point calibration with a fibre optic multiple analyte meter FireSting PRO (PyroScience, Aachen, Germany). The oxygen partial pressure data was used to calculate the OTR' according to equation (11) during the measurement phase of the RAMOS.

6.3 Results and discussion

6.3.1 Respiration monitoring for cultivations on agar medium allows tracking of the growth of *Escherichia coli* colonies

Gas uptake and evolution can lead to gradient formation of oxygen and carbon dioxide concentration above the cultures on solid media. These concentration gradients may result in an inaccurate determination of the real gas transfer rates. Hence, a homogenous gas phase is required for a successful respiration monitoring of microbial growth on agar.

In the applied RAMOS device, a convective gas flow is generated by a piezo-membrane pump, which circulates the gas phase of the Erlenmeyer flasks through a loop with oxygen, carbon dioxide and pressure sensors. To prove the successful homogenization of the gas phase, respiration measurements were conducted at different heights above the LB-agar during the cultivation of *E. coli* (Figure 21, Appendix Figure A20 and Appendix Figure A21).

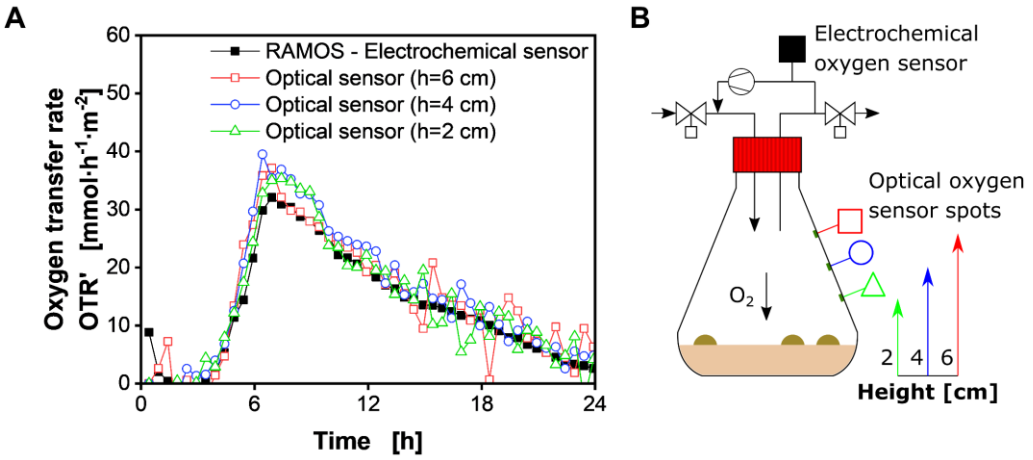

Figure 21. Comparison of the (**A**) area-specific oxygen transfer rates OTR' of an *Escherichia coli* BL21 cultivation on a solid LB-agar medium monitored with the (**B**) respiratory activity monitoring system (RAMOS) and optical oxygen sensor spots. The RAMOS is equipped with a gas circulation pump. Further details are depicted in Appendix Figure A19 and described in chapter 6.2.3. Sensor spots were glued to the inner flask wall at a height of 2 (green triangles), 4 (blue circles) and 6 cm (red squares). Culture conditions: Non-shaken 250 mL Erlenmeyer flasks, V_L = 20 mL, T = 37 °C, $V_{X,0}$ = 200 µL with OD of 10^{-1}.

Thereby, it was assessed if insufficient gas homogenization occurs and, thus, influences the measurement. The determined course of the oxygen partial pressure values over time of the cultivation can be found in Appendix Figure A21A. Despite a slight calibration offset, the general course of all measurements is highly similar. The measurements did not deviate by more than 1.7 hPa from each other in the last hour, when respiratory activity ceased. No influence of the measurement position on the online signal of the oxygen partial pressures could be noticed (Appendix Figure A21A, red, blue and green lines). The measurement with the electrochemical sensor in the RAMOS was less noisy compared to the optical sensors. Over a 5 min period without respiratory activity, the signal standard deviation was ±0.02 hPa for the electrochemical sensor. In contrast, the deviation for the optical sensors was ±0.11 hPa, ±0.10 hPa and ±0.25 hPa (2, 4 and 6 cm). The spikes occurring in regular intervals are due to the measurement principle of the RAMOS [51, 52]. The gas phase in the Erlenmeyer flask represents a closed system during the measurement phase by closing the in- and outlet valves. Therefore, depending on the oxygen uptake of the *E. coli* cultivation, the oxygen partial pressure decreases more or less rapidly. With this decrease, the OTR' can be determined (Appendix Figure A21B, grey area). After the measurement phase, the valves are opened. Gassing with an airflow

of 60 smL·min^{-1} leads to equilibration of the gas phase. The different intensities of the spikes, which indicate the oxygen partial pressure decrease during the measurement phase (Appendix Figure A21A), are represented by the OTR' values depicted in Figure 21A. Similar to the partial pressure trajectories, the heights of the measurement positions did not influence the calculated OTR'. The increased data scattering at low OTR' (Figure 21A) results from the noise of the oxygen partial pressure signal of the sensor spots [54]. The resulting OTR' signals start increasing after approximately 3 h, due to the growth and colony formation of *E. coli* (Figure 21A). After a rapid exponential increase, a peak value of 36.0 ± 3.1 mmol·h^{-1}·m^{-2} is reached after 6.9 ± 0.4 h. Thereafter, the OTR' steadily declines and reaches almost 0 mmol·h^{-1}·m^{-2} at 24 h. However, these findings solely indicate that the respiration monitoring is independent of the measurement height. For further validation, a visual comparison with biomass formation was conducted.

The observable increase in the OTR' (Figure 22A) over time is caused by biomass growth resulting in colony formation. To prove this, *E. coli* cultivations conducted on LB-agar in Erlenmeyer flasks were additionally monitored with a camera from below (Figure 22B). Frames taken during the cultivation are depicted in Figure 22C. Colony formation becomes noticeable once the OTR' increases exponentially. The OTR' reaches a peak at around 14 h, and subsequently, the OTR' steadily decreases. During the decreasing phase, the size of colonies is observed to remain similar. These observations can be explained by the competition for nutrients in the agar, which also depends on the initial inoculum density and the inoculum distribution on the agar. The inoculum density defines how many colonies are formed, whereas the distribution relates to the available space on the agar and, thus, the available nutrients. In liquid cultivations up to a scale of several dozen cubic meters, unicellular organisms experience homogenous environmental conditions due to good mixing. Here, the growth is dependent on the nutrient diffusion in the agar. Neighbouring colonies lead to a decreased nutrient availability and therefore, the colony sizes vary depending on the spatial proximity to other colonies. Similar colony size responses to other colonies' spatial proximity are reported in the literature [155, 156]. This effect is represented in the respiratory activity and is further illustrated in 6.3.2.

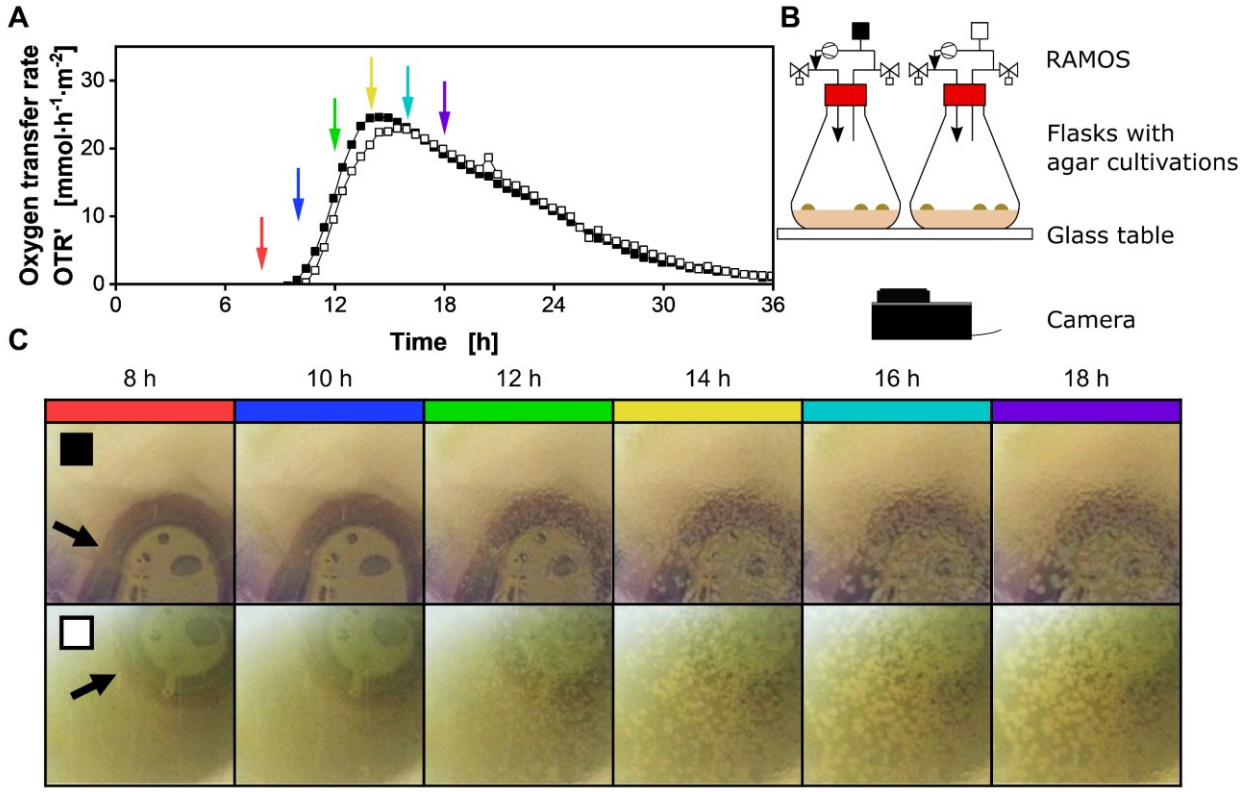

Figure 22. Cultivation of *Escherichia coli* BL21 on LB-agar in Erlenmeyer flasks. Two parallel agar cultures were monitored with the respiratory activity monitoring system (RAMOS). (**A**) Area-specific oxygen transfer rates OTR'. (**B**) Pictures were taken every minute of cultivation with a GoPro HERO4 camera from below. (**C**) Pictures at 8, 10, 12, 14, 16 and 18 h (coloured in the same way as the arrows in (A)) are depicted for the respective parallel measurements (filled and empty square symbols). The contrast of the pictures was increased by 40 % for a better visualization of colony formation. The round, grey and red cap of the RAMOS flasks (black arrows in (C)) can be seen in the background of the pictures. Culture conditions: Non-shaken 250 mL Erlenmeyer flasks, V_L = 20 mL, T = 33.5 °C, $V_{X,0}$ = 200 µL with OD of 10^{-3}, duplicate.

6.3.2 The inoculum density of *Escherichia coli* defines the trajectory of the respiratory activity

The viable cell count content or correlating colony forming units in a sample are crucial parameters for microbiological methods such as antimicrobial susceptibility testing [157]. Standard procedures to determine the cell count include plating a sample dilution on agar plates and counting the formed colonies [158]. However, not all organisms form defined colonies, and a suitable sample dilution is

necessary to allow colony counting. Hence, it was tested, whether the respiratory activity of such cultivations can assist in evaluating the viable cell count or colony forming units.

The initial inoculum density of *E. coli* for agar cultivations was varied over seven orders of magnitude at two different temperatures (Figure 23). At a high inoculum density and a temperature of 30 °C, *E. coli* colonies become indistinguishable (Figure 23A, black square). The OTR' data of these cultivations (Figure 23B, black squares) indicate a sharp peak resulting from a rapid initial biomass increase. With the decrease in the inoculum density, the colony count decreases, whereas the area between colonies increases (Figure 23A, red circle, blue inverted triangle and green diamond). This is in accordance with the observations in 6.3.1. Lowering the OD of the inoculum leads to a decline in the OTR' peak height and an increase in the peak broadness (Figure 23B). The OTR' was negligible for the lowest inoculum density (10^{-7} a.u. OD of inoculum). The OTR' of the cultivations performed at 37 °C (Figure 23C) indicates a similar pattern to the cultivations at 30 °C. However, the increased temperature resulted in faster growth and, therefore, an earlier and steeper increase in the OTR'. This also holds true for the time at which the OTR' peaks are reached at these temperatures. For the varying inoculation densities with an OD of 10^{-1}, 10^{-3} and 10^{-5}, the increase from 30 °C to 37 °C results in the OTR' peak to occur approximately 4.1, 5.1 and 9.1 h earlier, respectively. The faster growth can be attributed to the temperature optimum of *E. coli* at about 37 °C [159].

An increase in the colony count leads to decreasing space between the colonies and, therefore, nutrients in the surrounding of the colonies on the agar [160]. The radial growth of each colony depends on available nutrients. Fewer colonies can grow larger in size (Figure 23A). This prolonged radial growth of colonies is represented by a prolongation of the OTR' peak. In contrast to these cultivations on agar, the effect of spatial nutrient limitations does not occur in liquid cultivations. In smaller-scale liquid cultivations, unicellular organisms experience homogenous environmental conditions due to mixing. Hence, for liquid cultivations of *E. coli* in LB-medium, the variation of the inoculum density resulted in almost no change in the OTR trajectory (Appendix Figure A22). As the respiration activity varies with the utilized inoculum density, the time shift until an increase in the OTR' is noticeable could be applied for the quantification of viable cell count or colony forming units in a sample. Similarly, the general OTR' shape or characteristic values, such as the peak OTR' value, could be utilized.

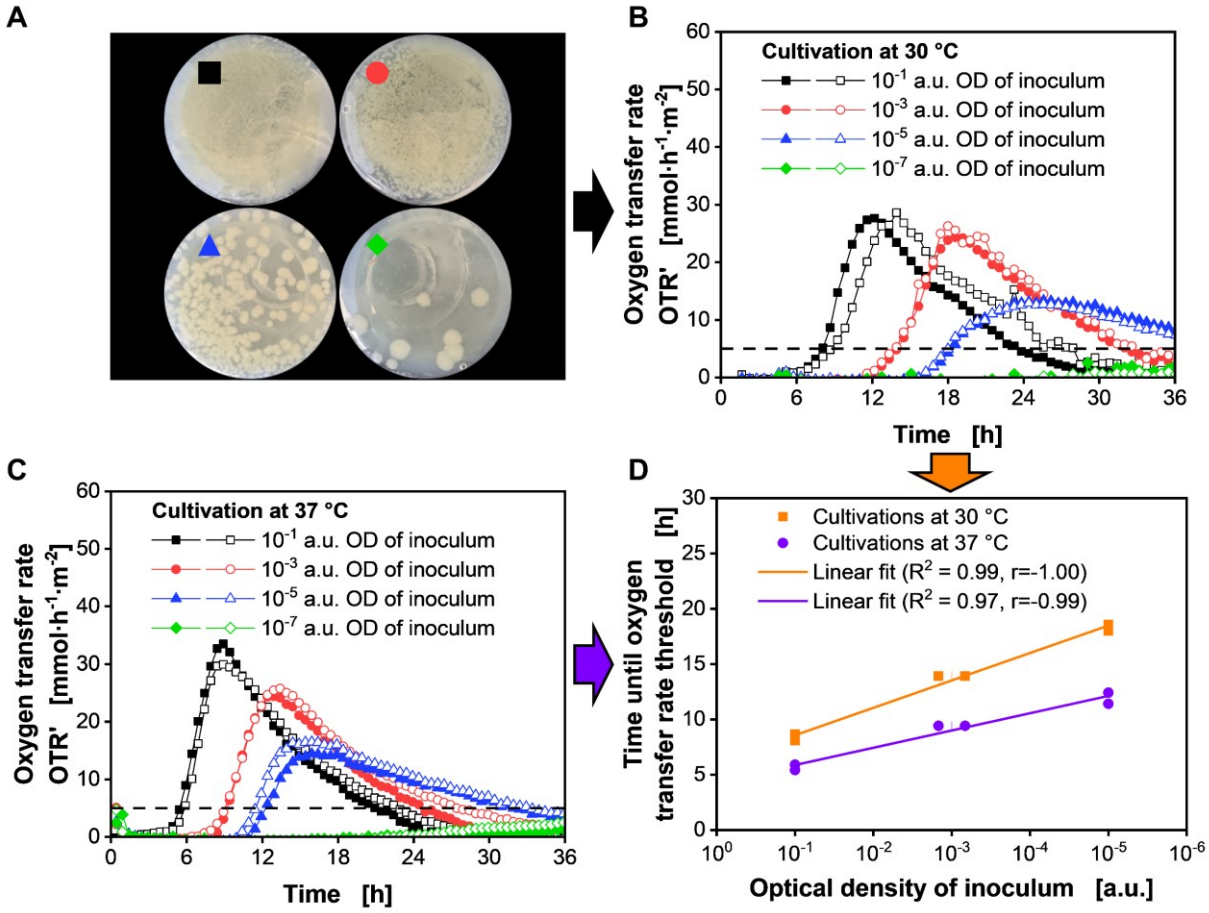

Figure 23. Cultivations of *Escherichia coli* BL21 on LB-agar in Erlenmeyer flasks with varying inoculation densities and temperatures. The inoculation density is defined by the arbitrary units of the optical density (a.u. OD of inoculum). (**A**) Pictures of the LB-agar at the end of cultivation at 30 °C. (**B**) Area-specific oxygen transfer rates OTR' for cultivations at 30 °C and (**C**) at 37 °C. (**D**) Correlation of the time until the oxygen transfer rate reaches a threshold of 5 mmol·h^{-1}·m^{-2} (Dashed line in (B) and (C)) is reached in the cultivation with the respective inoculum density. The optical density of inoculum is presented on a logarithmic scale. Culture conditions: Non-shaken 250 mL Erlenmeyer flasks, V_L = 20 mL, T = 30 °C or 37 °C, $V_{X,0}$ = 200 µL with varying OD, duplicates.

For the *E. coli* cultivations presented, an OTR' threshold of 5 mmol·h^{-1}·m^{-2} was chosen to define the time of the initial increase in OTR' (Figure 23D). The cultivations with the lowest inoculum density (10^{-7} a.u. OD of inoculum) did not reach the set threshold and were not considered. The other data indicates an excellent linear fit (R^2 for 30 °C = 0.99, R^2 for 37 °C = 0.97) of the time until the OTR' threshold is reached and the logarithmically scaled OD of the inoculum. A correlation over five orders

of magnitude in the inoculum of *E. coli* and the respiratory activity is obtained. For a standard determination of colony forming units, about two orders of magnitude, between 30 and 300 colonies of *E. coli*, are optimal for manual counting on a Petri dish of 8 cm in diameter [161, 162]. A broader range for colony forming units is countable with the respiratory method, presented in this work, while additionally providing an objective and quantitative evaluation parameter. However, further tests with different organisms should be conducted comparing respiration monitoring with automated counting techniques. It has to be examined, whether the proposed method is beneficial in conditions, where visual evaluation is challenging. More complex morphologies of the tested organisms such as filaments and, particularly, hyphal growth into the agar media, can hardly be observed visually. This is the case for many Streptomyces sp., of which the model representative S. coelicolor was examined in chapter 6.3.4.

6.3.3 Respiration monitoring allows for the evaluation of agar diffusion tests

Agar diffusion tests are most commonly used to examine the susceptibility of bacteria to an antibiotic substance. Despite the continued development of methods for antibiotic susceptibility testing over the years, the antibiotic disk diffusion method by Bauer and Kirby remains the gold standard [163, 164]. Similar to colony counting, automated image analysis systems are utilized for the evaluation of inhibition zones forming around the disk containing the antibiotic [165]. Hence, similarly, a respiratory evaluation can be applied, if an optical analysis is difficult or even impossible. Furthermore, the information on the respiratory activity could indicate the antibiotic's mechanism of action. For example, whether an antibiotic is bacteriostatic or bactericidal. An exemplary antibiotic disk diffusion test was conducted with *E. coli* and the antibiotic tetracycline (Figure 24). Tetracyclines exert a bacteriostatic effect by inhibiting bacterial protein synthesis. This is achieved by blockage of the ribosomal acceptor site for aminoacyl-tRNA [166]. The amount of tested tetracycline was chosen to range up to 30 µg and applied to the respective filter disks. Furthermore, the tests were simultaneously performed in Petri dishes and Erlenmeyer flasks to evaluate, whether there was a difference due to the cultivation vessel and the active aeration in the RAMOS device. The same volume of LB-agar was used in both cultivation vessels.

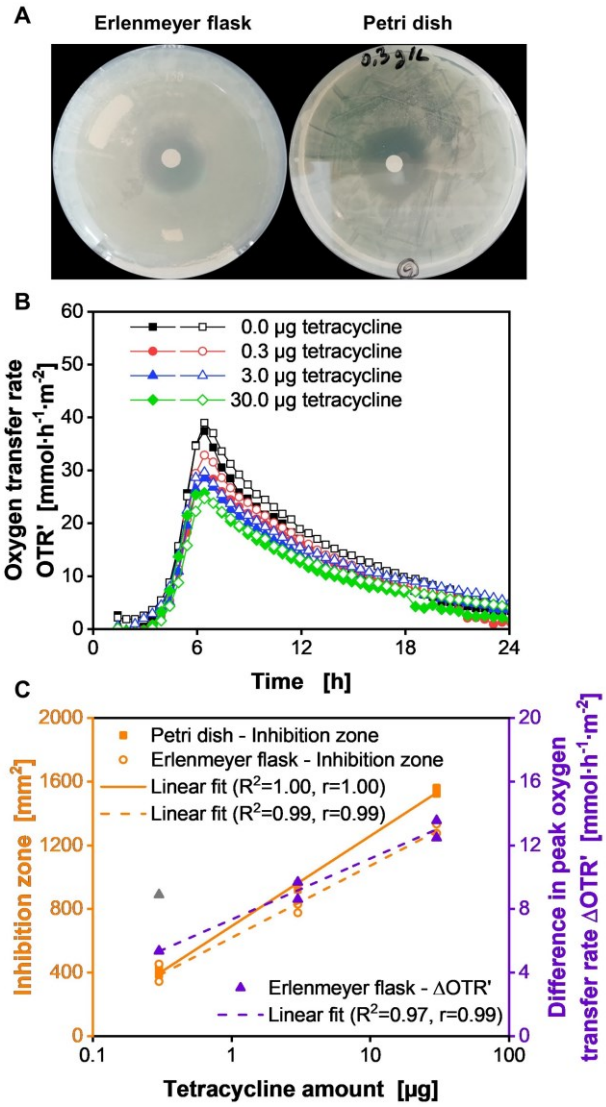

Figure 24. Tetracycline disk diffusion test with *Escherichia coli* BL21 on LB-agar in Erlenmeyer flasks and Petri dishes. (**A**) Representative pictures after the cultivation (0.3 µg tetracycline). (**B**) Area-specific oxygen transfer rates OTR'. (**C**) Inhibition zones and difference in peak oxygen transfer rates in relation to the samples with 0 µg tetracycline. The tetracycline amount is presented on a logarithmic scale. One measurement point (grey upward triangle) was neglected due to a setup error. Culture conditions: V_L = 20 mL, T = 30 °C, $V_{X,0}$ = 200 µL with OD of 10^{-1}, duplicates.

The visual examination of the bacterial lawn and inhibition zones in the Erlenmeyer flask and Petri dish (Figure 24A) indicates differences. The bacterial lawn in the Erlenmeyer flask is homogenous compared to the Petri dish. Therefore, the circular shape of the inhibition zone is clearer presented. This could indicate better growth of *E. coli* in the Erlenmeyer flask with active aeration by the RAMOS device. However, the improved growth is not necessarily a result of active aeration. The cross-sectional area in Petri dishes is slightly larger compared to the Erlenmeyer flasks. Hence, the ratio of the nutrients to the growth area is improved for the cultivations in Erlenmeyer flasks, potentially leading to a homogeneous bacterial lawn. The different cross-sectional areas also affect, to a certain extent, the diffusion of tetracycline. As the volume of LB-agar was kept constant, the agar height was different, depending on the cross-sectional area. In Petri dishes, the agar height is lower than in the Erlenmeyer flasks, resulting in increased radial diffusion of tetracycline and, therefore, increased inhibition zones. The measured inhibition zones (Figure 24C) for Petri dishes were slightly increased

compared to the zones recorded for Erlenmeyer flasks. Nonetheless, inhibition zones and the tetracycline amount on a logarithmic scale have a nearly perfect linear correlation (R^2 for Petri dishes = 1.00, R^2 for Erlenmeyer flasks = 0.99) for both cultivation vessels. A linear correlation of the logarithmic antibiotic amount and the size of the inhibition zone is well expected and described in the literature [167].

For the cultivations in Erlenmeyer flasks, the OTR' was additionally monitored with the RAMOS (Figure 24B). The overall trajectory matches the previous measurements reported in chapter 6.3.1 and 6.3.2. However, with increasing amounts of applied tetracycline on the filter disk, the peak OTR' at about 6.5 h was successively reduced. From a reference value of approximately 38 $mmol \cdot h^{-1} \cdot m^{-2}$ without the addition of tetracycline, the peak OTR' was reduced to about 25 $mmol \cdot h^{-1} \cdot m^{-2}$ for the condition with 30 µg tetracycline. One of the duplicates with 0.3 µg tetracycline (Figure 24B, red line and filled circles) did not follow the general trend and indicated an even lower peak OTR' than for the condition with 3 µg tetracycline. The lower peak OTR' was not an erroneous measurement, but resulted from a moved filter disk during the setup of the experiment. Due to the movement of the disc, tetracycline was further spread on the agar surface, leading to an enlarged inhibition area. Therefore, the respiration measurement of this cultivation was not considered for the evaluation (Figure 24C, grey upward triangle).

For comparing the respiratory activity with inhibition zones, the differences in the peak OTR' of the conditions with tetracycline to the average of the condition without tetracycline (0 µg) are presented (Figure 24C). The linear fit of this respiration data ($R^2 = 0.97$) yields a comparable result to the fit of the inhibition zones in Erlenmeyer flasks ($R^2 = 0.99$). The general deviating trend of the linear fits for inhibition zones and the difference in the peak OTR' could indicate the bacteriostatic effect of tetracycline on *E. coli*. However, an antibiotic exhibiting a bactericidal effect needs to be tested for confirmation.

6.3.4 Respiration monitoring can assist in standardization of agar cultivations for pro- and eukaryotic microorganisms

Depending on the metabolism and growth type, different organisms should exhibit a characteristic respiratory pattern in agar cultivations. Hence, it is to be assessed how the respiratory signal changes and whether it could be used to standardize pre-cultivations or spore production protocols on agar. In addition, it is conceivable that contaminants attached to mycelia or hidden under produced spores could change the respiration trajectory, serving as a simple online quality indicator.

For these purposes, it was examined, whether the presented method can be applied for various representative pro- and eukaryotic microorganisms (Figure 25). As prokaryotic organisms, *P. putida* and *S. coelicolor* were chosen. *P. putida* is of interest, due to its ability to oxidize glucose into gluconate and further into 2-ketogluconate within the periplasm [168]. This leads to increased oxygen consumption and elevated OTR' compared to *E. coli* cultures (Figure 25A) [169]. Thereby, even though for both cultivations LB-agar was used, the cultivations can be clearly distinguished from each other. Additionally, *S. coelicolor* was cultivated on SFM-agar. It is a gram-positive soil bacterium which forms filamentous structures and is able to produce spores [170]. For the cultivation, spores were spread on the agar. Therefore, and due to the slow growth rate of *S. coelicolor*, only after 16 h a linear increase of the OTR' can be noticed. After 44 h, the growth slows down, and the OTR' approaches a value of 20 $mmol \cdot h^{-1} \cdot m^{-2}$, until it drops at around 120 h. Although not investigated further, the OTR' trajectory of *S. coelicolor* is also clearly distinguishable from the tested unicellular and non-sporulating bacteria. While for *E. coli* and *P. putida* almost no OTR' is noticeable after 32 h, elevated respiratory activities of the *S. coelicolor* cultivations can be detected even after 144 h. This prolonged respiratory activity could be attributed to the complex life cycle of *S. coelicolor*. At first, a vegetative mycelium is formed, which can serve as the substrate for the aerial mycelium upon nutrient depletion [171]. However, also prolonged substrate availability due to a slow hydrolysis and consumption of the soy flour in the medium could cause the differences in the respiratory activity. Nonetheless, the two replicates indicated excellent reproducibility, which underlines the robustness of the presented method.

As representative eukaryotic organisms, the yeasts *S. cerevisiae* and *P. pastoris*, as well as the fungus *T. reesei*, were examined (Figure 25B). Again, the OTR' over time indicate a unique trajectory for each studied organism. Especially noticeable is the formation of a declining plateau in the OTR' at 24 h for the *P. pastoris* and *T. reesei* cultivations. In liquid cultivations, a declining plateau shape in the OTR

could be attributed to a secondary substrate limitation [51]. It has to be verified, whether this explanation also applies to these cultures on agar. At first glance, the late increase of the OTR' for *S. cerevisiae*, which appears at 20 h, is peculiar. However, as *S. cerevisiae* can utilize carbon sources with the respiro-fermentative metabolism and can form and grow on ethanol, the simultaneous monitoring of the by-product carbon dioxide is necessary to fully understand the late increase in the OTR' [172].

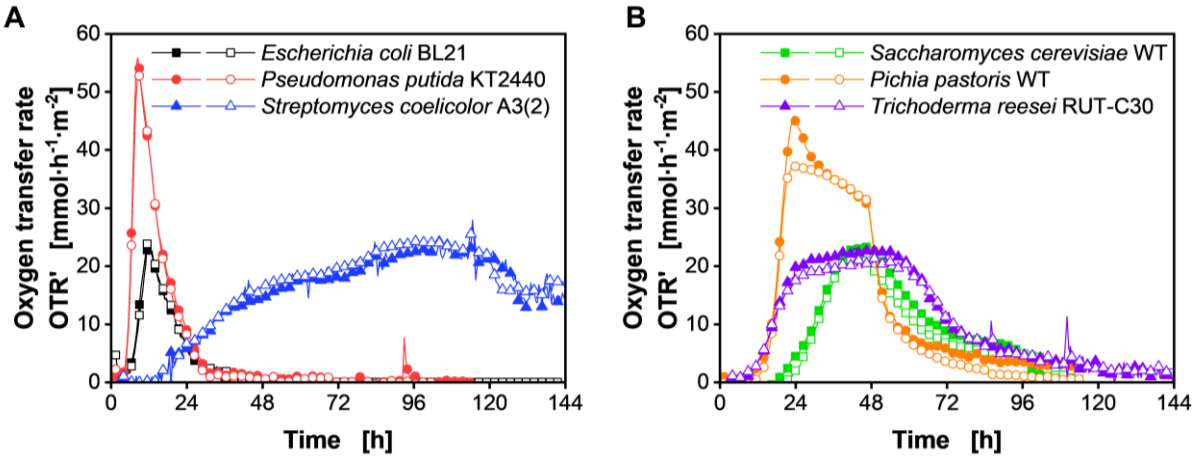

Figure 25. Area-specific oxygen transfer rates OTR' of cultivations with various microorganisms on different agar-types. (**A**) Prokaryotic representatives: *Escherichia coli* BL21 (LB-agar), *Pseudomonas putida* KT2440 (LB-agar), *Streptomyces coelicolor* A3(2) (SFM-agar). (**B**) Eukaryotic representatives: *Saccharomyces cerevisiae* WT (YPD-agar), *Pichia pastoris* WT (YPD-agar), *Trichoderma reesei* RUT-C30 (PD-agar). For clarity, only every 5th data point over time is indicated by the corresponding symbol. Culture conditions: Non-shaken 250 mL Erlenmeyer flasks, V_L = 20 mL, T = 30 °C, duplicates.

6.3.5 Additional monitoring of carbon dioxide transfer rates and respiratory quotient reveals substrate consumption and product formation phenomena

The addition of an infrared carbon dioxide sensor to the measurement loop of the RAMOS device allows to determine the CTR' of the conducted agar cultivations (Figure 26 and Appendix Figure A23-A28). Thereby, the RQ can be calculated and thus, the early respiro-fermentative activity of the Crabtree-positive *S. cerevisiae* can be quantified [172]. A rise in the CTR' could be detected after 10 h and, therefore, approximately 10 h before the OTR' increase (Figure 26). This indicates two phases with an initial ethanol production (10 - 30 h), whereas a transition towards ethanol consumption takes place with the rise of the OTR'. The calculated RQ also validates this observation. Initially, the RQ

exceeded 1, representing the formation of the reduced product ethanol. However, once the OTR' increased, the RQ approached a value of around 0.7. For the pure oxidation of the reduced compound ethanol, a RQ of 0.67 should be observed. This respiratory pattern and the occurrence of the different metabolic phases are in excellent agreement with results for liquid batch cultivations of *S. cerevisiae* [52, 173]. However, the two phases of ethanol production and consumption are more clearly distinguishable in liquid cultivations, whereas for agar cultivations both phases overlap. This effect can be attributed to the distribution of cells on the agar and the associated heterogeneity within a colony resulting in potentially multiple phenotypes [174, 175]. Considering the different phenotypes and cross-feeding of products such as acetate or ethanol within a colony, as well as the fact that the respiration monitoring yields a sum signal of the whole cultivation, the observation of these phases in agar cultivations is noteworthy [175]. The respiration monitoring of agar cultivations does not allow for the differentiation of subpopulations and only summarizes the total gas consumption and production. However, depending on the synchronization of the colony growth, the data is useful for validating single colony respiration models.

In contrast to the Crabtree-positive *S. cerevisiae*, *P. pastoris* is regarded as a Crabtree-negative yeast [176]. Therefore, ethanol is only produced under oxygen-limiting conditions [177]. Oxygen is increasingly limiting in the centre of expanding colonies [178]. Accordingly, the CTR' does not rise before the OTR' (Appendix Figure A27), in contrast to the *S. cerevisiae* cultivation (Figure 26). For *P. pastoris*, the initial growth and ethanol production are indicated by an RQ greater than 1. Afterwards, the RQ drops below 1 due to the sequential ethanol consumption. The CTR' and the resulting RQ also underline the observations regarding oxidation reactions in the *P. putida* cultivations (Appendix Figure A25). The RQ below 1 between approximately 5 - 26 h indicates the formation of an oxidized product, which may be metabolites, such as gluconate and 2-ketogluconate [168]. After about 26 h, the OTR' drops below the CTR', suggesting the consumption of oxidized products. Comparable to the *S. cerevisiae* cultivation, for *P. putida*, the observed trajectories fit respiratory and product formation data from liquid cultivations [169, 179].

Similar to liquid cultivations, respiration monitoring of cultivations on solid medium could also assist in designing and optimizing solid medium compositions. To showcase this possibility, an *E. coli* cultivation was performed on a defined medium without complex components (Appendix Figure A24).

In contrast to the cultivation of *E. coli* on LB-agar (Appendix Figure A23), a delayed and slower increase of the OTR' and CTR' can be noticed for the cultivation on synthetic Wilms-MOPS-agar. This effect can be attributed to the faster growth on complex components.

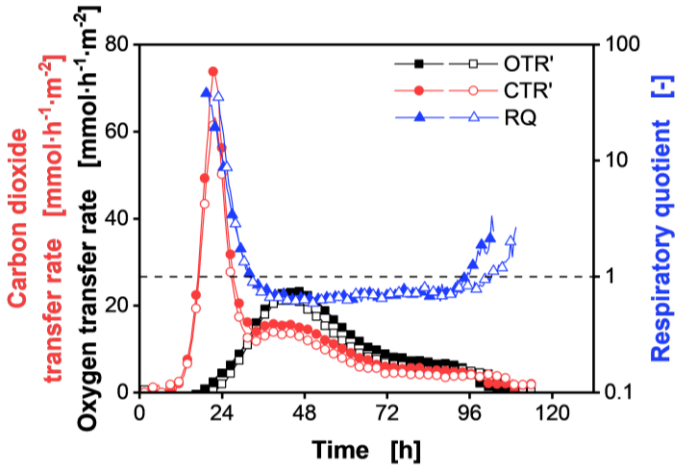

Figure 26. Cultivation of *Saccharomyces cerevisiae* WT on YPD-agar, depicted in Figure 25B, with area-specific oxygen transfer rate (OTR') and carbon dioxide transfer rate (CTR'), as well as the resulting respiratory quotient (RQ). A RQ = 1 is indicated by the horizontal dashed line. Values calculated from oxygen and carbon dioxide transfer rates smaller than 1 mmol·h^{-1}·m^{-2} were omitted. For clarity, only every 5th data point over time is indicated by the corresponding symbol. Culture conditions: Non-shaken 250 mL Erlenmeyer flasks, V_L = 20 mL, T = 30 °C, $V_{X,0}$ = 200 µL with OD of 10^{-1}, duplicates.

6.3.6 Further potential of respiration monitoring in solid medium cultivations

Based on the showcased adaption of the RAMOS technology for solid media cultivations, future applications are conceivable, especially for research areas where solid media cultivations are widely established.

In chapter 6.3.4, *S. coelicolor* was briefly introduced as a spore-forming bacterium with a complex life cycle. However, in liquid media, specifically *S. coelicolor* does not form spores. In fact, most *Streptomyces* strain do not form spores in liquid cultivations [180]. Instead, spores develop out of the aerial hyphae, by which they can escape nutrient-depleted aqueous environments [181]. Upon depletion of nutrients as well as due to other signals, the initial vegetative mycelium of *Streptomyces* undergoes programmed cell death, leading to the formation of aerial hyphae [182]. This is not the case in liquid cultivations. Hence, spore production and differentiation-associated antibiotic production are

frequently observed on solid media [183]. The proposed respiration monitoring could assist in these studies. The respiratory signal should indicate nutrient depletion and programmed cell death. Thereby, influencing factors on sporulation and, ultimately, antibiotic production could be investigated in more detail.

Additionally, the method can be applied to plant cell cultures or adherent mammalian cell cultures. For example, plant cell cultures were already cultivated in liquid media in the RAMOS device, while monitoring the oxygen and the plant cell hormone ethylene [149]. However, plant callus induction is mainly performed on solid media, as some callus can not be induced in liquid media [184]. Hence, it is conceivable that the presented method might prove useful in tracking the callus induction and the proliferation on solid media. Thereby, respiration could potentially serve as an online indicator for the induction rate and proliferation efficiency, which could help in selecting optimal culture conditions.

6.4 Conclusion

The introduced application of the RAMOS for cultivations on solid medium provides valuable information on the respiration activity. It was demonstrated that the respiration activity can indicate growth trajectories, metabolic state, and particular production and consumption phenomena of carbon sources. The OTR' and CTR' allow for a quantitative evaluation and comparison with cultivations in liquid media. Gathering such data is crucial for mass balancing and is especially beneficial, if gaseous substrates and products are to be investigated. Conclusions can be drawn, validating models of the respiration for single colonies. The respiratory method provides an online and objective process indicator, which can substitute subjective visual evaluations by the naked eye for agar cultivations. Furthermore, the method can assist and be used in combination with automated optical monitoring techniques. It was showcased that respiration monitoring is independent of the growth phenotype and can be applied for various pro- and eukaryotic organisms. In the future, a more detailed investigation of some presented application areas could be of interest. For example, it could be examined, whether the method can be used to evaluate a positive effector (e.g. disc soaked with an essential nutrient, which is limiting in the agar medium) in an agar diffusion test. Furthermore, the handling and measurement resolution could be improved with an adapter design for single-use Petri dishes with a low gas phase volume.

Parts of the following chapter have been published previously in

Finger, M.; Schröder, E.; Berg, C.; Dinger, R.; Büchs, J.; *Towards standardized solid medium cultivations: microbial online monitoring based on respiration activity*. Biotechnology Journal, 2023, 1-12.

Michelle Peiffer (AVT - Biochemical Engineering, RWTH Aachen University, Aachen, Germany) assisted with construction of the RAMOS-adapter and the cultivations presented in chapter 7.3.1.

7 Improving precision and throughput for respiration monitoring of cultivations on solid media

7.1 Background

The respiration monitoring of agar cultivations in chapter 6 was solely conducted in Erlenmeyer flasks. However, agar cultivations are mainly conducted within Petri dishes. The geometry of Erlenmeyer flasks is highly different compared to Petri dishes leading to different results, as could be noted for the agar disk diffusion test in chapter 6.3.3. Due to the different diameters of both cultivation vessels, the thickness of the agar is different, if the same agar volume is used. Hence, for comparison with data from the literature, agar cultivations should be performed in Petri dishes. Additionally, the measurement precision of the RAMOS device could be improved by utilizing Petri dishes. The measurement precision depends on the respective gas partial pressure in- or decreases during the measurement phase. The gas volume in a standard Petri dish is considerably lower compared to an Erlenmeyer flask. However, both vessels provide a similar area for the agar cultivations and hence, gas uptake or evolution rate. Therefore, a more rapid change of partial pressures should be monitorable during measurement phases in Petri dishes leading to improved measurement precision. To utilize Petri dishes in combination with the RAMOS device, an adapter is required.

In this chapter, the design and construction of a RAMOS-adapter for Petri dishes is showcased. Furthermore, respiration monitoring in MTPs is presented as a proof-of-concept to increase the throughput. Thereby, the respiration of 48 or 96 simultaneous agar cultivations can be monitored.

7.2 Material and methods

7.2.1 Microorganisms, media composition and cultivation procedures

All cultivations were conducted with *E. coli* BL21 and LB-agar according to chapter 6.2.1 and 6.2.2. For the tetracycline test, tetracycline was dissolved in water, sterile filtered and a tetracycline dilution series was prepared. Then, the required amount of tetracycline was applied to the agar by pipetting 10 µL of the needed concentration from the dilution series on top.

7.2.2 Respiration monitoring of agar cultivations

The monitoring of agar cultivations in Petri dishes and Erlenmeyer flasks was done as described in chapter 6.2.3. For the calculation of the OTR' of cultivations conducted in Petri dishes, an area of 55.4 cm^2 ($r_{Petri\ dish}$ = 4.2 cm) was assumed. The OTR' in 48-well MTPs and 96-deepwell MTPs were monitored with the µRAMOS and µTOM similar as described in 2.2.3 and 5.2 assuming an area for the respective wells of 1.21 cm^2 ($r_{MTP,48\text{-}well}$ = 0.62 cm) and 0.50 cm^2 ($r_{MTP,96\text{-}deepwell}$ = 0.40 cm). Wells were filled with 500 µL or 200 µL of LB-agar and inoculated with 20 µL or 10 µL of a solution containing *E. coli* with the required inoculation density, respectively.

7.2.3 Design of a 3D-printed RAMOS-adapter for Petri dishes

RAMOS-adapters for Petri dishes were designed using Solidworks (Dassault Systèmes, Vélizy-Villacoublay, France). Stereolithographic manufacturing of the RAMOS-adapters was done with a Form 2 3D-printer (Formlabs, Somerville, USA). A high temp resin (Formlabs, Somerville, USA) with a heat distortion temperature of 238 °C at 0.45 MPa was used for the RAMOS-adapter to allow multiple autoclaving cycles. After printing, the support structure was mechanically removed. The data presented in this work were obtained with the first version of the RAMOS-adapter. The gas volume of the RAMOS-adapter in combination with a Petri dish was approximately 104.4 ± 1.8 mL. For the first version, an ethylene propylene diene monomer (EPDM) sealing was fixated with silicone glue at the inner wall to ensure gas tightness. For the second version, EPDM O-rings 88x3 mm (ERIKS, Halle, Germany) are used, allowing for easier handling. A technical drawing is presented in Appendix Figure A29. Cotton plugs were inserted into the in- and outlets as a sterile barrier. The RAMOS-adapters were wrapped in aluminium foil and autoclaved at 121 °C for 20 min.

7.3 Results and discussion

7.3.1 Utilization of a custom Petri dish RAMOS-adapter for more precise respiration measurements of agar cultivations

Petri dishes are usually used for handling agar cultivations. Hence, an adapter was designed to allow respiration monitoring of agar cultivations performed in single-use Petri dishes with the RAMOS device (Figure 27). The RAMOS-adapter can endure multiple autoclaving cycles and can be quickly customized for other Petri dish sizes or containers by stereolithographic 3D-printing.

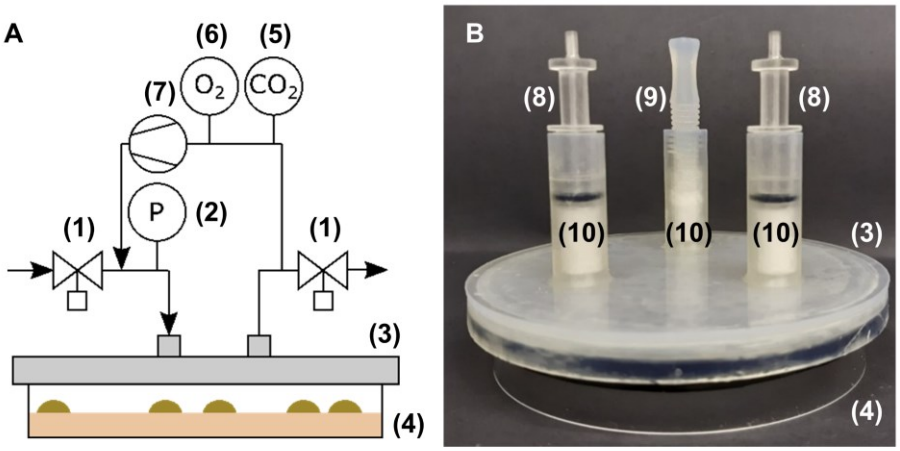

Figure 27. (**A**) Schematic presentation of the respiratory activity monitoring system (RAMOS), similar as presented by Anderlei et al. (2001 and 2004), Schulte et al. (2018), Munch et al. (2020) and Mann et al. (2021) with an adapter for Petri dishes [51, 52, 148, 149, 154]. (**B**) Foto of the first version of the stereolithographically manufactured RAMOS-adapter. Setup: (**1**) In- and outlet 3/2-way flipper solenoid valves (**2**) Differential pressure sensor (**3**) RAMOS-adapter for petri dishes (**4**) Petri dish (**5**) Infrared carbon dioxide sensor (**6**) Electrochemical oxygen sensor (**7**) Microfluidic piezomembrane pump (**8**) Attachments for the RAMOS tubes (**9**) Sealed additional port (**10**) Sterile barrier.

An additional advantage of the RAMOS-adapter for Petri dishes is a reduction of the gas volume compared to Erlenmeyer flasks and, thereby, an improved measurement precision. This was illustrated by a repetition of the experiment presented in chapter 6.3.2 with a varying inoculum of *E. coli* on LB-agar. The experiment was conducted simultaneously in Petri dishes with the RAMOS-adapter and Erlenmeyer flasks (Figure 28). The oxygen sensor signal, which corresponds to the oxygen partial pressure, is exemplarily represented in Figure 28A for the cultivation with an OD for the inoculum of 10^{-1} a.u. The general trajectory of the oxygen sensor signals indicates a similar trend in both cultivation vessels. After 6 h, both signals decrease until 8 h and, thereafter, slowly increase again. However, for the cultivation in the Petri dish, the in- and decrease are more pronounced. This holds true especially for the rapid decline of the oxygen sensor signal during the measurement phase, which leads to the regularly occurring spikes. The ratio of these spikes to the inherent oxygen sensor signal noise describes the precision for the OTR' determination. At similar oxygen consumptions in both systems, the amplitudes of the spikes for the Petri dish with the RAMOS-adapter are more than 3-fold increased. This is in accordance with the more than 3-fold decreased gas phase volume for the RAMOS-adapter

system (Approximately 84.4 mL compared to 290 mL for Erlenmeyer flasks at a filling volume of 20 mL), which leads to improved measurement precision. This can also be recognized by the smoother OTR' trajectories for the Petri dish system (Figure 28C) compared to Erlenmeyer flasks (Figure 28B). The OTR' values in both systems have the same trajectory and reach a similar maximum depending on the inoculum. The average values for the condition with 10^{-1} a.u. OD of inoculum is 34 mmol·h^{-1}·m^{-2} compared to 33 mmol·h^{-1}·m^{-2} for the Erlenmeyer flask and Petri dish system, respectively. For the condition with 10^{-3} a.u. OD of inoculum, 31 mmol·h^{-1}·m^{-2} compared to 30 mmol·h^{-1}·m^{-2} are reached. However, the single measurement conducted for 10^{-5} a.u. OD of inoculum in the Erlenmeyer flask does not fit the data obtained in Petri dishes. This could be explained by an error in the experimental procedure, for example, by a falsely diluted inoculum. Nonetheless, the obtained results indicate an improvement in the respiratory monitoring method for agar cultivations by applying Petri dishes combined with the designed RAMOS-adapter.

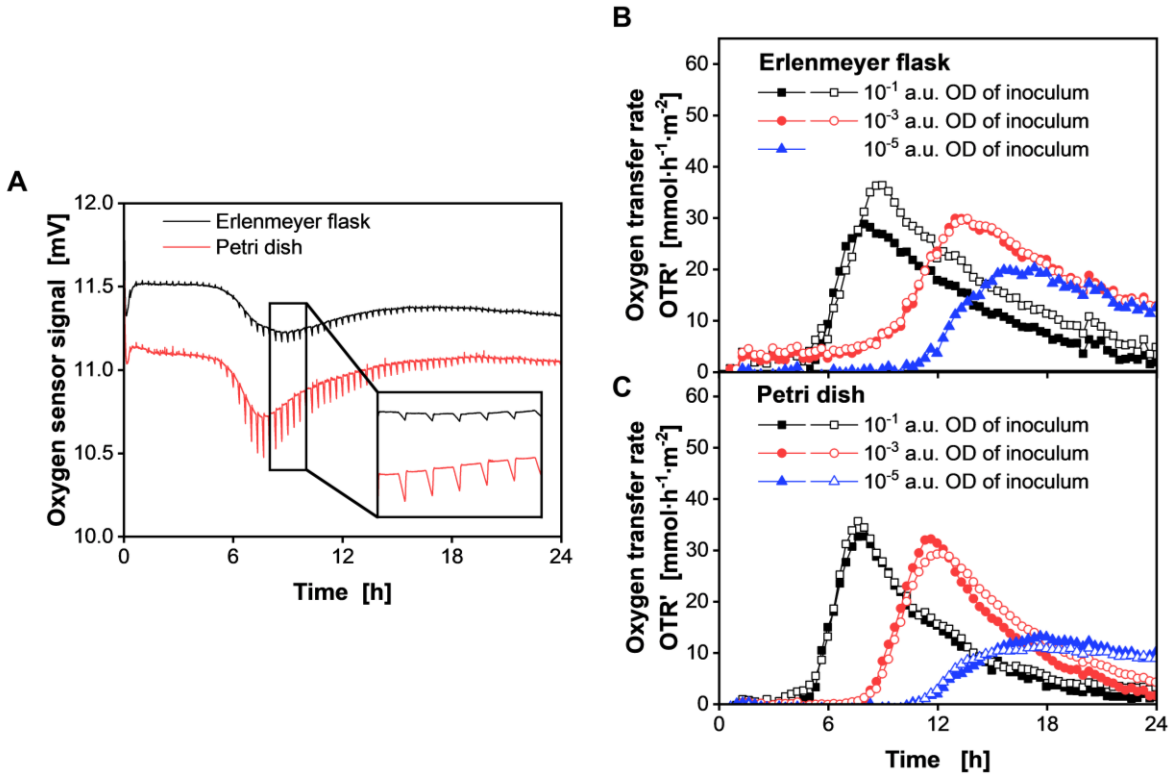

Figure 28. Cultivations of *Escherichia coli* BL21 on LB-agar in Erlenmeyer flasks and Petri dishes with varying inoculation densities. (**A**) Comparison of the oxygen sensor signal for the condition with 10^{-1} a.u. OD of inoculum. (**B**) Area-specific oxygen transfer rates OTR' of cultivations performed in Erlenmeyer

flasks. (**C**) Area-specific oxygen transfer rates OTR' of cultivations performed in Petri dishes. Culture conditions: V_L = 20 mL, T = 30 °C, $V_{X,0}$ = 200 µL with varying OD, duplicates except for an Erlenmeyer flask with 10^{-5} a.u. OD of inoculum.

7.3.2 Respiration monitoring of agar cultivations in microtiter plates

The RAMOS allows only for the respiration monitoring of up to 16 cultivations. Hence, for liquid cultivations, the µRAMOS and the µTOM were constructed to enable the respiration monitoring of up to 48 and 96 cultivations, respectively [53, 54]. High-throughput is often also required for agar cultivations. The throughput for experiments in Petri dishes can be achieved by segmenting the agar surface for the different conditions. However, the segmentation approach is not applicable in combination with the respiration monitoring. Only the respiratory sum signal is observed with the RAMOS. Therefore, it was evaluated whether a high-throughput respiration monitoring of agar cultivations can be conducted in the µRAMOS or µTOM devices.

As presented in chapter 6.3.2, varying inoculum densities were distributed on LB-agar in a 48-well MTP (Figure 29). The resulting OTR' trajectory matches the pattern in Erlenmeyer flasks (Figure 23). With a successively decreasing inoculation density, the OTR' increase appears later and becomes less steep (Figure 29A). Furthermore, the determined OTR' values are in good agreement with the values determined within the RAMOS. Hence, the evaluation was also performed in accordance with chapter 6.3.2 by plotting the time until an arbitrary OTR' threshold is reached against the utilized inoculum density (Figure 29B). An OTR' threshold of 10 $mmol \cdot h^{-1} \cdot m^{-2}$ was chosen, and the condition with the lowest inoculum density (10^{-7} a.u. OD of inoculum) was excluded. For the conditions ranging from 10^{0}-10^{-6} OD of inoculum, a perfect linear fit (R^2 = 1.00) indicates that the respiration monitoring method is applicable for the µRAMOS. Apparently, the measurements are not falsified by oxygen diffusion limitations. However, this has to be further tested in detail.

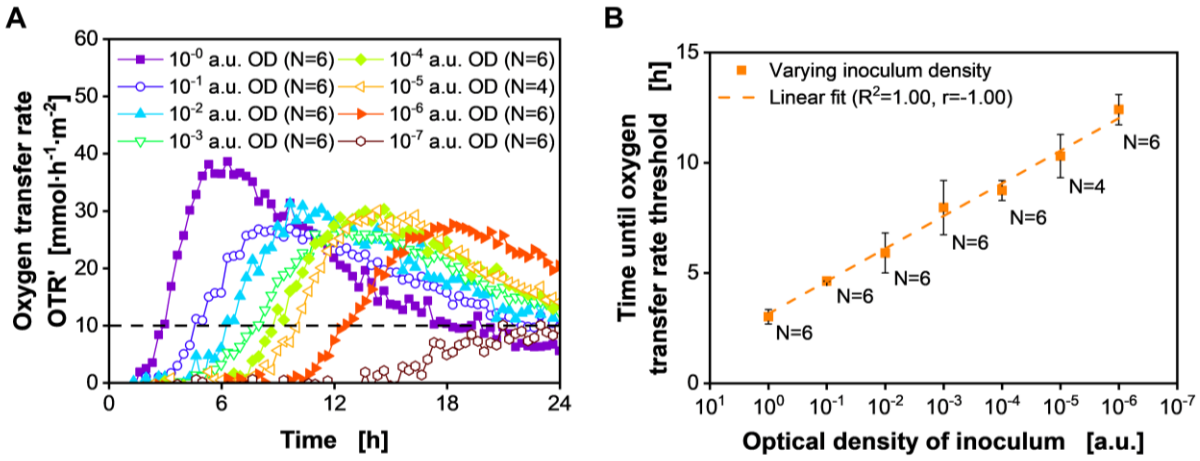

Figure 29. Cultivations of *Escherichia coli* BL21 on LB-agar in 48-well microtiter plate with varying inoculation densities. (**A**) Area-specific oxygen transfer rates OTR'. (**B**) Correlation of the time until the oxygen transfer rate threshold of 10 mmol·h^{-1}·m^{-2} (Dashed line in (A)) is reached in the cultivation with the respective inoculum density. The optical density of the inoculum is presented on a logarithmic scale. Culture conditions: 48-well microtiter plate, V_L = 0.5 mL, T = 37 °C, $V_{X,0}$ = 20 µL with varying OD, N=4-6.

The respiration monitoring was also conducted in the µTOM. Instead of varying inoculation densities, different amounts of the antibiotic tetracycline were applied (Figure 30). In contrast to the agar disk diffusion test presented in chapter 6.3.3, the tetracycline was directly pipetted on top of the agar. For the agar disk diffusion test, the antibiotic concentration decreases in the radial direction of the disk, which leads to the formation of inhibition zones (Figure 24). However, for the MTP experiment, the antibiotic concentration at the agar surface can be assumed to be homogenous. This is due to the small well radius ($r_{MTP,96\text{-}deepwell}$ = 0.40 cm) and applying the antibiotic directly onto the agar instead of a disk. Hence, the observed respiration (Figure 30A) also indicates a different pattern.No growth occurs, if a particular tetracycline threshold concentration is reached (Figure 30A). In the agar disk diffusion test, the respiratory signal is reduced depending on the size of the inhibition zone. In contrast, for the presented diffusion test in the MTP, the overall OTR' trajectory shifts with the amount of applied tetracycline. For 0-0.010 µg applied to the agar, the time is approximately linearly prolonged (Figure 30B) until an arbitrary threshold of 20 mmol·h^{-1}·m^{-2} is reached. Tetracycline amounts exceeding 0.010 µg prevented growth, as indicated by the OTR', which remained below 10 mmol·h^{-1}·m^{-2}. Overall, respiration monitoring in the µTOM was proven to be possible.

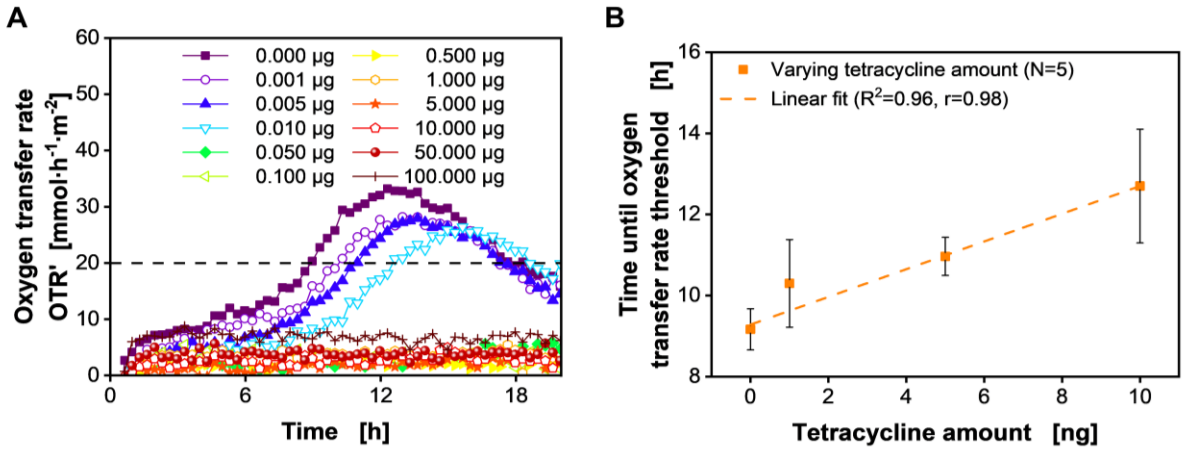

Figure 30. Tetracycline test with cultivations of *Escherichia coli* BL21 on LB-agar in 96-deepwell plates. (**A**) Area-specific oxygen transfer rates OTR'. (**B**) Correlation of the time until the oxygen transfer rate threshold of 20 mmol·h^{-1}·m^{-2} (Dashed line in (A)) is reached in the cultivation with the respective tetracycline amount. The tetracycline amount is presented on a logarithmic scale. Culture conditions: V_L = 200 µL, T = 37 °C, $V_{X,0}$ = 10 µL with OD of 10^{-1}, $V_{Tetracycline}$ = 10 µL, N=5.

7.4 Conclusion

The precision and throughput of the respiration monitoring of agar cultivations were successfully improved. A RAMOS-adapter was designed and constructed, allowing for respiration monitoring within Petri dishes. Thereby, the handling and measurement precision was enhanced. The gas volume is reduced over 3-fold compared to Erlenmeyer flasks, and the design can be adapted to varying Petri dish sizes, ensuring the broad applicability of the presented method. Furthermore, it was showcased that respiration monitoring is possible within 48- and 96-well MTPs with the µRAMOS and µTOM. Thereby, the throughput can be increased more than 15-fold compared to the RAMOS with eight measurement positions [54]. This makes the method applicable for agar-based procedures requiring many replicates or different tested parameters.

8 Summary and outlook

Co-cultivations are scarcely performed in laboratories and are rather conducted by accidental contamination. In contrast, the majority of cultivations in natural habitats of microorganisms are co-cultivations. Additionally, nutrients such as the carbon source are not abundantly available in the natural environment. However, it is suspected that these nutrient-limited co-cultivations favour the formation of natural products. Especially filamentous microorganisms possess a high potential for the formation of natural products. Still, due to the inherent complexity of nutrient-limited filamentous co-cultivations, detailed investigations are seldomly performed. In this thesis, a model cellulolytic co-cultivation system consisting of the filamentous organisms *T. reesei* and *S. coelicolor*, was studied. The complexity of this co-cultivation was tackled by the application of high-throughput online monitoring techniques.

Initially, the growth and product formation of *S. coelicolor* was defined and characterized in axenic conditions. An in-house built 48-well microtiter plate-based system was used to enable the monitoring of the respiration activity as well as the fluorescence and scattered light. It was demonstrated that the formation of the pigmented antibiotics undecylprodigiosin and actinorhodin affect the optical signals and, thereby, can be tracked. Furthermore, it was presented that the growth trajectory of *S. coelicolor* can be heavily influenced by varying specific power inputs. Based on this knowledge, co-cultivations with *T. reesei* and cellulose as the primary carbon source were conducted. To control the population dynamics, different parameters were varied. It was demonstrated that the inoculation ratio, the osmolality, as well as the specific power input can be used to steer the population dynamics. Conditions favouring *S. coelicolor* over *T. reesei* growth with a simultaneously slow carbon release by cellulose hydrolysis were beneficial for pigment formation. The co-cultivation was successfully scaled up into a STR. The population dynamics changed in the STR due to the increased specific power input compared to the MTP. However, similar to the observations for cultivations conducted in MTPs, conditions favouring *S. coelicolor* over *T. reesei* growth lead to abundant pigment formation with actinorhodin titers up to 352 µmol·L^{-1}. The titer was more than 2-fold increased compared to glucose-limited axenic cultivations of *S. coelicolor*, in which the highest titer was 143 ± 2 µmol·L^{-1}.

The investigated co-cultivation depends on the release of glucose by cellulose hydrolysis. Hence, the co-cultivation is mostly carbon-limited, which describes a glucose concentration within the order of the

substrate affinity k_S. Therefore, the k_S value of the co-cultivation partners for glucose is a critical parameter. However, as the determination of k_S values is laborious and requires precise analytical procedures, data on k_S values are scarce in the literature. To this end, a novel respiratory method, called sl-RA, was developed for simple and fast initial estimation of the k_S value. By utilizing the µTOM device, the change in the OTR after the spiking of different glucose concentrations is monitored. The correlation of respiration with growth leads to an approximation for the k_S value. The method was successfully applied for three organisms. For *T. reesei*, a k_S value of 12.69 ± 3.25 mg·L^{-1} was obtained.

As an additional respiratory method, the respiration monitoring of agar cultivations was presented in this thesis. By utilizing the RAMOS device, an objective respiration parameter was provided for the evaluation of applications based on agar cultivations, which were conducted in non-shaken Erlenmeyer flasks. The method was successfully demonstrated for potential use cases, including the determination of colony forming units, antibiotic disk diffusion tests, quality control for spore production or for pre-cultures and the investigation of the metabolic activity in cultivations on solid media. Furthermore, an adapter was constructed for respiration monitoring with the RAMOS device in Petri dishes to increase the measurement precision. In contrast to the Erlenmeyer flasks used before, the gas volume was reduced more than 3-fold. Finally, it was proven that the respiration activity of agar cultivations could also be monitored in MTPs with the µRAMOS and µTOM devices.

The next step for the presented co-cultivation system should be the investigation of the complete natural product profile and not just the pigmented antibiotics undecylprodigiosin and actinorhodin. Analysis of the gathered samples with tandem mass spectrometry could lead to the identification of novel compounds not produced in axenic cultivations. It would be particularly interesting to examine, how different population compositions affect these natural product profiles. Furthermore, if the analysis of the natural product profiles is established, the presented cellulolytic system can be used as a platform for co-cultivation with other *Streptomyces sp*. Thereby, many different co-cultivations can be easily screened in the used MTP systems. If interesting compounds are found, the co-cultivation can be scaled up in a similar manner as presented within this thesis.

The presented respiratory k_S estimation method has to be applied for *S. coelicolor* to quantify how glucose-limited conditions affect the growth in the cellulolytic co-cultivation with *T. reesei*. However, as *S. coelicolor* has a pelleted morphology, only an apparent k_S value would be estimated. Therefore, it would be interesting to study how this value is affected depending on the morphology and the pellet size. Furthermore, up to now, the k_S values are inherently overestimated depending on the measurement phase length. The method could be further improved, for example, by a continuous OTR calculation.

The respiration monitoring for cultivations on solid media can also be used in various other applications. This can be the investigation of anaerobic waste valorization or cell culture applications such as plant callus induction. It is also conceivable that the method is applicable for adherent cell cultures. Thereby, the respiratory signal could improve cultivation and seeding strategies for adherent cells. To this end, the measurement precision has to be further enhanced. Due to the increased throughput, the µTOM device could be a powerful tool for studying respiration in adherent cell cultures.

In summary, a model cellulolytic filamentous co-cultivation for the production of pigmented antibiotics was successfully established within this thesis. The presented research lays the foundation to set up similar filamentous co-cultivations for natural product synthesis. Furthermore, two respiratory methods were developed for the fast estimation of the substrate affinity k_S as well as for the respiration monitoring of cultivations on solid media.

9 Bibliography

[1] Procópio, R. E. d. L., Silva, I. R. d., Martins, M. K., Azevedo, J. L. d. et al., Antibiotics produced by *Streptomyces*. *The Brazilian Journal of Infectious Diseases: An Official Publication of the Brazilian Society of Infectious Diseases* 2012, *16*, 466-471.

[2] Bérdy, J., Bioactive microbial metabolites. *The Journal of Antibiotics* 2005, *58*, 1-26.

[3] Antoraz, S., Santamaría, R. I., Díaz, M., Sanz, D. et al., Toward a new focus in antibiotic and drug discovery from the *Streptomyces* arsenal. *Frontiers in Microbiology* 2015, *6*, 461.

[4] Bentley, S. D., Chater, K. F., Cerdeño-Tárraga, A.-M., Challis, G. L. et al., Complete genome sequence of the model actinomycete *Streptomyces coelicolor* A3(2). *Nature* 2002, *417*, 141-147.

[5] Xu, Z., Wang, Y., Chater, K. F., Ou, H.-Y. et al., Large-Scale Transposition Mutagenesis of *Streptomyces coelicolor* Identifies Hundreds of Genes Influencing Antibiotic Biosynthesis. *Applied and Environmental Microbiology* 2017, *83*.

[6] Bhatia, S. K., Lee, B.-R., Sathiyanarayanan, G., Song, H. S. et al., Biomass-derived molecules modulate the behavior of *Streptomyces coelicolor* for antibiotic production. *3 Biotech* 2016, *6*, 223.

[7] Park, S.-S., Yang, Y.-H., Song, E., Kim, E.-J. et al., Mass spectrometric screening of transcriptional regulators involved in antibiotic biosynthesis in *Streptomyces coelicolor* A3(2). *Journal of Industrial Microbiology & Biotechnology* 2009, *36*, 1073-1083.

[8] Gramajo, H. C., Takano, E., Bibb, M. J., Stationary-phase production of the antibiotic actinorhodin in *Streptomyces coelicolor* A3(2) is transcriptionally regulated. *Molecular Microbiology* 1993, *7*, 837-845.

[9] Kang, S. G., Jin, W., Bibb, M., Lee, K. J., Actinorhodin and undecylprodigiosin production in wild-type and relA mutant strains of *Streptomyces coelicolor* A3(2) grown in continuous culture. *FEMS Microbiology Letters* 1998, *168*, 221-226.

[10] Tough, A. J., Prosser, J. I., Experimental verification of a mathematical model for pelleted growth of *Streptomyces coelicolor* A3(2) in submerged batch culture. *Microbiology (Reading, England)* 1996, *142 (Pt 3)*, 639-648.

[11] Bibb, M., 1995 Colworth Prize Lecture. The regulation of antibiotic production in *Streptomyces coelicolor* A3(2). *Microbiology (Reading, England)* 1996, *142 (Pt 6)*, 1335-1344.

[12] Kawabuchi, M., Hara, Y., Nihira, T., Yamada, Y., Production of butyrolactone autoregulators by *Streptomyces coelicolor* A3(2). *FEMS Microbiology Letters* 1997, *157*, 81-85.

[13] Takano, E., Chakraburtty, R., Nihira, T., Yamada, Y. et al., A complex role for the gamma-butyrolactone SCB1 in regulating antibiotic production in *Streptomyces coelicolor* A3(2). *Molecular Microbiology* 2001, *41*, 1015-1028.

[14] Biarnes-Carrera, M., Lee, C.-K., Nihira, T., Breitling, R. et al., Orthogonal regulatory circuits for *Escherichia coli* based on the γ-butyrolactone system of *Streptomyces coelicolor*. *ACS Synthetic Biology* 2018, *7*, 1043-1055.

[15] Luti, K. J. K., Mavituna, F., Elicitation of *Streptomyces coelicolor* with dead cells of *Bacillus subtilis* and *Staphylococcus aureus* in a bioreactor increases production of undecylprodigiosin. *Applied Microbiology and Biotechnology* 2011, *90*, 461-466.

[16] Sanitá Lima, M., Coutinho de Lucas, R., Co-cultivation, co-culture, mixed culture, and microbial consortium of fungi: An understudied strategy for biomass conversion. *Frontiers in Microbiology* 2021, *12*, 837685.

[17] Knowles, S. L., Raja, H. A., Roberts, C. D., Oberlies, N. H., Fungal-fungal co-culture: a primer for generating chemical diversity. *Natural Product Reports* 2022, *39*, 1557-1573.

[18] Arora, D., Gupta, P., Jaglan, S., Roullier, C. et al., Expanding the chemical diversity through microorganisms co-culture: Current status and outlook. *Biotechnology Advances* 2020, *40*, 107521.

[19] Scherlach, K., Sarkar, A., Schroeckh, V., Dahse, H.-M. et al., Two induced fungal polyketide pathways converge into antiproliferative spiroanthrones. *Chembiochem: A European Journal of Chemical Biology* 2011, *12*, 1836-1839.

[20] Doull, J. L., Vining, L. C., Nutritional control of actinorhodin production by *Streptomyces coelicolor* A3(2): suppressive effects of nitrogen and phosphate. *Applied Microbiology and Biotechnology* 1990, *32*, 449-454.

[21] Boruta, T., Marczyk, A., Rychta, K., Przydacz, K. et al., Confrontation between *Penicillium rubens* and *Aspergillus terreus*: Investigating the production of fungal secondary metabolites in submerged co-cultures. *Journal of Bioscience and Bioengineering* 2020, *130*, 503-513.

[22] Netzker, T., Flak, M., Krespach, M. K. C., Stroe, M. C. et al., Microbial interactions trigger the production of antibiotics. *Current Opinion in Microbiology* 2018, *45*, 117–123.

[23] Arn, F., Frasson, D., Kroslakova, I., Rezzonico, F. et al., Isolation and identification of actinomycetes strains from switzerland and their biotechnological potential. *Chimia* 2020, *74*, 382-390.

[24] Cibichakravarthy, B., Jose, P. A., Biosynthetic potential of *Streptomyces* rationalizes genome-based bioprospecting. *Antibiotics* 2021, *10*, 873.

[25] Schneider, O., Simic, N., Aachmann, F. L., Rückert, C. et al., Genome mining of *Streptomyces sp.* YIM 130001 isolated from lichen affords new thiopeptide antibiotic. *Frontiers in Microbiology* 2018, *9*.

[26] Zothanpuia, Passari, A. K., Chandra, P., Leo, V. V. et al., Production of potent antimicrobial compounds from *Streptomyces cyaneofuscatus* associated with fresh water sediment. *Frontiers in Microbiology* 2017, *8*, 1-13.

[27] Boruta, T., A bioprocess perspective on the production of secondary metabolites by *Streptomyces* in submerged co-cultures. *World Journal of Microbiology and Biotechnology* 2021, *37*, 1–15.

[28] Onaka, H., Mori, Y., Igarashi, Y., Furumai, T., Mycolic acid-containing bacteria induce natural-product biosynthesis in *Streptomyces* species. *Applied and Environmental Microbiology* 2011, *77*, 400-406.

[29] Traxler, M. F., Watrous, J. D., Alexandrov, T., Dorrestein, P. C. et al., Interspecies interactions stimulate diversification of the *Streptomyces coelicolor* secreted metabolome. *mBio* 2013, *4*, 1-12.

[30] Luti, K. J. K., Mavituna, F., *Streptomyces coelicolor* increases the production of undecylprodigiosin when interacted with *Bacillus subtilis*. *Biotechnology Letters* 2011, *33*, 113-118.

[31] Schäberle, T. F., Orland, A., König, G. M., Enhanced production of undecylprodigiosin in *Streptomyces coelicolor* by co-cultivation with the corallopyronin A-producing myxobacterium, *Corallococcus coralloides*. *Biotechnology letters* 2014, *36*, 641-648.

[32] Barka, E. A., Vatsa, P., Sanchez, L., Gaveau-Vaillant, N. et al., Taxonomy, physiology, and natural products of actinobacteria. *Microbiology and Molecular Biology Reviews: MMBR* 2016, *80*, 1-43.

[33] Boer, W. d., Folman, L. B., Summerbell, R. C., Boddy, L., Living in a fungal world: impact of fungi on soil bacterial niche development. *FEMS Microbiology Reviews* 2005, *29*, 795-811.

[34] Bertrand, S., Azzollini, A., Schumpp, O., Bohni, N. et al., Multi-well fungal co-culture for de novo metabolite-induction in time-series studies based on untargeted metabolomics. *Molecular bioSystems* 2014, *10*, 2289-2298.

[35] Azzollini, A., Boggia, L., Boccard, J., Sgorbini, B. et al., Dynamics of metabolite induction in fungal co-cultures by metabolomics at both volatile and non-volatile levels. *Frontiers in Microbiology* 2018, *9*.

[36] Zhang, S., Zhu, J., Untargeted metabolomics sensitively differentiates gut bacterial species in single culture and co-culture systems. *ACS Omega* 2022, *7*, 14643-14652.

[37] Schlembach, I., Grünberger, A., Rosenbaum, M. A., Regestein, L., Measurement techniques to resolve and control population dynamics of mixed-culture processes. *Trends in Biotechnology* 2021, *39*, 1093-1109.

[38] Spiegelman, D., Whissell, G., Greer, C. W., A survey of the methods for the characterization of microbial consortia and communities. *Canadian Journal of Microbiology* 2005, *51*, 355-386.

[39] Noonan, A. J. C., Qiu, Y., Ho, J. C. H., Ocampo, J. et al., CRAGE-mediated insertion of fluorescent chromosomal markers for accurate and scalable measurement of co-culture dynamics in *Escherichia coli*. *Synthetic Biology* 2020, *5*, 1-12.

[40] Geinitz, B., Rehmann, L., Büchs, J., Regestein, L., Noninvasive tool for optical online monitoring of individual biomass concentrations in a defined coculture. *Biotechnology and Bioengineering* 2020, *117*, 999-1011.

[41] Gao, C. H., Cao, H., Cai, P., Sørensen, S. J., The initial inoculation ratio regulates bacterial coculture interactions and metabolic capacity. *The ISME Journal* 2021, *15*, 29-40.

[42] Li, H., Zhong, Y., Lu, Q., Zhang, X. et al., Co-cultivation of *Rhodotorula glutinis* and *Chlorella pyrenoidosa* to improve nutrient removal and protein content by their synergistic relationship. *RSC Advances* 2019, *9*, 14331-14342.

[43] Wang, Y., Yang, Y., Ma, F., Xuan, L. et al., Optimization of *Chlorella vulgaris* and bioflocculant-producing bacteria co-culture: enhancing microalgae harvesting and lipid content. *Letters in Applied Microbiology* 2015, *60*, 497-503.

[44] Kunze, M., Lattermann, C., Diederichs, S., Kroutil, W. et al., Minireactor-based high-throughput temperature profiling for the optimization of microbial and enzymatic processes. *Journal of Biological Engineering* 2014, *8*, 22.

[45] Stöckmann, C., Palmen, T. G., Schroer, K., Kunze, G. et al., Definition of culture conditions for *Arxula adeninivorans*, a rational basis for studying heterologous gene expression in this dimorphic yeast. *Journal of Industrial Microbiology & Biotechnology* 2014, *41*, 965-976.

[46] Luchterhand, B., Fischöder, T., Grimm, A. R., Wewetzer, S. et al., Quantifying the sensitivity of *G. oxydans* ATCC 621H and DSM 3504 to osmotic stress triggered by soluble buffers. *Journal of Industrial Microbiology & Biotechnology* 2015, *42*, 585-600.

[47] Lüders, S., David, F., Steinwand, M., Jordan, E. et al., Influence of the hydromechanical stress and temperature on growth and antibody fragment production with *Bacillus megaterium*. *Applied Microbiology and Biotechnology* 2011, *91*, 81-90.

[48] Davison, B. H., Stephanopoulos, G., Effect of pH oscillations on a competing mixed culture. *Biotechnology and Bioengineering* 1986, *28*, 1127-1137.

[49] Krieger, A. G., Zhang, J., Lin, X. N., Temperature regulation as a tool to program synthetic microbial community composition. *Biotechnology and Bioengineering* 2021, *118*, 1381-1392.

[50] Panda, T., Bisaria, V. S., Ghose, T. K., Method to estimate growth of *Trichoderma reesei* and *Aspergillus wentii* in mixed culture on cellulosic substrates. *Applied and Environmental Microbiology* 1989, *55*, 1044-1046.

[51] Anderlei, T., Büchs, J., Device for sterile online measurement of the oxygen transfer rate in shaking flasks. *Biochemical Engineering Journal* 2001, *7*, 157-162.

[52] Anderlei, T., Zang, W., Papaspyrou, M., Büchs, J., Online respiration activity measurement (OTR, CTR, RQ) in shake flasks. *Biochemical Engineering Journal* 2004, *17*, 187-194.

[53] Flitsch, D., Krabbe, S., Ladner, T., Beckers, M. et al., Respiration activity monitoring system for any individual well of a 48-well microtiter plate. *Journal of Biological Engineering* 2016, *10*, 14.

[54] Dinger, R., Lattermann, C., Flitsch, D., Fischer, J. P. et al., Device for respiration activity measurement enables the determination of oxygen transfer rates of microbial cultures in shaken 96-deepwell microtiter plates. *Biotechnology and Bioengineering* 2022, *119*, 881-894.

[55] Rubinstein-Litwak, S., Energy metabolism, in:, *Encyclopedia of food sciences and nutrition*, Elsevier, 2003, 2108-2114.

[56] Silberbach, M., Maier, B., Zimmermann, M., Büchs, J., Glucose oxidation by *Gluconobacter oxydans*: characterization in shaking-flasks, scale-up and optimization of the pH profile. *Applied Microbiology and Biotechnology* 2003, *62*, 92-98.

[57] Losen, M., Frölich, B., Pohl, M., Büchs, J., Effect of oxygen limitation and medium composition on *Escherichia coli* fermentation in shake-flask cultures. *Biotechnology Progress* 2004, *20*, 1062-1068.

[58] Wechselberger, P., Sagmeister, P., Herwig, C., Real-time estimation of biomass and specific growth rate in physiologically variable recombinant fed-batch processes. *Bioprocess and Biosystems Engineering* 2013, *36*, 1205-1218.

[59] Kensy, F., Engelbrecht, C., Büchs, J., Scale-up from microtiter plate to laboratory fermenter: evaluation by online monitoring techniques of growth and protein expression in *Escherichia coli* and *Hansenula polymorpha* fermentations. *Microbial Cell Factories* 2009, *8*, 68.

[60] Antonov, E., Dissertation, *Ein Reaktoransatz zur Produktion von Plattformchemikalien aus Cellulose mittels einer Mischkultur*, 2017.

[61] Giese, H., Kruithof, P., Meier, K., Sieben, M. et al., Improvement and scale-down of a *Trichoderma reesei* shake flask protocol to microtiter plates enables high-throughput screening. *Journal of Bioscience and Bioengineering* 2014, *118*, 702-709.

[62] Hobbs, G., Frazer, C., Gardner, D., Cullum, J. et al., Dispersed growth of *Streptomyces* in liquid culture. *Applied Microbiology and Biotechnology* 1989, *31*.

[63] Antonov, E., Schlembach, I., Regestein, L., Rosenbaum, M. A. et al., Process relevant screening of cellulolytic organisms for consolidated bioprocessing. *Biotechnology for Biofuels* 2017, *10*, 106.

[64] Ladner, T., Held, M., Flitsch, D., Beckers, M. et al., Quasi-continuous parallel online scattered light, fluorescence and dissolved oxygen tension measurement combined with monitoring of the oxygen transfer rate in each well of a shaken microtiter plate. *Microbial Cell Factories* 2016, *15*, 206.

[65] Ladner, T., Beckers, M., Hitzmann, B., Büchs, J., Parallel online multi-wavelength (2D) fluorescence spectroscopy in each well of a continuously shaken microtiter plate. *Biotechnology Journal* 2016, *11*, 1605-1616.

[66] Schneider, C. A., Rasband, W. S., Eliceiri, K. W., NIH Image to ImageJ: 25 years of image analysis. *Nature Methods* 2012, *9*, 671-675.

[67] Philip, P., Meier, K., Kern, D., Goldmanns, J. et al., Systematic evaluation of characteristics of the membrane-based fed-batch shake flask. *Microbial Cell Factories* 2017, *16*, 122.

[68] Faassen, S. M., Hitzmann, B., Fluorescence spectroscopy and chemometric modeling for bioprocess monitoring. *Sensors (Basel, Switzerland)* 2015, *15*, 10271-10291.

[69] Hartmann, S. K., Stockdreher, Y., Wandrey, G., Hosseinpour Tehrani, H. et al., Online in vivo monitoring of cytosolic NAD redox dynamics in *Ustilago maydis*. *Biochimica et Biophysica Acta. Bioenergetics* 2018, *1859*, 1015-1024.

[70] Surre, J., Saint-Ruf, C., Collin, V., Orenga, S. et al., Strong increase in the autofluorescence of cells signals struggle for survival. *Scientific Reports* 2018, *8*, 12088.

[71] Wucherpfennig, T., Hestler, T., Krull, R., Morphology engineering - osmolality and its effect on *Aspergillus niger* morphology and productivity. *Microbial Cell Factories* 2011, *10*, 58.

[72] Krull, R., Bley, T., *Filaments in Bioprocesses*, Vol. *149*, Springer International Publishing, 2015.

[73] Sohoni, S. V., Bapat, P. M., Lantz, A. E., Robust, small-scale cultivation platform for *Streptomyces coelicolor*. *Microbial Cell Factories* 2012, *11*, 9.

[74] Koepff, J., Keller, M., Tsolis, K. C., Busche, T. et al., Fast and reliable strain characterization of *Streptomyces lividans* through micro-scale cultivation. *Biotechnology and Bioengineering* 2017, *114*, 2011-2022.

[75] Montes-Serrano, I., Satzer, P., Jungbauer, A., Dürauer, A., Characterization of hydrodynamics and volumetric power input in microtiter plates for the scale-up of downstream operations. *Biotechnology and Bioengineering* 2022, *119*, 523-534.

[76] Büchs, J., Maier, U., Milbradt, C., Zoels, B., Power consumption in shaking flasks on rotary shaking machines: II. Nondimensional description of specific power consumption and flow regimes in unbaffled flasks at elevated liquid viscosity. *Biotechnology and Bioengineering* 2000, *68*, 594-601.

[77] Klöckner, W., Tissot, S., Wurm, F., Büchs, J., Power input correlation to characterize the hydrodynamics of cylindrical orbitally shaken bioreactors. *Biochemical Engineering Journal* 2012, *65*, 63-69.

[78] Klöckner, W., Lattermann, C., Pursche, F., Büchs, J. et al., Time efficient way to calculate oxygen transfer areas and power input in cylindrical disposable shaken bioreactors. *Biotechnology Progress* 2014, *30*, 1441-1456.

[79] Kunze, M., Roth, S., Gartz, E., Büchs, J., Pitfalls in optical on-line monitoring for high-throughput screening of microbial systems. *Microbial Cell Factories* 2014, *13*, 53.

[80] Stankovic, N., Radulovic, V., Petkovic, M., Vuckovic, I. et al., *Streptomyces sp.* JS520 produces exceptionally high quantities of undecylprodigiosin with antibacterial, antioxidative, and UV-protective properties. *Applied Microbiology and Biotechnology* 2012, *96*, 1217-1231.

[81] Bystrykh, L. V., Fernández-Moreno, M. A., Herrema, J. K., Malpartida, F. et al., Production of actinorhodin-related "blue pigments" by *Streptomyces coelicolor* A3(2). *Journal of Bacteriology* 1996, *178*, 2238-2244.

[82] Takano, E., Nihira, T., Hara, Y., Jones, J. J. et al., Purification and structural determination of SCB1, a gamma-butyrolactone that elicits antibiotic production in *Streptomyces coelicolor* A3(2). *The Journal of Biological Chemistry* 2000, *275*, 11010-11016.

[83] Zhou, S., Bhukya, H., Malet, N., Harrison, P. J. et al., Molecular basis for control of antibiotic production by a bacterial hormone. *Nature* 2021, *590*, 463-467.

[84] Ates, S., Elibol, M., Mavituna, F., Production of actinorhodin by *Streptomyces coelicolor* in batch and fed-batch cultures. *Process Biochemistry* 1997, *32*, 273-278.

[85] Aldén, L., Demoling, F., Bååth, E., Rapid method of determining factors limiting bacterial growth in soil. *Applied and Environmental Microbiology* 2001, *67*, 1830-1838.

[86] Romero-Rodríguez, A., Rocha, D., Ruiz-Villafán, B., Guzmán-Trampe, S. et al., Carbon catabolite regulation in *Streptomyces*: new insights and lessons learned. *World Journal of Microbiology & Biotechnology* 2017, *33*, 162.

[87] Antonov, E., Wirth, S., Gerlach, T., Schlembach, I. et al., Efficient evaluation of cellulose digestibility by *Trichoderma reesei* Rut-C30 cultures in online monitored shake flasks. *Microbial Cell Factories* 2016, *15*, 164.

[88] Schlembach, I., Hosseinpour Tehrani, H., Blank, L. M., Büchs, J. et al., Consolidated bioprocessing of cellulose to itaconic acid by a co-culture of *Trichoderma reesei* and *Ustilago maydis*. *Biotechnology for Biofuels* 2020, *13*, 207.

[89] Palacio-Barrera, A., Schlembach, I., Finger, M., Büchs, J. et al., Reliable online measurement of population dynamics for filamentous co-cultures. *Microbial Biotechnology* 2022, 1-13.

[90] Finger, M., Sentek, F., Hartmann, L., Palacio-Barrera, A. et al., Insights into *Streptomyces coelicolor* A3(2) growth and pigment formation with high-throughput online monitoring. *Engineering in Life Sciences* 2022, *23*, e2100151.

[91] Wucherpfennig, T., Hestler, T., Krull, R., Morphology engineering - Osmolality and its effect on *Aspergillus niger* morphology and productivity. *Microbial Cell Factories* 2011, *10*, 1-15.

[92] Boruta, T., Górnicka, A., Grzybowska, I., Stefaniak, I. et al., Exploring the extremes: applying high concentration of yeast extract leads to drastic morphological changes and elimination of (+)-geodin and asterric acid production in *Aspergillus terreus* submerged cultures. *Biotechnology Letters* 2021, *43*, 61-71.

[93] Kensy, F., Zang, E., Faulhammer, C., Tan, R. et al., Validation of a high-throughput fermentation system based on online monitoring of biomass and fluorescence in continuously shaken microtiter plates. *Microbial Cell Factories* 2009, *17*, 1-17.

[94] Bradford, M. M., A rapid and sensitive method for the quantitation of microgram quantities of protein utilizing the principle of protein-dye binding. *Analytical Biochemistry* 1976, *72*, 248-254.

[95] Lim, J.-H., Lee, C.-R., Dhakshnamoorthy, V., Park, J. S. et al., Molecular characterization of *Streptomyces coelicolor* A(3) SCO6548 as a cellulose 1,4-β-cellobiosidase. *FEMS Microbiology Letters* 2016, *363*.

[96] Kredics, L., Manczinger, L., Antal, Z., Pénzes, Z. et al., In vitro water activity and pH dependence of mycelial growth and extracellular enzyme activities of *Trichoderma* strains with biocontrol potential. *Journal of Applied Microbiology* 2004, *96*, 491-498.

[97] Malin, G., Lapidot, A., Induction of synthesis of tetrahydropyrimidine derivatives in *Streptomyces* strains and their effect on *Escherichia coli* in response to osmotic and heat stress. *Journal of Bacteriology* 1996, *178*, 385-395.

[98] Sevcikova, B., Kormanec, J., Differential production of two antibiotics of *Streptomyces coelicolor* A3(2), actinorhodin and undecylprodigiosin, upon salt stress conditions. *Archives of Microbiology* 2004, *181*, 384-389.

[99] Hobbs, G., Frazer, C. M., Gardner, D. C. J., Flett, F. et al., Pigmented antibiotic production by *Streptomyces coelicolor* A3(2): kinetics and the influence of nutrients. *Journal of General Microbiology* 1990, *136*, 2291–2296.

[100] Jäger, G., Wulfhorst, H., Zeithammel, E. U., Elinidou, E. et al., Screening of cellulases for biofuel production: online monitoring of the enzymatic hydrolysis of insoluble cellulose using high-throughput scattered light detection. *Biotechnology Journal* 2011, *6*, 74-85.

[101] Neves, A. A., Pereira, D. A., Vieira, L. M., Menezes, J. C., Real time monitoring biomass concentration in *Streptomyces clavuligerus* cultivations with industrial media using a capacitance probe. *Journal of Biotechnology* 2000, *84*, 45-52.

[102] Fehrenbach, R., Comberbach, M., Pêtre, J. O., On-line biomass monitoring by capacitance measurement. *Journal of Biotechnology* 1992, *23*, 303-314.

[103] Monod, J., The growth of bacterial cultures. *Annual review of microbiology* 1949, *3*, 371-394.

[104] Ferenci, T., 'Growth of bacterial cultures' 50 years on: towards an uncertainty principle instead of constants in bacterial growth kinetics. *Research in Microbiology* 1999, *150*, 431-438.

[105] Takors, R., Scale-up of microbial processes: impacts, tools and open questions. *Journal of Biotechnology* 2012, *160*, 3-9.

[106] Junker, B. H., Scale-up methodologies for *Escherichia coli* and yeast fermentation processes. *Journal of Bioscience and Bioengineering* 2004, *97*, 347-364.

[107] Enfors, S.-O., Jahic, M., Rozkov, A., Xu, B. et al., Physiological responses to mixing in large scale bioreactors. *Journal of Biotechnology* 2001, *85*, 175-185.

[108] Bylund, F., Collet, E., Enfors, S.-O., Larsson, G., Substrate gradient formation in the large-scale bioreactor lowers cell yield and increases by-product formation. *Bioprocess Engineering* 1998, *18*, 171.

[109] Mandenius, C.-F. (Ed.), *Bioreactors: Design, operation and novel applications*, 1st Ed., Wiley-VCH, Weinheim 2016.

[110] Harrison, D. E., Studies on the affinity of methanol- and methane-utilizing bacteria for their carbon substrates. *The Journal of Applied Bacteriology* 1973, *36*, 301-308.

[111] Kell, D. B., Sonnleitner, B., GMP - good modelling practice: an essential component of good manufacturing practice. *Trends in Biotechnology* 1995, *13*, 481-492.

[112] Schmideder, A., Severin, T. S., Cremer, J. H., Weuster-Botz, D., A novel milliliter-scale chemostat system for parallel cultivation of microorganisms in stirred-tank bioreactors. *Journal of Biotechnology* 2015, *210*, 19-24.

[113] Graf, M., Haas, T., Teleki, A., Feith, A. et al., Revisiting the growth modulon of *Corynebacterium glutamicum* under glucose limited chemostat conditions. *Frontiers in Bioengineering and Biotechnology* 2020, *8*, 584614.

[114] Senn, H., Lendenmann, U., Snozzi, M., Hamer, G. et al., The growth of *Escherichia coli* in glucose-limited chemostat cultures: a re-examination of the kinetics. *Biochimica et Biophysica Acta (BBA) - General Subjects* 1994, *1201*, 424-436.

[115] Lindner, S. N., Seibold, G. M., Henrich, A., Krämer, R. et al., Phosphotransferase system-independent glucose utilization in *Corynebacterium glutamicum* by inositol permeases and glucokinases. *Applied and Environmental Microbiology* 2011, *77*, 3571-3581.

[116] Stöckmann, C., Maier, U., Anderlei, T., Knocke, C. et al., The oxygen transfer rate as key parameter for the characterization of *Hansenula polymorpha* screening cultures. *Journal of Industrial Microbiology & Biotechnology* 2003, *30*, 613-622.

[117] Oliveira, C. S., Ordaz, A., Alba, J., Alves, M. et al., Determination of kinetic and stoichiometric parameters of *Pseudomonas putida* F1 by chemostat and in situ pulse respirometry. *Chemical Product and Process Modeling* 2009, *4*.

[118] Legan, J. D., Owens, J. D., Determination of growth parameters of methylamine-using bacteria. *Microbiology* 1987, *133*, 1075-1080.

[119] Ordaz, A., Oliveira, C. S., Aguilar, R., Carrión, M. et al., Kinetic and stoichiometric parameters estimation in a nitrifying bubble column through "in-situ" pulse respirometry. *Biotechnology and Bioengineering* 2008, *100*, 94-102.

[120] Goudar, C. T., Strevett, K. A., Estimating growth kinetics of *Penicillium chrysogenum* through the use of respirometry. *Journal of Chemical Technology & Biotechnology* 1998, *72*, 207-212.

[121] Hermann, T., Industrial production of amino acids by coryneform bacteria. *Journal of Biotechnology* 2003, *104*, 155-172.

[122] Wendisch, V. F., Bott, M., Eikmanns, B. J., Metabolic engineering of *Escherichia coli* and *Corynebacterium glutamicum* for biotechnological production of organic acids and amino acids. *Current Opinion in Microbiology* 2006, *9*, 268-274.

[123] Becker, J., Rohles, C. M., Wittmann, C., Metabolically engineered *Corynebacterium glutamicum* for bio-based production of chemicals, fuels, materials, and healthcare products. *Metabolic Engineering* 2018, *50*, 122-141.

[124] Wendisch, V. F., Jorge, J. M. P., Pérez-García, F., Sgobba, E., Updates on industrial production of amino acids using *Corynebacterium glutamicum*. *World Journal of Microbiology & Biotechnology* 2016, *32*, 105.

[125] Freudl, R., Beyond amino acids: Use of the *Corynebacterium glutamicum* cell factory for the secretion of heterologous proteins. *Journal of Biotechnology* 2017, *258*, 101-109.

[126] Vertès, A. A., Inui, M., Yukawa, H., Postgenomic approaches to using corynebacteria as biocatalysts. *Annual review of Microbiology* 2012, *66*, 521-550.

[127] Uhde, A., Youn, J.-W., Maeda, T., Clermont, L. et al., Glucosamine as carbon source for amino acid-producing *Corynebacterium glutamicum*. *Applied Microbiology and Biotechnology* 2013, *97*, 1679-1687.

[128] Kovárová-Kovar, K., Egli, T., Growth kinetics of suspended microbial cells: from single-substrate-controlled growth to mixed-substrate kinetics. *Microbiology and Molecular Biology Reviews: MMBR* 1998, *62*, 646-666.

[129] Siemen, A., Kosciow, K., Schweiger, P., Deppenmeier, U., Production of 5-ketofructose from fructose or sucrose using genetically modified *Gluconobacter oxydans* strains. *Applied Microbiology and Biotechnology* 2018, *102*, 1699-1710.

[130] Ameyama, M., Shinagawa, E., Matsushita, K., Adachi, O., D-fructose dehydrogenase of *Gluconobacter industrius*: purification, characterization, and application to enzymatic microdetermination of D-fructose. *Journal of Bacteriology* 1981, *145*, 814-823.

[131] Kallnik, V., Meyer, M., Deppenmeier, U., Schweiger, P., Construction of expression vectors for protein production in *Gluconobacter oxydans*. *Journal of Biotechnology* 2010, *150*, 460-465.

[132] Unthan, S., Grünberger, A., van Ooyen, J., Gätgens, J. et al., Beyond growth rate 0.6: What drives *Corynebacterium glutamicum* to higher growth rates in defined medium. *Biotechnology and Bioengineering* 2014, *111*, 359-371.

[133] Ho, P., Täuber, S., Stute, B., Grünberger, A. et al., Microfluidic reproduction of dynamic bioreactor environment based on computational lifelines. *Frontiers in Chemical Engineering* 2022, *4*, 826485.

[134] Liebl, W., Klamer, R., Schleifer, K.-H., Requirement of chelating compounds for the growth of *Corynebacterium glutamicum* in synthetic media. *Applied Microbiology and Biotechnology* 1989, *32*, 205-210.

[135] Osten, C. H. von der, Gioannetti, C., Sinskey, A. J., Design of a defined medium for growth of *Corynebacterium glutamicum* in which citrate facilitates iron uptake. *Biotechnology Letters* 1989, *11*, 11-16.

[136] Richhardt, J., Bringer, S., Bott, M., Role of the pentose phosphate pathway and the Entner-Doudoroff pathway in glucose metabolism of *Gluconobacter oxydans* 621H. *Applied Microbiology and Biotechnology* 2013, *97*, 4315-4323.

[137] Ihling, N., Munkler, L. P., Berg, C., Reichenbächer, B. et al., Time-resolved monitoring of the oxygen transfer rate of chinese hamster ovary cells provides insights into culture behavior in shake flasks. *Frontiers in Bioengineering and Biotechnology* 2021, *9*, 725498.

[138] Mühlmann, M. J., Forsten, E., Noack, S., Büchs, J., Prediction of recombinant protein production by *Escherichia coli* derived online from indicators of metabolic burden. *Biotechnology Progress* 2018, *34*, 1543-1552.

[139] Bäumchen, C., Knoll, A., Husemann, B., Seletzky, J. et al., Effect of elevated dissolved carbon dioxide concentrations on growth of *Corynebacterium glutamicum* on D-glucose and L-lactate. *Journal of Biotechnology* 2007, *128*, 868-874.

[140] Pirt, S. J., A theory of the mode of growth of fungi in the form of pellets in submerged culture. *Proceedings of the Royal Society of London. Series B, Biological Sciences* 1966, *166*, 369-373.

[141] Minty, J. J., Singer, M. E., Scholz, S. A., Bae, C.-H. et al., Design and characterization of synthetic fungal-bacterial consortia for direct production of isobutanol from cellulosic biomass. *Proceedings of the National Academy of Sciences of the United States of America* 2013, *110*, 14592-14597.

[142] Herweg, E., Schöpping, M., Rohr, K., Siemen, A. et al., Production of the potential sweetener 5-ketofructose from fructose in fed-batch cultivation with *Gluconobacter oxydans*. *Bioresource Technology* 2018, *259*, 164-172.

[143] Geissmann, Q., OpenCFU, A new free and open-source software to count cell colonies and other circular objects. *PloS One* 2013, *8*, e54072.

[144] Levin-Reisman, I., Fridman, O., Balaban, N. Q., ScanLag: High-throughput quantification of colony growth and lag time. *Journal of visualized experiments: JoVE* 2014.

[145] Bär, J., Boumasmoud, M., Kouyos, R. D., Zinkernagel, A. S. et al., Efficient microbial colony growth dynamics quantification with ColTapp, an automated image analysis application. *Scientific Reports* 2020, *10*, 16084.

[146] Tschiersch, H., Liebsch, G., Borisjuk, L., Stangelmayer, A. et al., An imaging method for oxygen distribution, respiration and photosynthesis at a microscopic level of resolution. *The New Phytologist* 2012, *196*, 926-936.

[147] Takahashi, M., Sawada, Y., Aoyagi, H., Development of a circulation direct sampling and monitoring system for O_2 and CO_2 concentrations in the gas-liquid phases of shake-flask systems during microbial cell culture. *AMB Express* 2017, *7*, 163.

[148] Munch, G., Schulte, A., Mann, M., Dinger, R. et al., Online measurement of CO_2 and total gas production in parallel anaerobic shake flask cultivations. *Biochemical Engineering Journal* 2020, *153*, 107418.

[149] Schulte, A., Schilling, J. V., Nolten, J., Korona, A. et al., Parallel online determination of ethylene release rate by shaken parsley cell cultures using a modified RAMOS device. *BMC Plant Biology* 2018, *18*, 101.

[150] Stöckmann, C., Losen, M., Dahlems, U., Knocke, C. et al., Effect of oxygen supply on passaging, stabilising and screening of recombinant production strains in test tube cultures. *FEMS Yeast Research* 2003, *4*, 195-205.

[151] Ihling, N., Munkler, L. P., Paul, R., Berg, C. et al., Non-invasive and time-resolved measurement of the respiration activity of chinese hamster ovary cells enables prediction of key culture parameters in shake flasks. *Biotechnology Journal* 2022, *17*, e2100677.

[152] Wilms, B., Hauck, A., Reuss, M., Syldatk, C. et al., High-cell-density fermentation for production of L-N-carbamoylase using an expression system based on the *Escherichia coli* rhaBAD promoter. *Biotechnology and Bioengineering* 2001, *73*, 95-103.

[153] Rahmen, N., Fulton, A., Ihling, N., Magni, M. et al., Exchange of single amino acids at different positions of a recombinant protein affects metabolic burden in *Escherichia coli*. *Microbial Cell Factories* 2015, *14*, 10.

[154] Mann, M., Hüser, A., Schick, B., Dinger, R. et al., Online monitoring of gas transfer rates during CO and CO/H_2 gas fermentation in quasi-continuously ventilated shake flasks. *Biotechnology and Bioengineering* 2021, *118*, 2092-2104.

[155] Chacón, J. M., Möbius, W., Harcombe, W. R., The spatial and metabolic basis of colony size variation. *The ISME Journal* 2018, *12*, 669-680.

[156] Xue, H., Kurokawa, M., Ying, B.-W., Correlation between the spatial distribution and colony size was common for monogenetic bacteria in laboratory conditions. *BMC Microbiology* 2021, *21*, 114.

[157] Hazan, R., Que, Y.-A., Maura, D., Rahme, L. G., A method for high throughput determination of viable bacteria cell counts in 96-well plates. *BMC Microbiology* 2012, *12*, 259.

[158] Sweeney, M. T., Martin-Jimenez, T., Diaz-Campos, D., *Performance standards for antimicrobial disk and dilution susceptibility tests for bacteria isolated from animals*. *CLSI*

supplement, *VET08 = v. 38, no. 13*, 5th Ed., Clinical and Laboratory Standards Institute, Wayne, PA 2018.

[159] Ferrer, M., Chernikova, T. N., Yakimov, M. M., Golyshin, P. N. et al., Chaperonins govern growth of *Escherichia coli* at low temperatures. *Nature Biotechnology* 2003, *21*, 1267.

[160] Cooper, A. L., Dean, A. C., Hinshelwood, C., Factors affecting the growth of bacterial colonies on agar plates. *Proceedings of the Royal Society of London. Series B, Biological Sciences* 1968, *171*, 175-199.

[161] Sieuwerts, S., Bok, F. A. M. de, Mols, E., vos, W. M. de et al., A simple and fast method for determining colony forming units. *Letters in Applied Microbiology* 2008, *47*, 275-278.

[162] Breed, R. S., Dotterrer, W. D., The number of colonies allowable on satisfactory agar plates. *Journal of Bacteriology* 1916, *1*, 321-331.

[163] Khan, Z. A., Siddiqui, M. F., Park, S., Current and emerging methods of antibiotic susceptibility testing. *Diagnostics (Basel, Switzerland)* 2019, *9*.

[164] Bauer, A. W., Kirby, W. M., Sherris, J. C., Turck, M., Antibiotic susceptibility testing by a standardized single disk method. *American Journal of Clinical Pathology* 1966, *45*, 493-496.

[165] Felmingham, D., Brown, D. F., Instrumentation in antimicrobial susceptibility testing. *The Journal of Antimicrobial Chemotherapy* 2001, *48*, 81-85.

[166] Chopra, I., Roberts, M., Tetracycline antibiotics: mode of action, applications, molecular biology, and epidemiology of bacterial resistance. *Microbiology and Molecular Biology Reviews: MMBR* 2001, *65*, 232-60.

[167] Ericsson, H., Tunevall, G., Wickmann, K., The paper disc method for determination of bacterial sensitivity to antibiotics. Relationship between the diameter of the zone of inhibition and the minimum inhibitory concentration. *Scandinavian Journal of Clinical and Laboratory Investigation* 1960, *12*, 414-422.

[168] Del Castillo, T., Ramos, J. L., Rodríguez-Herva, J. J., Fuhrer, T. et al., Convergent peripheral pathways catalyze initial glucose catabolism in *Pseudomonas putida*: Genomic and flux analysis. *Journal of Bacteriology* 2007, *189*, 5142-5152.

[169] Latrach Tlemçani, L., Corroler, D., Barillier, D., Mosrati, R., Physiological states and energetic adaptation during growth of *Pseudomonas putida* mt-2 on glucose. *Archives of Microbiology* 2008, *190*, 141-150.

[170] Hopwood, D. A., Forty years of genetics with *Streptomyces*: From in vivo through *in vitro* to *in silico*. *Microbiology (Reading, England)* 1999, *145 (Pt 9)*, 2183-2202.

[171] Urem, M., van Rossum, T., Bucca, G., Moolenaar, G. F. et al., OsdR of *Streptomyces coelicolor* and the dormancy regulator DevR of *Mycobacterium tuberculosis* control overlapping regulons. *mSystems* 2016, *1*.

[172] Käppeli, O., Regulation of carbon metabolism in *Saccharomyces cerevisiae* and related yeasts. *Advances in Microbial Physiology* 1987, 181-209.

[173] Bijkerk, A. H., Hall, R. J., A mechanistic model of the aerobic growth of *Saccharomyces cerevisiae*. *Biotechnology and Bioengineering* 1977, *19*, 267-296.

[174] Pirt, S. J., A kinetic study of the mode of growth of surface colonies of bacteria and fungi. *Journal of General Microbiology* 1967, *47*, 181-197.

[175] Cole, J. A., Kohler, L., Hedhli, J., Luthey-Schulten, Z., Spatially-resolved metabolic cooperativity within dense bacterial colonies. *BMC Systems Biology* 2015, *9*, 15.

[176] Baumann, K., Dato, L., Graf, A. B., Frascotti, G. et al., The impact of oxygen on the transcriptome of recombinant *S. cerevisiae* and *P. pastoris* - a comparative analysis. *BMC Genomics* 2011, *12*, 218.

[177] Baumann, K., Carnicer, M., Dragosits, M., Graf, A. B. et al., A multi-level study of recombinant *Pichia pastoris* in different oxygen conditions. *BMC systems biology* 2010, *4*, 141.

[178] Peters, A. C., Wimpenny, J. W., Coombs, J. P., Oxygen profiles in, and in the agar beneath, colonies of *Bacillus cereus*, *Staphylococcus albus* and *Escherichia coli*. *Journal of General Microbiology* 1987, *133*, 1257-1263.

[179] Tiso, T., Ihling, N., Kubicki, S., Biselli, A. et al., Integration of genetic and process engineering for optimized rhamnolipid production using *Pseudomonas putida*. *Frontiers in Bioengineering and Biotechnology* 2020, *8*, 976.

[180] Manteca, Á., Yagüe, P., *Streptomyces* differentiation in liquid cultures as a trigger of secondary metabolism. *Antibiotics (Basel, Switzerland)* 2018, *7*.

[181] Flärdh, K., Buttner, M. J., *Streptomyces* morphogenetics: dissecting differentiation in a filamentous bacterium. *Nature reviews. Microbiology* 2009, *7*, 36-49.

[182] Manteca, A., Jung, H. R., Schwämmle, V., Jensen, O. N. et al., Quantitative proteome analysis of *Streptomyces coelicolor* nonsporulating liquid cultures demonstrates a complex differentiation process comparable to that occurring in sporulating solid cultures. *Journal of Proteome Research* 2010, *9*, 4801-4811.

[183] Tenconi, E., Traxler, M., Tellatin, D., van Wezel, G. P. et al., Prodiginines postpone the onset of sporulation in *Streptomyces coelicolor*. *Antibiotics (Basel, Switzerland)* 2020, *9*.

[184] Muhamad, S. N. S., Ling, A. P.-K., Wong, C.-L., Effect of plant growth regulators on direct regeneration and callus induction from *Sargassum polycystum* C. Agardh. *Journal of Applied Phycology* 2018, *30*, 3299-3310.

[185] Lichten, C. A., White, R., Clark, I. B. N., Swain, P. S., Unmixing of fluorescence spectra to resolve quantitative time-series measurements of gene expression in plate readers. *BMC Biotechnology* 2014, *14*, 11.

10 Appendix

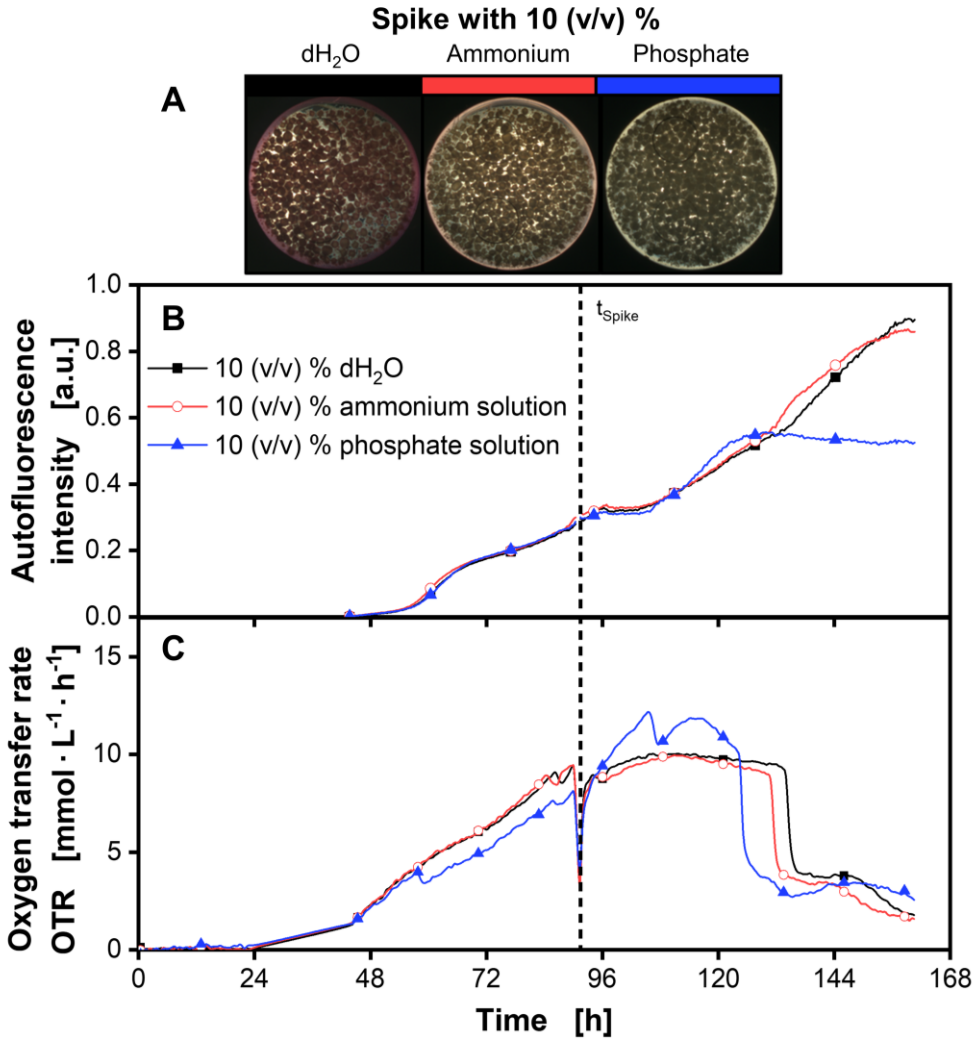

Appendix Figure A1. Cultivation of *Streptomyces coelicolor* A3(2) spiked with different solutions at t_{Spike} = 91 h (dashed line). Concentrations for the ammonium and phosphate solution were chosen that the final concentration after spiking resembles the initial medium composition. (**A**) Macroscopic pictures of pellets after termination of the cultivation. The pellet size was in the order of 300 µm. (**B**) Normalized autofluorescence intensity signals (Excitation: 483 nm; Emission: 520 nm). (**C**) Oxygen transfer rates. For clarity, only every 50th data point over time is indicated by the corresponding symbol in (B) and (C). Pictures shown in (A) and data presented in (B) and (C) originate from the same well for each condition, respectively. Culture conditions: 48-well round well plate, V_L = 1000 µL, n = 800 rpm, d_0 = 3 mm, T = 30 °C, $X_0 = 10^6$ spores·mL^{-1}, LNP medium with 30 g·L^{-1} glucose.

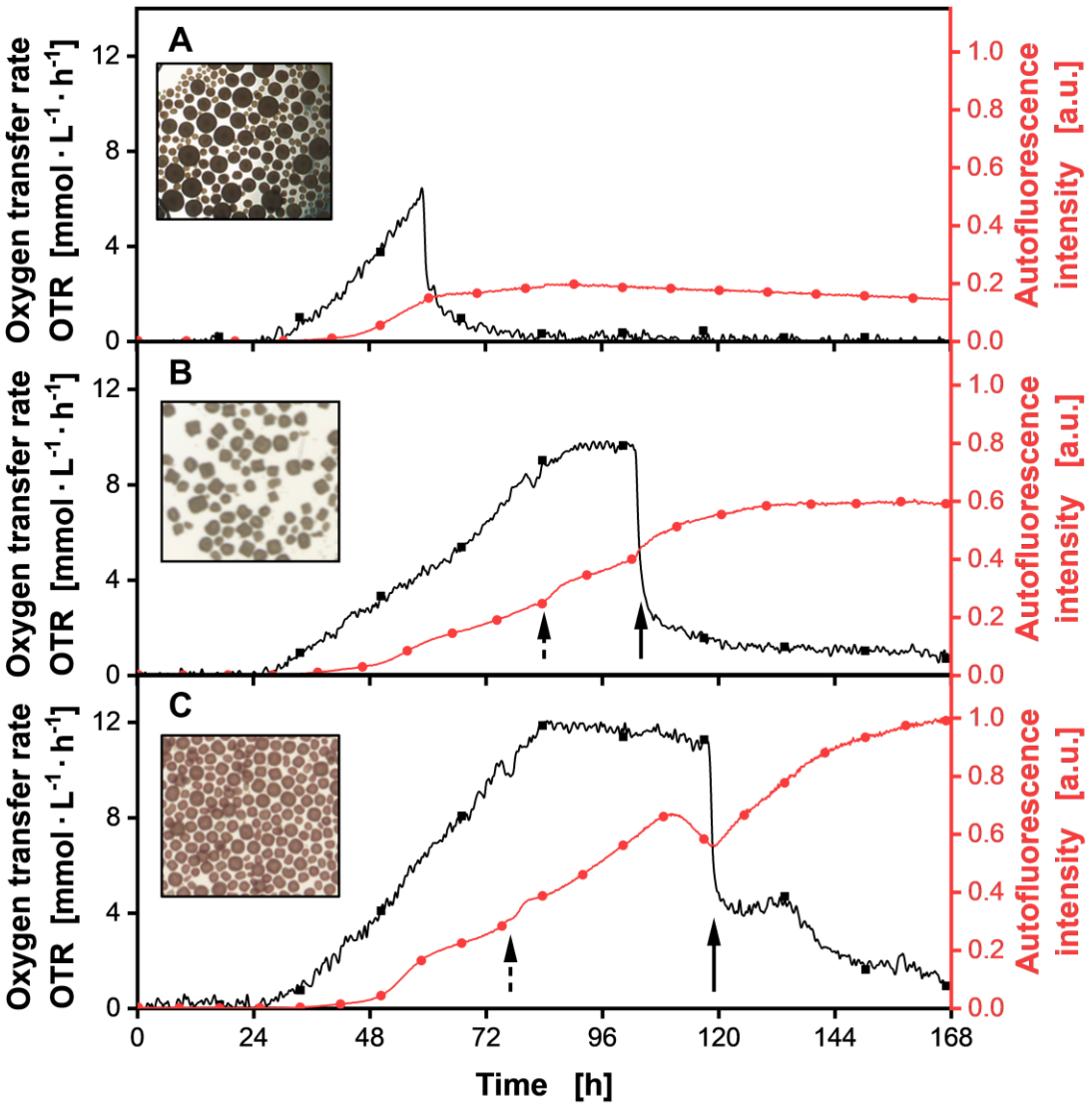

Appendix Figure A2. Cultivation of *Streptomyces coelicolor* A3(2) with (**A**) 5 g·L^{-1} glucose (No phosphate limitation and no pigmentation), (**B**) 20 g·L^{-1} glucose (Phosphate limitation and no pigmentation, dataset from Figure 2) and (**C**) 30 g·L^{-1} glucose (Phosphate limitation and pigmentation, dataset from Figure 3). Oxygen transfer rates are depicted in black and normalized autofluorescence intensity signals (Excitation: 483 nm; Emission: 520 nm) in red. Dashed arrows mark phosphate limitation and solid arrows glucose exhaustion. For clarity, only every 50th data point over time is indicated by the corresponding symbol in (A)-(C). Culture conditions: 48-well round well plate, V_L = 1000 µL, n = 800 rpm, d_0 = 3 mm, T = 30 °C, X_0 = 10^6 spores·mL^{-1}, LNP medium with varying glucose concentrations.

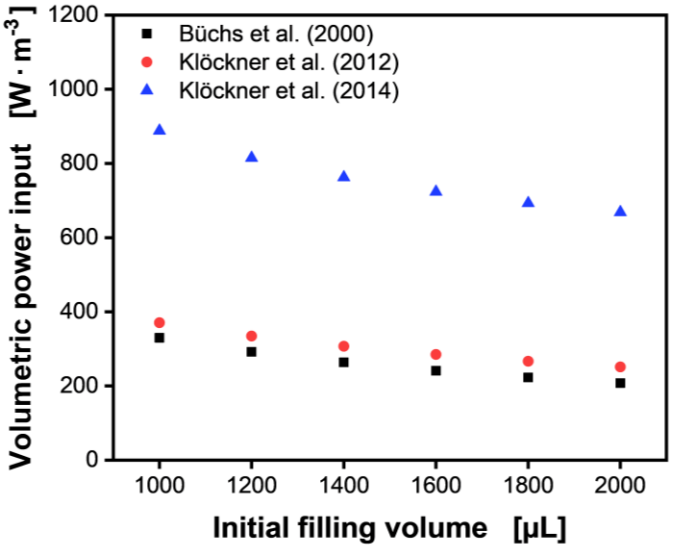

Appendix Figure A3. Estimation of volumetric power inputs for varying filling volumes in 48-round well plates with the models of Büchs et al. (2000) for shake flasks, Klöckner et al. (2012) for shaken bioreactors and Klöckner et al. (2014) also for shaken bioreactors [76–78]. Conditions: 48-well round well plate, V_L = 1000 - 2000 µL, n = 800 rpm, d_0 = 3 mm.

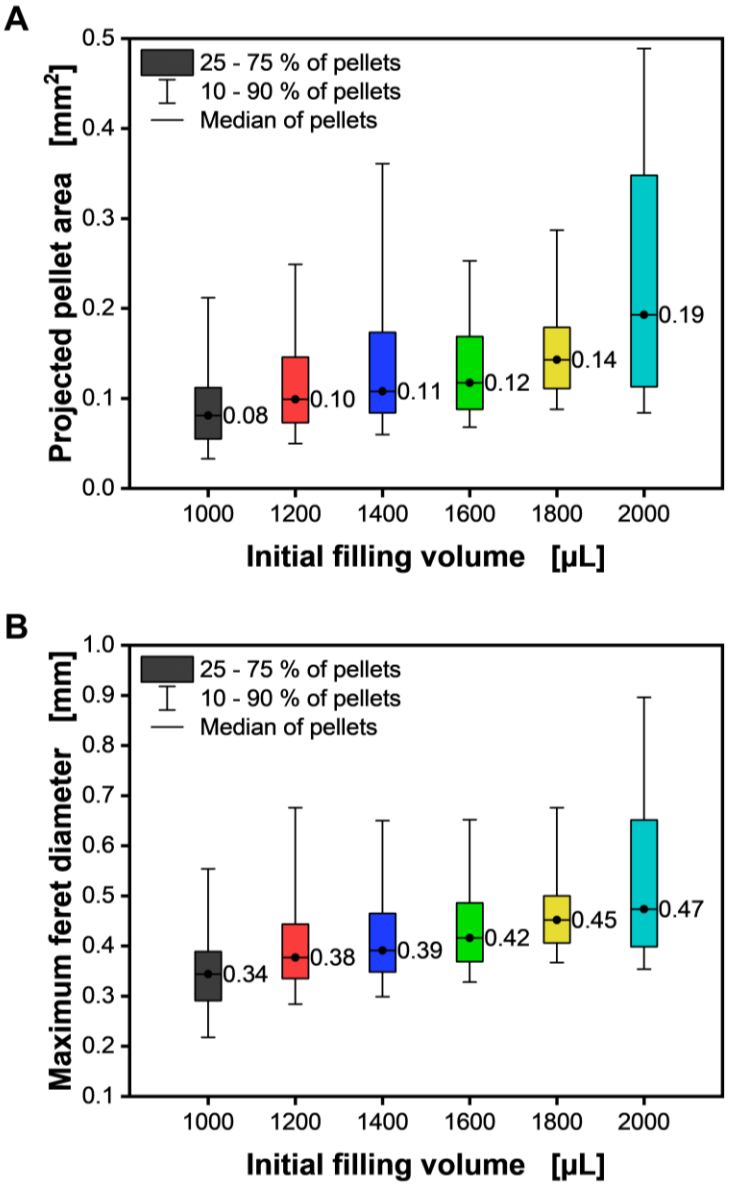

Appendix Figure A4. Correlation of the filling volume and the pellet size described by (**A**) projected pellet area and the (**B**) maximum feret diameter. Projected pellet area and maximum ferret diameter were determined by analysis of >50 pellets from the respective pictures (Figure 3A) with the program ImageJ.

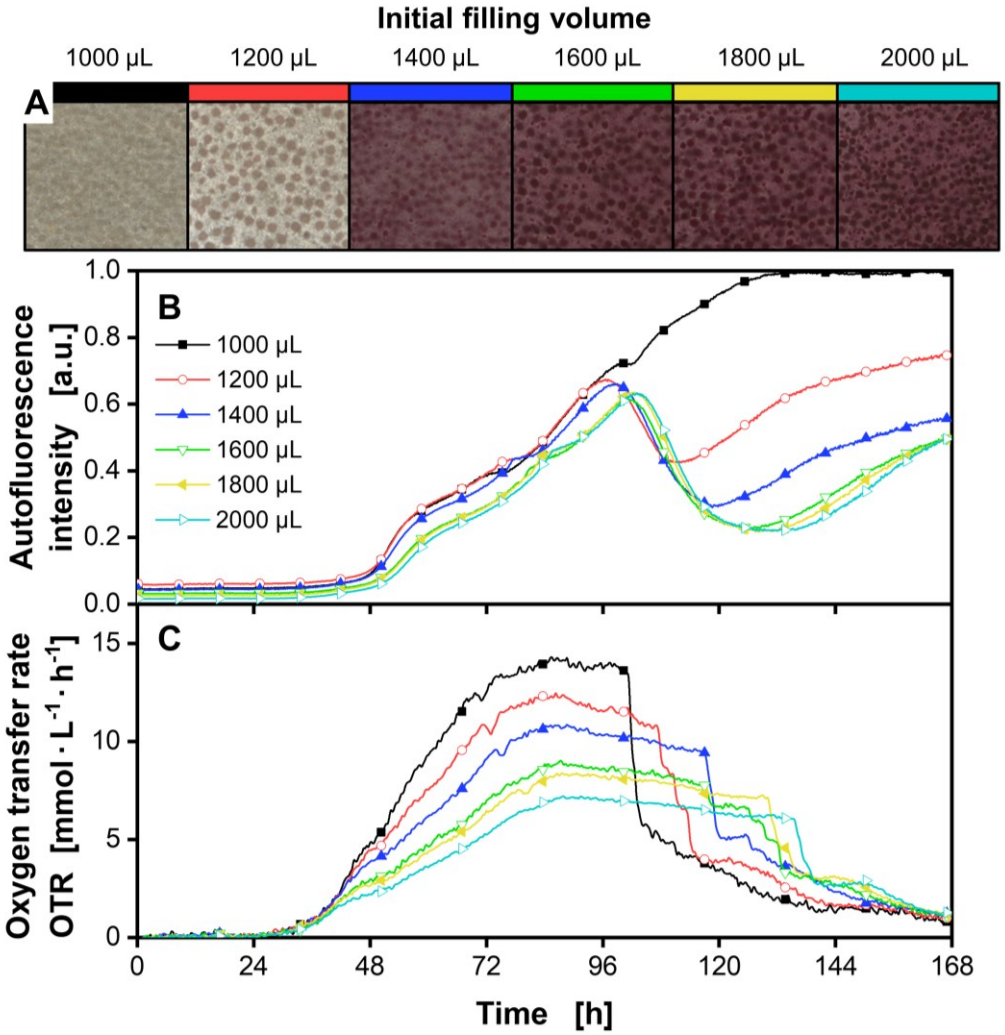

Appendix Figure A5. Cultivation of *Streptomyces coelicolor* A3(2) with varying filling volumes, supplemented with 30 mg α-cellulose per well. (**A**) Macroscopic pictures of pellets after termination of the cultivation. The pellet size was in the order of 300 µm. (**B**) Normalized autofluorescence intensity signals (Excitation: 483 nm; Emission: 520 nm). (**C**) Oxygen transfer rates. For clarity, only every 50th data point over time is indicated by the corresponding symbol in (B) and (C). Pictures shown in (A) and data presented in (B) and (C) originate from the same well for each condition, respectively. Culture conditions: 48-well round well plate, 30 mg α-cellulose per well, V_L = 1000 - 2000 µL, n = 800 rpm, d_0 = 3 mm, T = 30 °C, $X_0 = 10^6$ spores·mL^{-1}, LNP medium with 30 g·L^{-1} glucose.

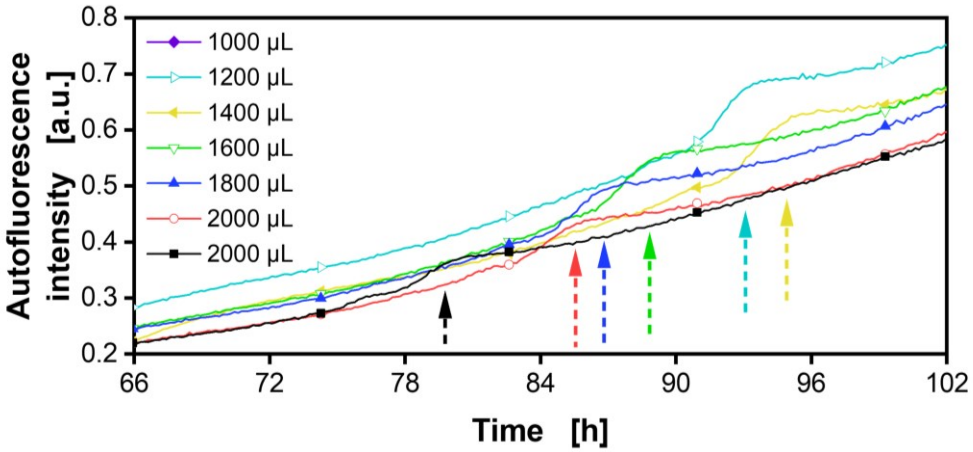

Appendix Figure A6. Enlarged version of Figure 3 from 66 – 102 h. Cultivation of *Streptomyces coelicolor* A3(2) with varying filling volumes. Normalized autofluorescence intensity signals (Excitation: 483 nm; Emission: 520 nm). Dashed arrows mark the stress signal due to phosphate limitation. For clarity, only every 50th data point over time is indicated by the corresponding symbol. Culture conditions: 48-well round well plate, V_L = 1000 - 2000 µL, n = 800 rpm, d_0 = 3 mm, T = 30 °C, $X_0 = 10^6$ spores·mL^{-1}, LNP medium with 30 g·L^{-1} glucose.

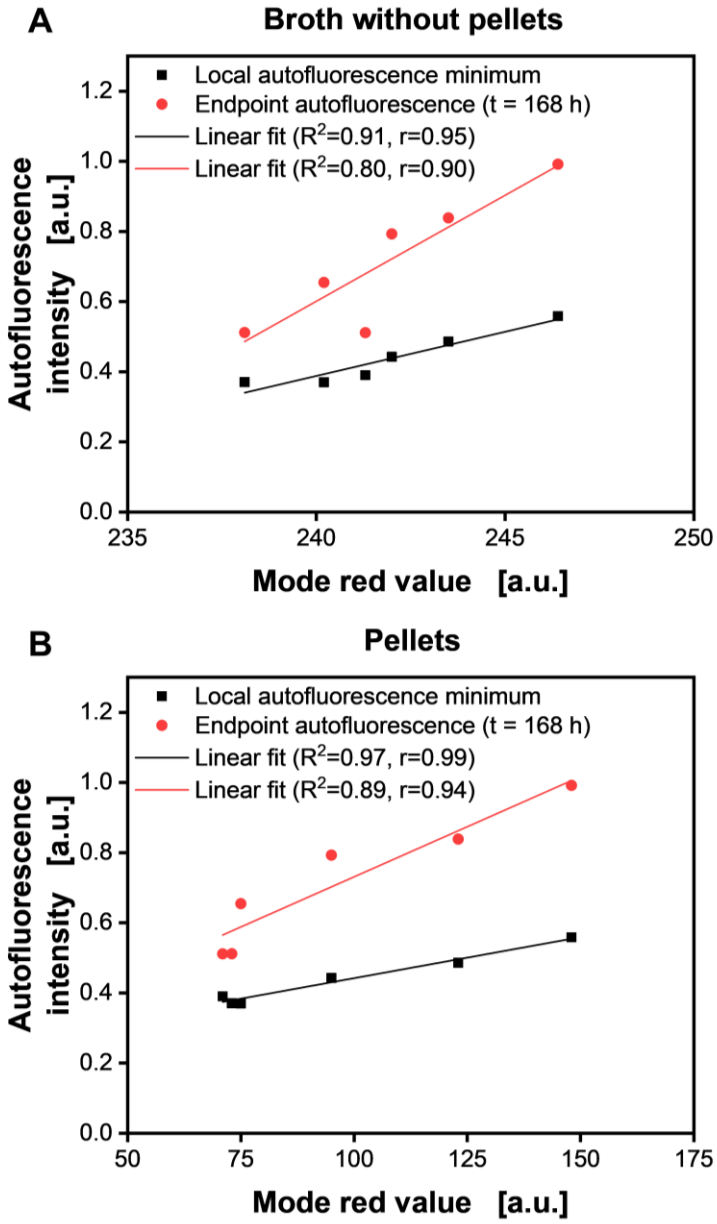

Appendix Figure A7. Correlation of the autofluorescence signals (Excitation: 483 nm; Emission: 520 nm) from the dataset of Figure 3 with the pigmentation intensity represented by the mode red value. The autofluorescence intensities were taken at the local minimum when glucose exhaustion occurred and from the endpoint at t = 168 h. The mode red value for the (**A**) culture broth (background) and the (**B**) pellets was determined by analysis of >5000 pixels from the respective pictures in Figure 3A with the program ImageJ.

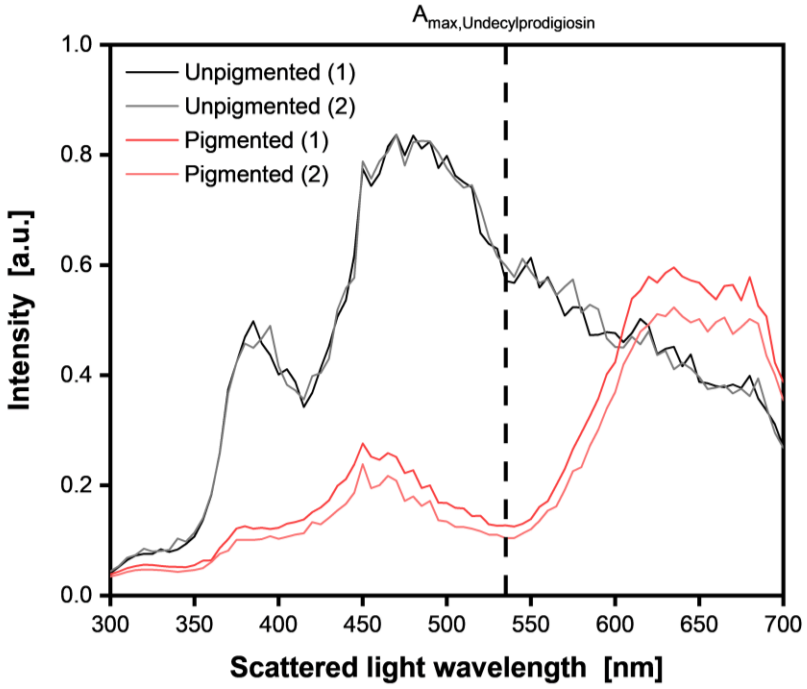

Appendix Figure A8. Comparison of scattered light signals of pigmented and unpigmented *Streptomyces coelicolor* A3(2) samples in duplicates taken from shake flask cultivations. Maximum absorption wavelength of undecylprodigiosin is indicated by the dashed line [80] Conditions: 48-well round well plate, V_L = 1000 µL, n = 800 rpm, d_0 = 3 mm, T = 30 °C.

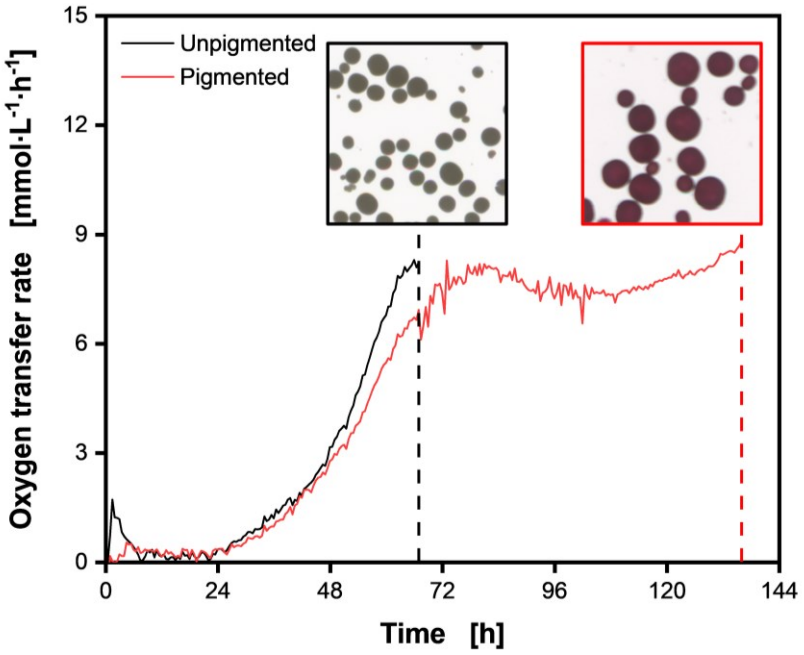

Appendix Figure A9. Cultivation of *Streptomyces coelicolor* A3(2) in shake flasks. Termination of cultivations are indicated by dashed lines. From these macroscopic pictures for unpigmented and pigmented conditions were taken and supernatant for supplementing was generated. Culture conditions: 250 mL shake flasks, V_L = 20 mL, n = 350 rpm, d_0 = 50 mm, T = 30 °C, $X_0 = 10^6$ spores·mL^{-1}, LNP medium with 30 g·L^{-1} glucose.

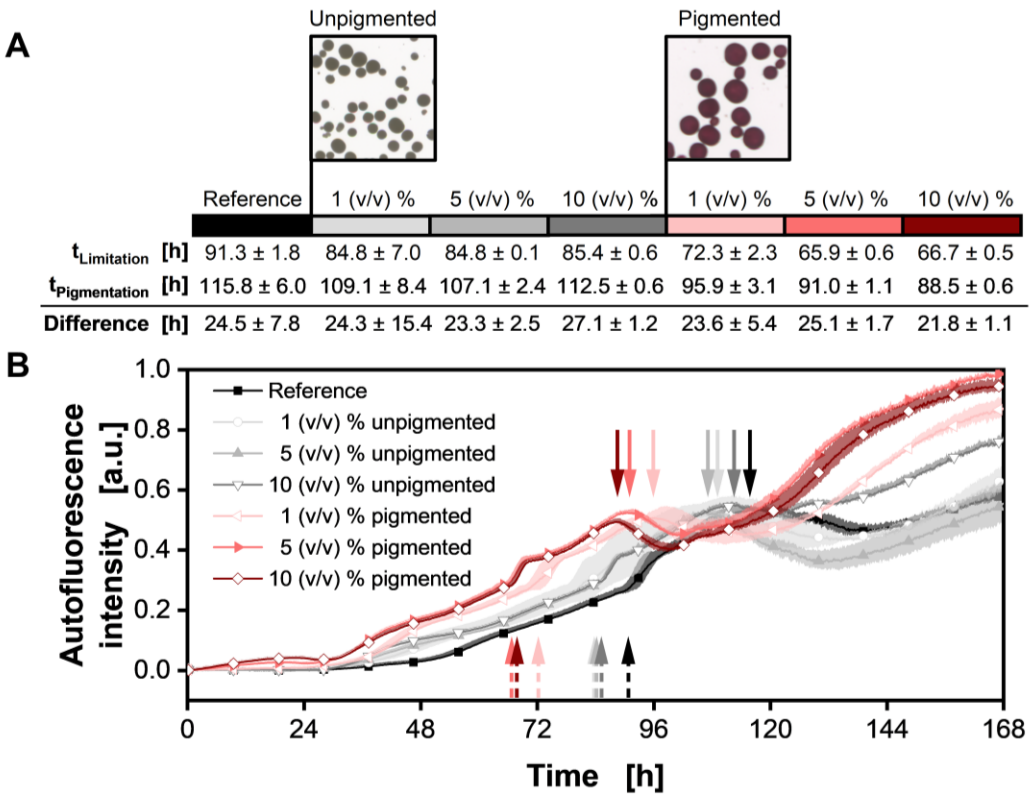

Appendix Figure A10. Cultivation of *Streptomyces coelicolor* A3(2) supplemented with different amounts of supernatants from unpigmented (grey scale) and pigmented (red scale) cultures. (**A**) Macroscopic pictures of the shake flasks cultivations from which the supernatant was taken. The added volumetric amount is stated in (v/v) %. The resulting time points of the stress signal due to phosphate limitation $t_{Limitation}$ and pigmentation onset $t_{Pigmentation}$ as well as the difference is given. (**B**) Normalized autofluorescence intensity signals (Excitation: 483 nm; Emission: 520 nm). Dashed arrows mark $t_{Limitation}$ and solid arrows mark $t_{Pigmentation}$. For clarity, only every 50th data point over time is indicated by the corresponding symbol. Data presented in (A) and (B) are mean values and originate from technical triplicates for each condition, respectively. Shaded areas represent standard deviations. Culture conditions: 48-well round well plate, V_L = 1000 µL, n = 800 rpm, d_0 = 3 mm, T = 30 °C, $X_0 = 10^6$ spores·mL^{-1}, LNP medium with 30 g·L^{-1} glucose.

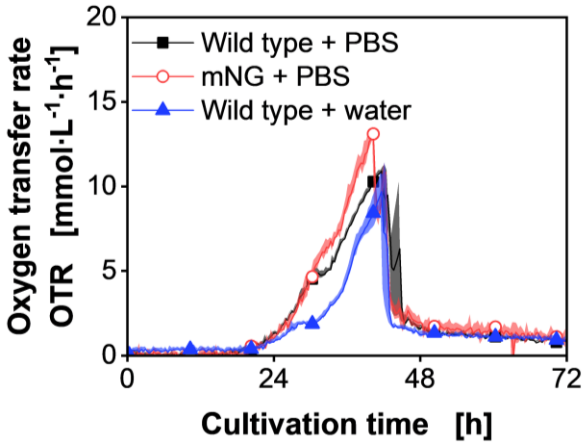

Appendix Figure A11. Oxygen transfer rates for axenic cultivations of *Streptomyces coelicolor* A3(2) WT from Figure 7 and Appendix Figure A13 and *Streptomyces coelicolor* A3(2) mNG from Figure 9. Spore stocks were prepared either with phosphate-buffered saline (PBS) or deionized water. For clarity, only a representative amount of data points is indicated by the corresponding symbols. Culture conditions: 48-well round well plate, N = 3, $X_0 = 10^6$ spores·mL^{-1}, V_L = 1000 µL, n = 800 rpm, d_0 = 3 mm, T = 30 °C, LNP medium with 5 g·L^{-1} glucose and 30 g·L^{-1} α-cellulose.

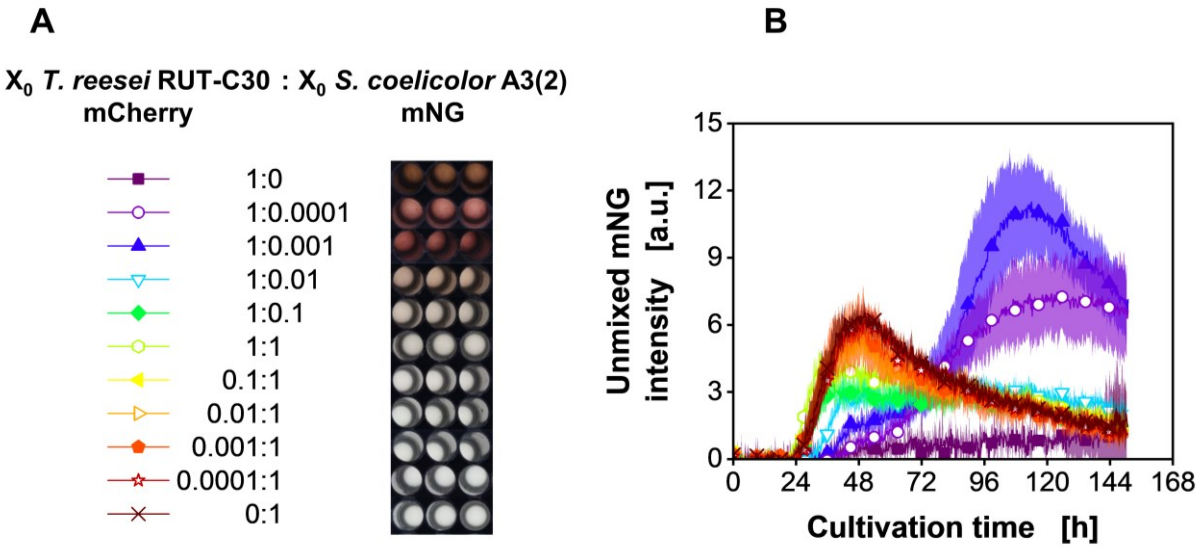

Appendix Figure A12. Co-cultivations of *Trichoderma reesei* RUT-C30 mCherry and *Streptomyces coelicolor* A3(2) mNG. Inoculation ratios were varied, as given relating to the standard inoculation size of $X_0 = 10^6$ spores·mL^{-1}. The spore stock of *S. coelicolor* was prepared with phosphate-buffered saline. (**A**) Macroscopic pictures of the culture broth after termination of the cultivation. (**B**) Unmixed mNG intensity signal from data obtained at channel 1 (Excitation: 480 nm; Emission: 520 nm) and channel 2 (Excitation: 450 nm; Emission: 520 nm). For clarity, only a representative amount of data points is indicated by the corresponding symbols in (A). Culture conditions: 48-well round well plate, N = 3, V_L = 1000 µL, n = 800 rpm, d_0 = 3 mm, T = 30 °C, LNP medium with 5 g·L^{-1} glucose and 30 g·L^{-1} α-cellulose.

Method - Unmixing of green fluorescence signals

The method reported by Lichten et. al (2014) was used for spectral unmixing of the online fluorescence signal corresponding to the mNG tag [185]. This method was validated and adapted for co-cultivations by Palacio-Barrera et al. (2022) [89]. Online green fluorescence signals of the mNG tag were unmixed using data of two channels: Data of Channel 1, corresponds to a green fluorescent protein (GFP) or GFP-like dominated signal (Excitation: 480 nm; Emission: 520 nm). Data of Channel 2, corresponds to an autofluorescence dominated signal (Excitation: 450 nm; Emission: 520 nm), which is mainly attributed to the biogenic fluorophore riboflavin. Measurements were performed with a gain of 100. Detailed description of method adaption can be found in the work of Palacio-Barrera et al. (2022) [89].

Discussion - Unmixing of green fluorescence signals

It can be observed that the trends for the unmixed signal (Appendix Figure A12) of all traces are very similar, when compared to the green fluorescence signal obtained from channel 1 and portrayed in Figure 8C. The fluorescence values are lower, since here, only the signal that comes from the mNeonGreen tag is considered. There is a drop of the unmixed fluorescence after 52 h, in the axenic culture of *S. coelicolor* mNG as well as the co-cultivations with low *T. reesei* to *S. coelicolor* ratio (Brown to green lines). As the mentioned co-cultivations were unpigmented, it can be hypothesized that after 52 h, there was either biomass death, or proteolytic degradation. Likewise, it can be suggested, that as in these co-cultivations production of fluorescence proteins was discontinued very early and photobleaching probably occurred. The mentioned drop in unmixed fluorescence is not pH related. The pKa of mNeonGreen is 5.7 and in these cases, the final pH of the broth was above 6.7 (Appendix Table A1). In contrast, for the co-cultivations with the two highest *T. reesei* to *S. coelicolor* ratios, which are highly pigmented, a drop in the unmixed signal is visible at the end of the culture. The onset of pigment formation might be the main cause of this drop, as already reported in chapter 2 and by Palacio-Barrera et al. (2022) [89, 90]. This exemplary process of unmixing the mNG fluorescence signal as specific biomass measure for *S. coelicolor* from the green autofluorescence signal shows for this co-cultivation that the overall green autofluorescence signal also gives a good relative account for the biomass of *S. coelicolor* (compare Figure Appendix A12B with Figure 8C of the main text). Since it was not possible in all used Biolector devices to measure two independent green fluorescence channels simultaneously, as is required for applying the unmixing process, only the total green

fluorescence as a relative signal for *S. coelicolor* biomass is presented for all other experiments of chapter 3.

Appendix Table A1. Final pH of broth for *T. reesei* mCherry : *S. coelicolor* mNG co-cultivations and axenic controls

T. reesei mCherry : *S. coelicolor* mNG	Final pH
1:0	5.81 ± 0.01
1:0.0001	5.78 ± 0.02
1:0.001	5.90 ± 0.01
1:0.01	6.74 ± 0.02
1:0.1	6.75 ± 0.01
1:1	6.73 ± 0.01
0.1:1	6.75 ± 0.00
0.01:1	6.74 ± 0.00
0.001:1	6.74 ± 0.01
0.0001:1	6.72 ± 0.00
0:1	6.74 ± 0.01

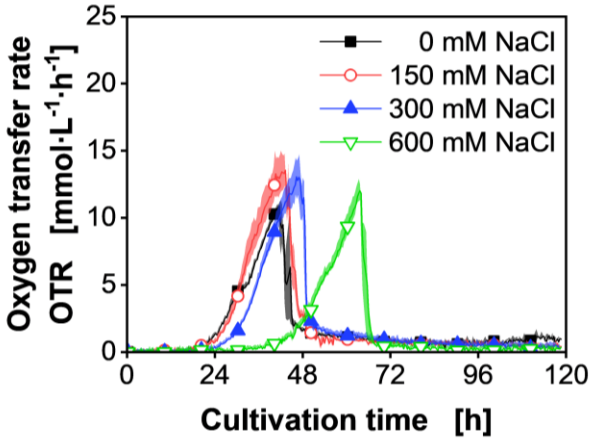

Appendix Figure A13. Oxygen transfer rates for axenic cultivations of *Streptomyces coelicolor* A3(2) WT with varying amounts of added sodium chloride. For clarity, only a representative amount of data points is indicated by the corresponding symbols. Culture conditions: 48-well round well plate, N = 3, $X_0 = 10^6$ spores·mL^{-1}, V_L = 1000 µL, n = 800 rpm, d_0 = 3 mm, T = 30 °C, LNP medium with 5 g·L^{-1} glucose and 30 g·L^{-1} α-cellulose.

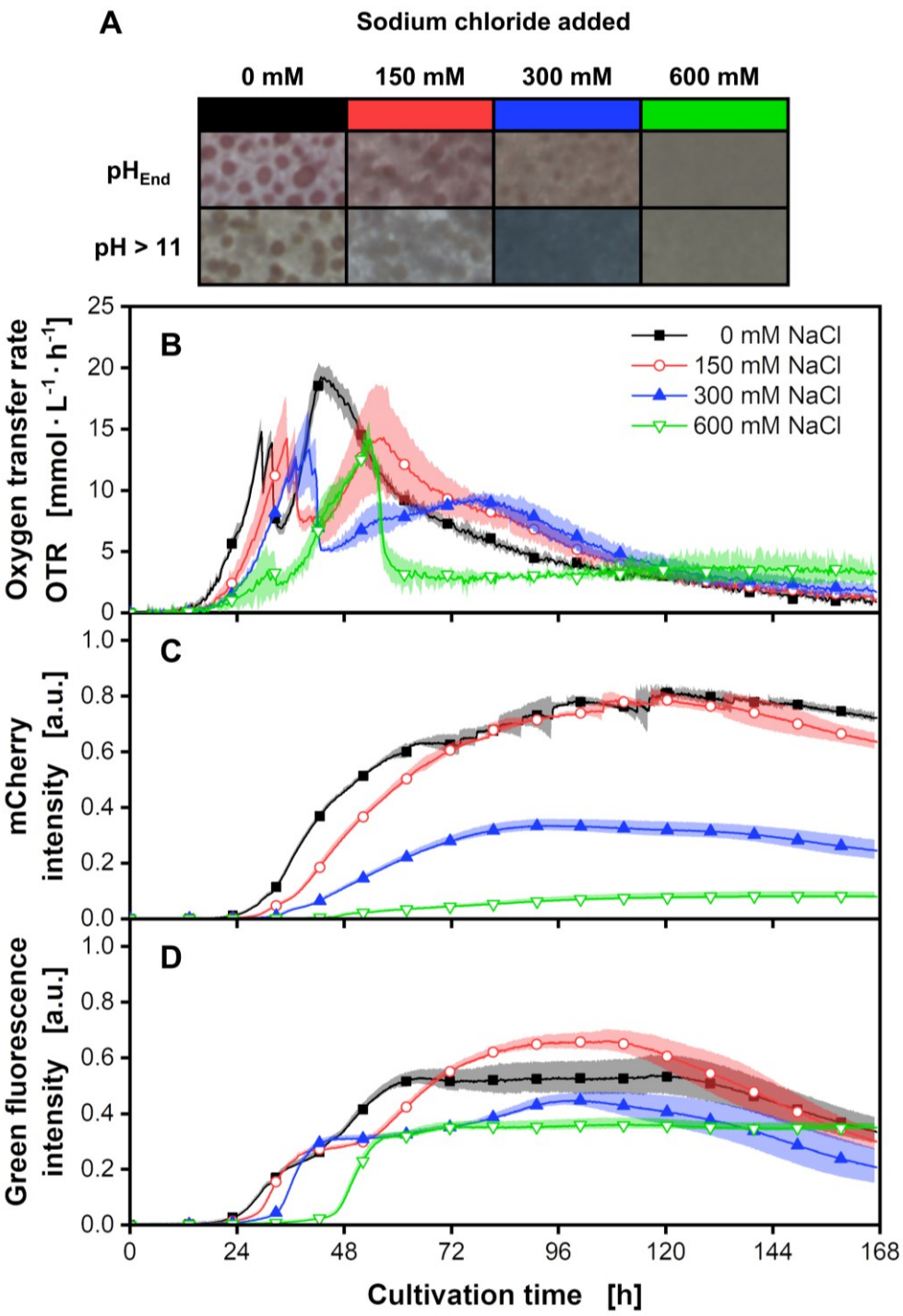

Appendix Figure A14. Co-cultivations of *Trichoderma reesei* RUT-C30 mCherry and *Streptomyces coelicolor* A3(2) WT with varying amounts of added sodium chloride. (**A**) Macroscopic pictures of the culture broth after termination of the cultivation. The pH was changed to a value of above 11 to determine production of the blue pigment actinorhodin (second row in (A)). (**B**) Oxygen transfer rates. (**C**) mCherry intensity signals (Excitation: 587 nm; Emission: 610 nm). (**D**) Green fluorescence intensity signals (Excitation: 483 nm; Emission: 520 nm). For clarity, only a representative

amount of data points is indicated by the corresponding symbols in (B) – (D). Culture conditions: 48-well round well plate, N = 3, $X_0 = 10^6$ spores·mL^{-1}, V_L = 1000 µL, n = 800 rpm, d_0 = 3 mm, T = 30 °C, LNP medium with 5 g·L^{-1} glucose and 30 g·L^{-1} α-cellulose.

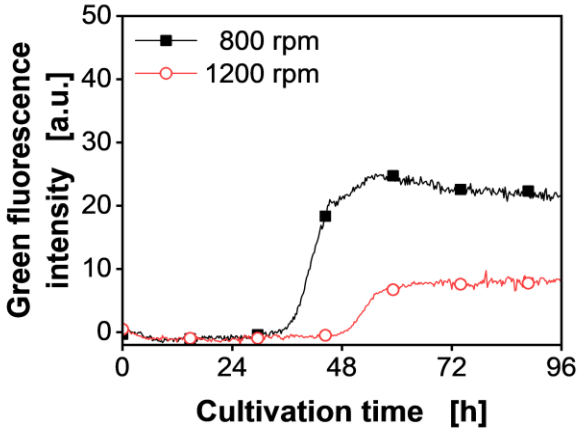

Appendix Figure A15. Biomass signal for axenic cultivations of *Streptomyces coelicolor* A3(2) WT with shaking frequencies of 800 and 1200 rpm. The green fluorescence intensity signals (Excitation: 480 nm; Emission: 520 nm) were monitored. For clarity, only a representative amount of data points is indicated by the corresponding symbols. Culture conditions: 48-well round well plate, $X_0 = 10^6$ spores·mL^{-1}, V_L = 1000 µL, n = 800 rpm, d_0 = 3 mm, T = 30 °C, LNP medium with 5 g·L^{-1} glucose and 30 g·L^{-1} α-cellulose.

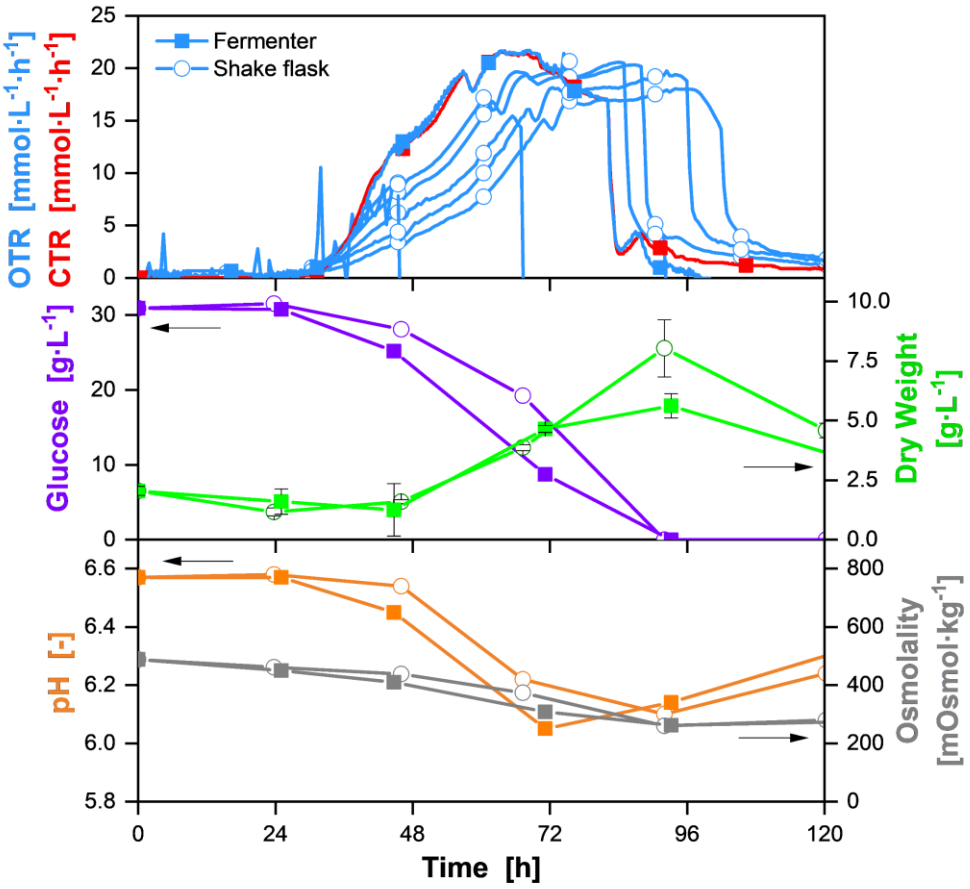

Appendix Figure A16. Comparison of simultaneous conducted cultivations of *Streptomyces coelicolor* A3(2) in shake flasks and a fermenter. For each sample for the shake flasks cultivations, one flask was taken out of the incubator and used for offline analytics. Fermenter culture conditions: 2 L fermenter, V_L = 1 L, n = 600 rpm, q_g = 1 vvm, T = 30 °C, X_0 = 1 (v/v) % washed pre-culture, LNP medium with antifoam agent. Shake flask culture conditions: 250 mL shake flasks, V_L = 20 mL, n = 320 rpm, d_0 = 50 mm, T = 30 °C, X_0 = 1 (v/v) % washed pre-culture, LNP medium with 30 g·L^{-1} glucose and antifoam agent.

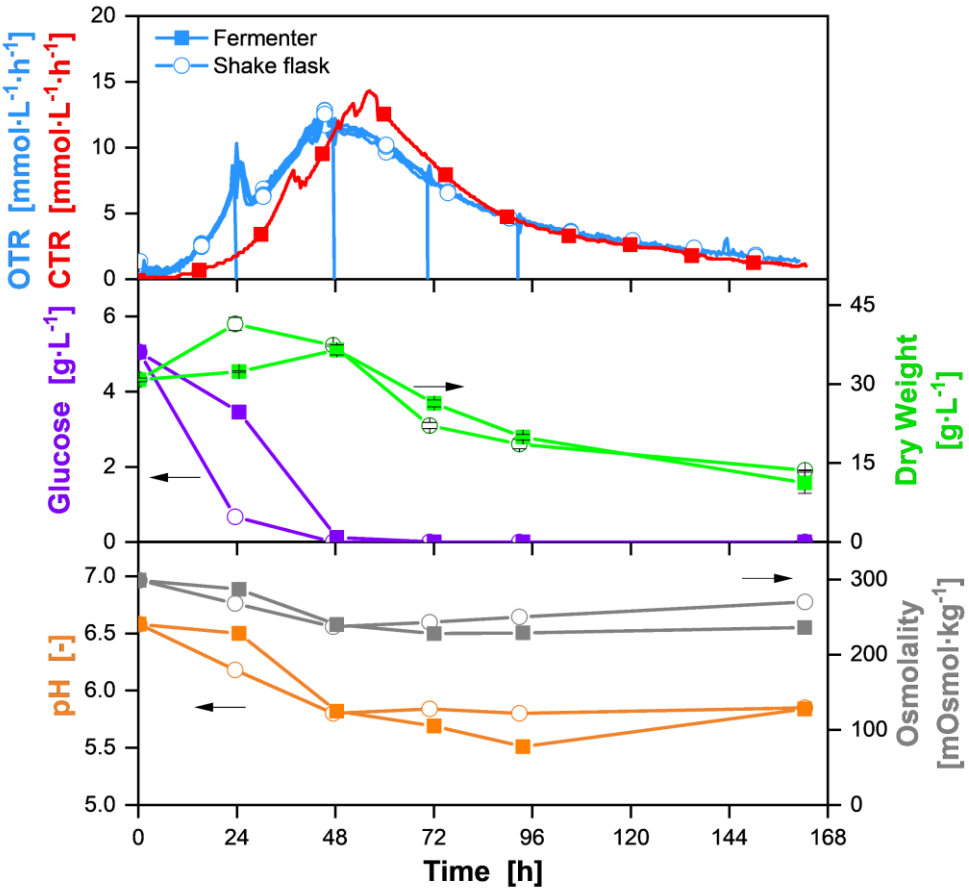

Appendix Figure A17. Comparison of simultaneous conducted cultivations of *Trichoderma reesei* RUT-C30 mCherry in shake flasks and a fermenter. For each sample for the shake flasks cultivations, one flask was taken out of the incubator and used for offline analytics. OTR data of the fermenter was omitted due to faulty measurements. Fermenter culture conditions: 2 L fermenter, V_L = 1 L, n = 1000 rpm, q_g = 1 vvm, T = 30 °C, X_0 = 1 (v/v) % washed pre-culture, LNP medium with antifoam agent. Shake flask culture conditions: 250 mL shake flasks, V_L = 20 mL, n = 320 rpm, d_0 = 50 mm, T = 30 °C, X_0 = 1 (v/v) % washed pre-culture, LNP medium with 5 g·L^{-1} glucose, 30 g·L^{-1} α-cellulose and antifoam agent.

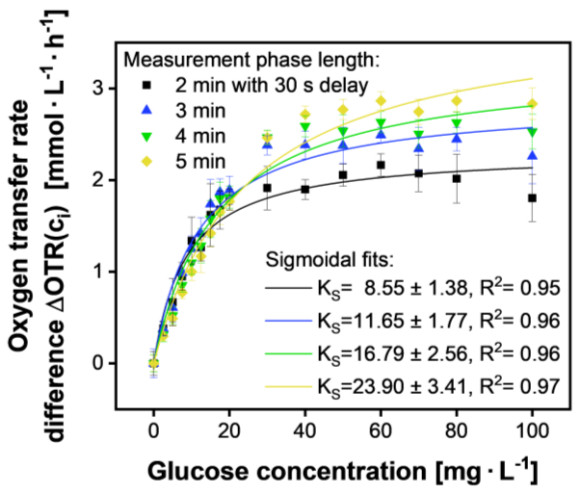

Appendix Figure A18. Correlation of the resulting oxygen transfer rate difference after the glucose spike to the respective initial glucose concentrations. The measurement phase lengths were varied. Due to the glucose depletion within the mesaurment phase, the k_S value is successively overstimated with the increasing measurement phase lengths. Culture conditions: 96-deepwell microtiter plate, V_L = 1 mL, n = 800 rpm, d_0 = 3 mm, T = 30 °C, CGXII medium without PCA, spike with 100 µL of 16 different glucose concentrations.

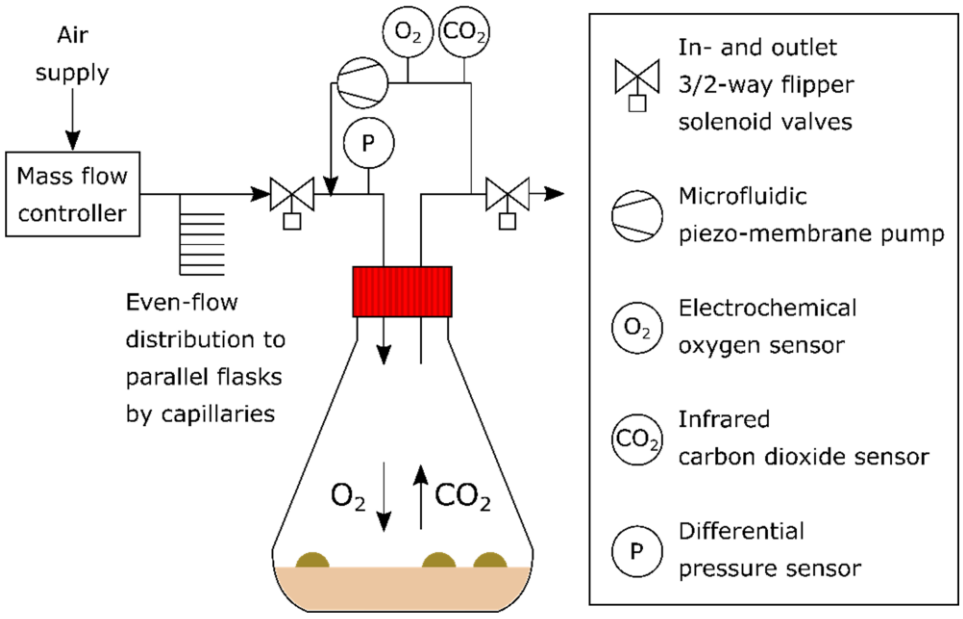

Appendix Figure A19. Schematic illustration of the respiratory activity monitoring system (RAMOS) used to monitor the respiratory activity of up to eight agar cultivations in shake flasks, similar as presented by Anderlei et al. (2001 and 2004), Schulte et al. (2018), Munch et al. (2020) and Mann et al. (2021) [51, 52, 148, 149, 154]. The Erlenmeyer flasks are not shaken for cultivations on solid media.

Appendix Figure A20. Erlenmeyer flask for the respiratory activity monitoring system (RAMOS) with three PyroScience optical oxygen sensor spots used to determine oxygen partial pressure p_{O2} at different heights above a LB-agar cultivation of *Escherichia coli* BL21.

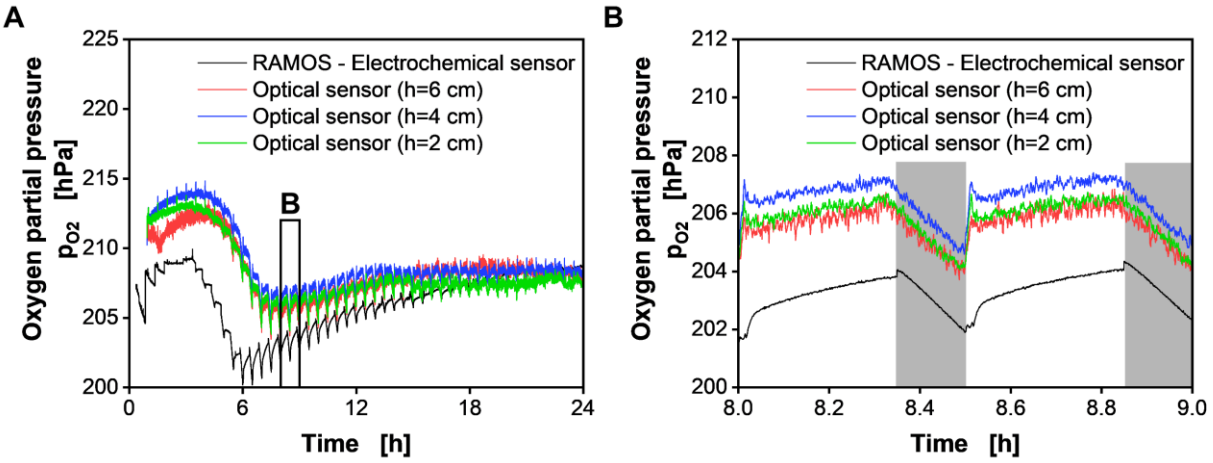

Appendix Figure A21. (**A**) Oxygen partial pressure p_{O2} profile determined by the respiratory activity monitoring system (RAMOS) and by optical oxygen sensor spots at different heights above a LB-agar cultivation of *Escherichia coli* BL21. In (**B**) an enlarged view from 8 to 9 h is depicted for a better visualization of measurement phases (grey area). Culture conditions: Non-shaken 250 mL Erlenmeyer flasks, V_L = 20 mL, T = 37 °C, $V_{X,0}$ = 200 µL with OD of 0.1.

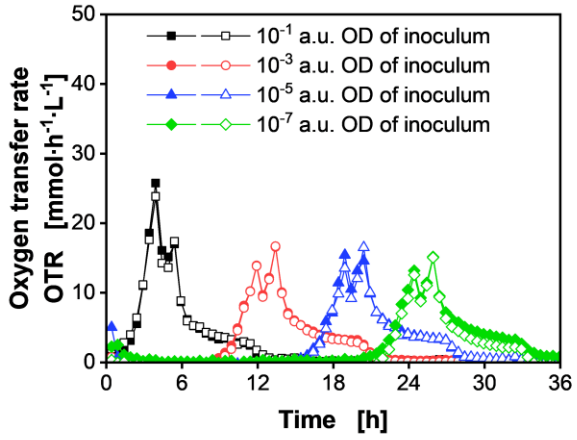

Appendix Figure A22. Cultivation of *Escherichia coli* BL21 in liquid LB-medium with varying inoculation densities. The inoculation density is defined by the arbitrary units of the optical density (a.u. OD of inoculum). The time until an increase in the OTR is noticed, varies depending on the inoculation density. However, in contrast to the cultivations on LB-agar, no other change in the OTR trajectory with successively decreasing inoculum densities can be monitored. Culture conditions: Shaken 250 mL Erlenmeyer flasks, V_L = 20 mL, n = 250 rpm, d_0 = 50 mm, T = 30 °C, $V_{X,0}$ = varying OD, duplicates.

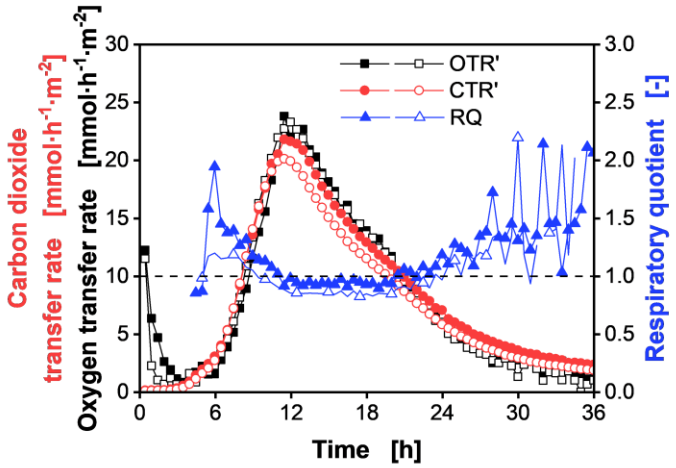

Appendix Figure A23. Cultivation of *Escherichia coli* BL21 on LB-agar, depicted in Figure 25A, with area-specific oxygen transfer rate (OTR') and area-specific carbon dioxide transfer rate (CTR') as well as the resulting respiratory quotient (RQ). A RQ = 1 is indicated by the horizontal dashed line. Values calculated from oxygen and carbon dioxide transfer rates smaller than 1 mmol·h^{-1}·m^{-2} were omitted. Culture conditions: Non-shaken 250 mL Erlenmeyer flasks, V_L = 20 mL, T = 30 °C, $V_{X,0}$ = 200 µL with an OD of 10^{-1}, duplicates.

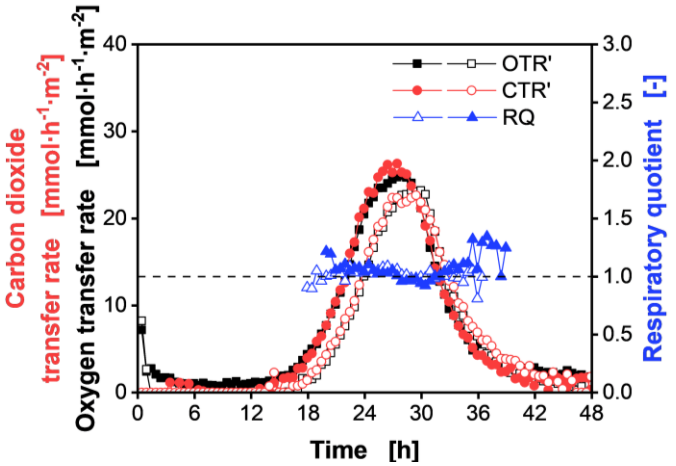

Appendix Figure A24. Cultivation of *Escherichia coli* BL21 on Wilms-MOPS-agar with area-specific oxygen transfer rate (OTR') and area-specific carbon dioxide transfer rate (CTR') as well as the resulting respiratory quotient (RQ). A RQ = 1 is indicated by the horizontal dashed line. Values calculated from oxygen and carbon dioxide transfer rates smaller than 1 mmol·h^{-1}·m^{-2} were omitted. Culture conditions: Non-shaken 250 mL Erlenmeyer flasks, V_L = 20 mL, T = 30 °C, $V_{X,0}$ = 200 µL with an OD of 10^{-1}, duplicates.

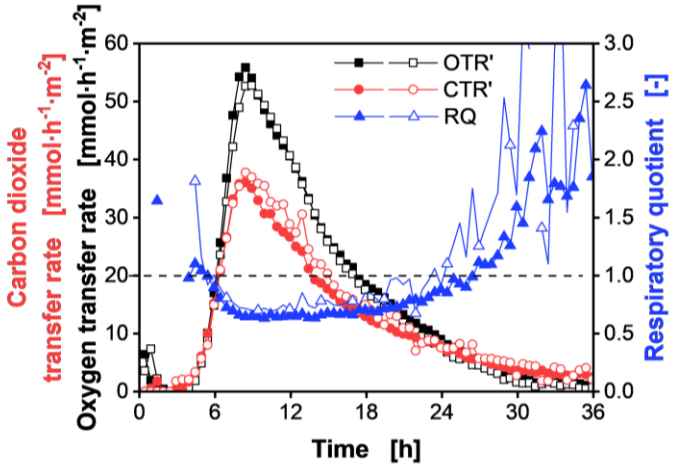

Appendix Figure A25. Cultivation of *Pseudomonas putida* KT2440 on LB-agar, depicted in Figure 25A, with area-specific oxygen transfer rate (OTR') and area-specific carbon dioxide transfer rate (CTR') as well as the resulting respiratory quotient (RQ). A RQ = 1 is indicated by the horizontal dashed line. Values calculated from oxygen and carbon dioxide transfer rates smaller than 1 mmol·h^{-1}·m^{-2} were omitted. Culture conditions: Non-shaken 250 mL Erlenmeyer flasks, V_L = 20 mL, T = 30 °C, duplicates.

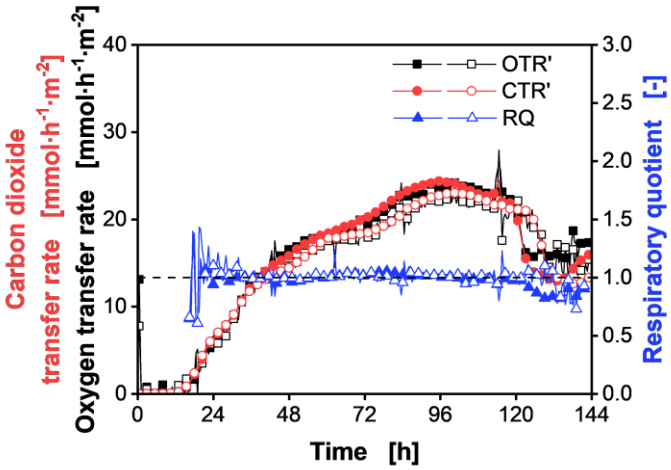

Appendix Figure A26. Cultivation of *Streptomyces coelicolor* A3(2) on SFM-agar, depicted in Figure 25A, with area-specific oxygen transfer rate (OTR') and area-specific carbon dioxide transfer rate (CTR') as well as the resulting respiratory quotient (RQ). A RQ = 1 is indicated by the horizontal dashed line. Values calculated from oxygen and carbon dioxide transfer rates smaller than 1 mmol·h^{-1}·m^{-2} were omitted. For clarity, only every 5th data point over time is indicated by the corresponding symbol. Culture conditions: Non-shaken 250 mL Erlenmeyer flasks, V_L = 20 mL, T = 30 °C, duplicates.

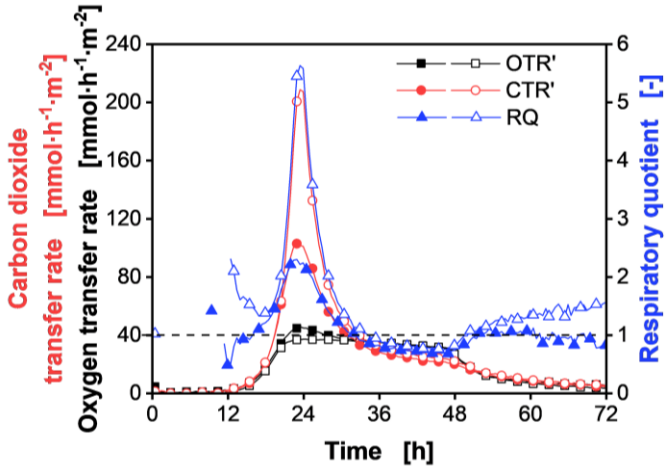

Appendix Figure A27. Cultivation of *Pichia pastoris* WT on YPD-agar, depicted in Figure 25B, with area-specific oxygen transfer rate (OTR') and area-specific carbon dioxide transfer rate (CTR') as well as the resulting respiratory quotient (RQ). A RQ = 1 is indicated by the horizontal dashed line. Values calculated from oxygen and carbon dioxide transfer rates smaller than 1 mmol·h^{-1}·m^{-2} were omitted. For clarity, only every 5th data point over time is indicated by the corresponding symbol. Culture conditions: Non-shaken 250 mL Erlenmeyer flasks, V_L = 20 mL, T = 30 °C, duplicates.

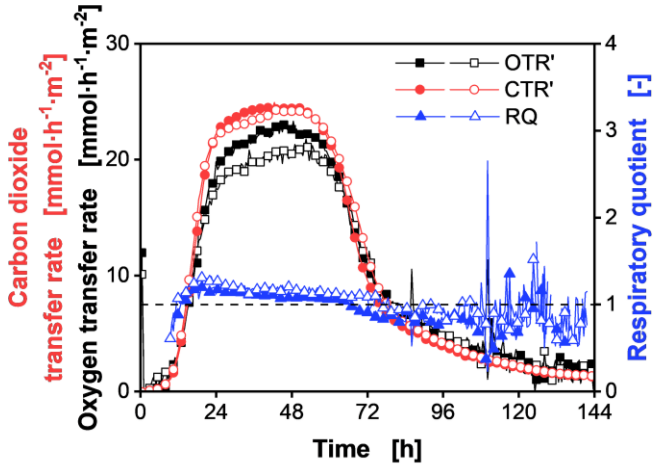

Appendix Figure A28. Cultivation of *Trichoderma reesei* RUT-C30 on PD-agar, depicted in Figure 25B, with area-specific oxygen transfer rate (OTR') and area-specific carbon dioxide transfer rate (CTR') as well as the resulting respiratory quotient (RQ). A RQ = 1 is indicated by the horizontal dashed line. Values calculated from oxygen and carbon dioxide transfer rates smaller than 1 mmol·h^{-1}·m^{-2} were omitted. For clarity, only every 5th data point over time is indicated by the corresponding symbol. Culture conditions: Non-shaken 250 mL Erlenmeyer flasks, V_L = 20 mL, T = 30 °C, duplicates.

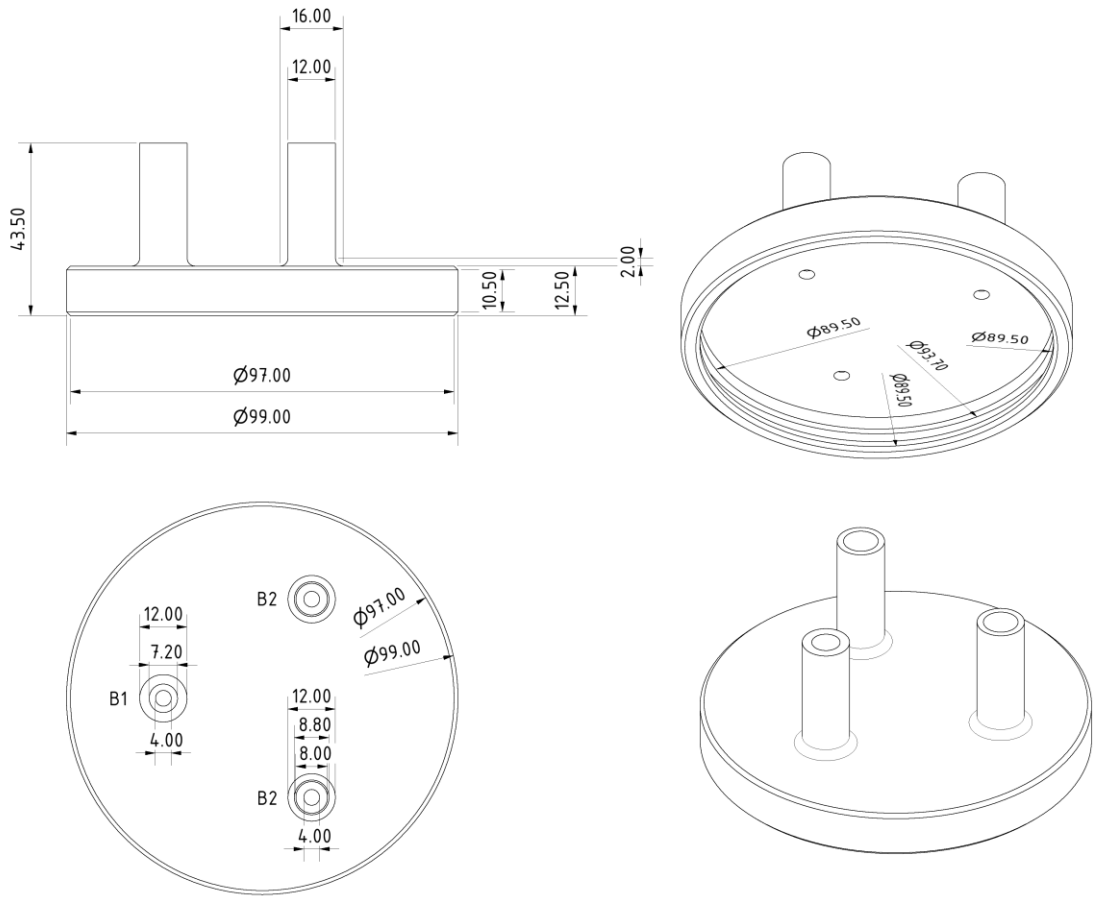

Appendix Figure A29. Technical drawing of the second version of an adapter to allow for the respiration monitoring of agar cultivations in Petri dishes with the RAMOS device. All dimensions are given in millimeters.